Universidade Federal do Rio Grande – FURG

Instituto de oceanografia

Programa de Pós-Graduação em oceanologia

DINÂMICA DA MATÉRIA ORGÂNICA PARTICULADA E DISTRIBUIÇÃO DE MASSAS DE ÁGUA NO ATLÂNTICO TROPICAL

ELIAS JOSE AZAR CEBALLOS

Dissertação apresentada ao Programa de Pós-Graduação em oceanologia, como parte dos requisitos para a obtenção do Título de Mestre.

Orientadora: *Profa. Dra.* MÔNICA WALLNER-KERSANACH

Universidade Federal do Rio Grande (FURG), Brasil.

Coorientadora: *Profa. Dra.* EUNICE DA COSTA MACHADO

Universidade Federal do Rio Grande (FURG), Brasil.

Rio Grande, RS, Brasil

Novembro, 2020

DINÂMICA DA MATÉRIA ORGÂNICA PARTICULADA E DISTRIBUIÇÃO DE MASSAS DE ÁGUA NO ATLÂNTICO TROPICAL

Dissertação apresentada ao Programa de Pós-Graduação em oceanologia, como parte dos requisitos para a obtenção do Título de Mestre

por

ELIAS JOSE AZAR CEBALLOS

Rio Grande, RS, Brasil

Novembro, 2020

AZAR CEBALLOS, ELIAS JOSE

Dinâmica da Matéria Orgânica Particulada e Distribuição de Massas de Água no Atlântico Tropical. / Elias Jose Azar Ceballos. – Rio Grande: FURG, Ano 2020.

Número de páginas p.114

Dissertação (Mestrado) – Universidade Federal do Rio Grande. Mestrado em oceanologia. Área de Concentração: Física dos oceanos e Clima; Biogeoquímica.

1. Termoclina. 2. Camada Central. 3. Massas de Água. 4. Matéria Orgânica Particulada. 5. Zona de Mínimo de Oxigênio. 6. Isótopos de Carbono e nitrogênio 7. Bomba Biológica.

Agradecimentos

Agradeço primeiramente a Deus por todas as bênçãos que tenho na minha vida.

Agradeço grandemente à minha esposa que sempre me apoia em cada coisa que eu faço, em cada ideia que eu tenho, você é a melhor companheira de vida. Sem ti e o meu filho, os dois tesouros que tenho na minha vida, nada desta aventura teria acontecido, obrigado por me acompanhar e apoiar em tudo.

Agradeço aos meus parceiros, colegas, e aqueles que foram minha família no Brasil, Karelys e Astolfo. Obrigado por ter me brindado com seu apoio, quando eu cheguei aqui, e pela amizade de anos.

Agradeço ao meu parceiro incondicional Andres, esse que sempre está quando eu preciso dele (sabe que eu também estou para ti). Obrigado por todo o tempo convivido, pela valiosa amizade, e pelo apoio em tudo MEU IRMÃO.

Aos professores do PPGO e da Hidroquímica que influenciaram muito no desenvolvimento pessoal e acadêmico ao logo dessa aventura chamada Mestrado. Especialmente à professora Mônica, à professora Eunice, e ao professor Rodrigo Kerr.

A toda a galera de Hidroquímica obrigado pelo tempo convivido e por fazer parte do meu crescimento pessoal.

Agradeço a todas as instituições que permitiram que este projeto fosse possível: à Universidade Federal de Rio Grande (FURG), à Marinha do Brasil, à equipe do navio Vital de Oliveira, ao laboratório de Hidroquímica, à Universidade Estadual Do Norte Fluminense Darcy Ribeiro (UENF), ao CNPq, a CAPES junto com o seu projeto PRINT da FURG, e ao Programa de Pós-graduação em Oceanologia.

Um grande agradecimento ao Brasil, por ter me brindado com essa grande oportunidade de continuar meus estudos.

Índice

Lista de figuras

Manuscrito I

<u>Manuscrito II</u>

Lista de tabelas

Manuscrito I

Manuscrito II

Lista de acrônimos e abreviações

AAIW – *Antarctic Intermediate Water*

ACAN – Água Central do Atlântico Norte

ACAS – Água Central do Atlântico Sul

ADT – *Absolute Dynamic Topography*

AIA – Água Intermediária Antártica

BC – *Brazil Current*

CCHDO – *Carbon Hydrographic Data Office*

COP – Carbono Orgânico Particulado

DO – *Dissolved Oxygen*

EDW – *Eighteen Degree Water*

ENSO – *El Niño Southern Oscillation*

ESACW – *Eastern South Atlantic Central Water*

GLODAPv2 – *Carbon Hydrographic Data Office second version*

GO-SHIP – *Global Ocean Ship-based Hydrographic Investigations Program*

INPE – Instituto Nacional de Pesquisa Espacial

ITCZ – *Intertropical Convergence Zone*

MMW – *Madeira Mode Water*

MLD – *Mixed Layer Depth*

MOP – Matéria Orgânica Particulada

NACW – *North Atlantic Central Water*

NASTMW – *North Atlantic Subtropical Mode Water*

NEC – *North Equatorial Current*

NOAA – *National Oceanographic and Atmospheric Administration*

NTP – Nitrogênio Total Particulado

OMZ – *Oxygen Minimum Zone*

PIRATA - *Prediction and Research Moored Array in the Tropical Atlantic*

POC – *Particulate Organic Carbon*

POM – *Particulate Organic Matter*

TPN – *Total Particulate Nitrogen*

PV – *Potential Vorticity*

SAMW – *Subantarctic Mode Water*

SASTMW – *South Atlantic Subtropical Mode Water*

SLA – *Sea Level Anomaly*

sSEC – *Southern South Equatorial Current*

SSS – *Sea Surface Salinity*

SST – *Sea Surface Temperature*

STIMW – *Subtropical Indian Mode Water*

STMW – *Subtropical Mode Water*

$STMW_{12}$ – *Subtropical Mode Water of 12°C*

$STMW_{14}$ – *Subtropical Mode Water of 14°C*

$STMW_{18}$ – *Subtropical Mode Water of 18°C*

SWT – *Source Water Type*

TW – *Tropical Water*

WOD18 – *World Ocean Database 2018*

WSACW – *Western South Atlantic Central Water*

ZCIT – Zona de Convergência Intertropical

ZMO – Zona de Mínimo de Oxigênio

$\delta^{13}C_{COP}$ – Delta de Carbono 13 no Carbono Orgânico Particulado

$\delta^{15}N_{NTP}$ – Delta de Nitrogênio 15 no Total Nitrogênio Particulado

$\delta^{13}C_{POC}$ – *Delta-Carbono-13 in the Particulate Organic Carbon*

$\delta^{15}N_{TPN}$ – *Delta-Nitrogen-15 in the Total Particulate Nitrogen*

Resumo

O oceano Atlântico Tropical é caracterizado por uma complexa dinâmica oceanográfica que afeta seus processos físicos e biogeoquímicos. O efeito dos processos sobre a matéria orgânica particulada (MOP) e na bomba biológica ainda estão em debate. Assim, neste trabalho a dinâmica das massas de água na termoclina foi primeiramente estudada através da análise otimizada com parâmetros múltiplos usando-se a base de dados hidrográficos disponíveis no *World Ocean Database 2018*. Na camada da Água Central do Atlântico Norte (ACAN), a contribuição da massa de água foi definida pela *Eighteen Degree Water (EDW)* e a *Madeira Mode Water (MMW)*, que seguem a Corrente Norte Equatorial estabelecendo o limite com a Água Central do Atlântico Sul (ACAS) em torno de 10ºN. No hemisfério sul, a fonte de água formada na região sudeste (em níveis superficiais) e aquela formada na borda da frente subtropical (em níveis mais densos) foram os principais contribuintes para a camada da ACAS no Atlântico Tropical. Além disso, na região subtropical, a *Subtropical Indian Mode Water* teve grande influência com uma contribuição média de ~ 34 ± 20% entre 20ºS e 30ºS principalmente nas isopicnais de 26,2 e 26,4 kg m^{-3} (100 - 400 m). Então, uma vez que essa dinâmica foi determinada, a MOP foi caracterizada pelo seu teor de carbono orgânico (COP) e nitrogênio (NTP) e as assinaturas isotópicas de $\delta^{13}C_{COP}$ e $\delta^{15}N_{NTP}$ em um transecto meridional (38 °O) do equador até 15°N na coluna d'água. O COP (~ 4 µmol L^{-1}) e o NTP (~ 0,2 µmol L^{-1}) foram maiores na subsuperfície em 8°N e o $\delta^{13}C_{COP}$ (- 25 ‰) foi relativamente mais pesado do que aqueles ao sul dessa latitude, sugerindo que o efeito de lastro devido às partículas terrígenas provenientes da entrada eólica aumentam as velocidades de afundamento da MOP. O mesmo padrão na MOP e $\delta^{13}C_{COP}$ foi encontrado na zona de mínimo de oxigênio e logo abaixo dela. Neste caso, isto provavelmente associado às mudanças no comportamento do zooplâncton devido à baixa concentração de oxigênio. Portanto, concluiu-se que a dinâmica física está afetando de diferentes maneiras a bomba biológica no Atlântico Tropical.

Palavras-Chave: Termoclina; Camada Central; Massas de Água; Matéria Orgânica Particulada; Zona de Mínimo de Oxigênio; Isótopos de Carbono e nitrogênio; Bomba Biológica.

Abstract

The tropical Atlantic Ocean is characterized by a complex oceanographic dynamic which affect its physical and biogeochemical processes. This effect on the particulate organic matter (POM) and the biological pump is still under debate. Thus, in this work it was first studied the thermocline water mass dynamic through the Optimum Multiparameter water mass analysis using the hydrographic dataset available from the World Ocean Database 2018. In the North Atlantic Central Water (NACW) layer, the water mass contribution was defined by the Eighteen Degree Water (EDW) and Madeira Mode Water (MMW), which follows the North Equatorial Current and setting up the limit with the South Atlantic Central Water (SACW) at about 10ºN. In the southern hemisphere, the source water formed in the southeastern area (on surface levels) and that formed in the edge of the subtropical front (on denser levels) were the main contributors to the SACW layer in the tropical Atlantic. Moreover, in the subtropical region, the Subtropical Indian Mode Water greatly influences with an average contribution of ~34 ± 20% between 20ºS and 30ºS, and mainly at the isopycnals layers between 26.2 and 26.4 kg m^{-3} (100 – 400 m). Then, once this dynamics was stablished it was characterized the POM by its organic carbon (POC) and nitrogen (TPN) content and the $\delta^{13}C_{POC}$ and $\delta^{15}N_{TPN}$ signatures in a meridional transect (38°W) from the equator to 15°N. POC (~ 4 µmol L^{-1}) and TPN (~ 0.2 µmol L^{-1}) were higher in the subsurface at 8°N and the $\delta^{13}C_{POC}$ (- 25 ‰) was relative heavier than those southern, suggesting that the ballast effect due to terrigenous particles coming from aeolian input, enhance the sinking velocities of the POM. The same patter in POM and $\delta^{13}C_{POC}$ was found in the oxygen minimum zone and just beneath it, in this case, it was likely associated with changes in zooplankton behaviour owing to poor oxygen concentration. Therefore, it was concluded that the physical dynamics is affecting in different ways the biological pump in the tropical Atlantic.

Keywords: Thermocline; Upper ocean; Water masses; Particulate Organic Matter; Oxygen Minimum Zone; Carbon and Nitrogen Isotopes; Biological Carbon Pump.

CAPÍTULO I:

Introdução

A bomba biológica é um conjunto de mecanismos complexos que transportam constantemente grandes quantidades de moléculas de carbono na forma de carbono orgânico particulado (COP) e biominerais ($CaCO_3$), da superfície do oceano para zonas mais profundas (Volk & Hoffert, 1985; Honjo et al., 2008). Esta bomba começa perto da superfície, onde o material inorgânico dissolvido (CO_2, nitrato, fosfato e silicato) é transformado em matéria orgânica (carboidratos, lipídios e proteínas) e biominerais (sílica e carbonato de cálcio) pelo fitoplâncton através da fotossíntese (Falkowski et al., 1998, De la Rocha & Passow, 2014). A produção primária líquida é responsável por 50 Pg C ano^{-1} (1 Pg ou 1 Gt é 10^{15} g) dos quais 10 Pg C ano^{-1} são exportados (da zona eufótica) e 2 Pg C ano^{-1} atingem o fundo do mar (De la Rocha & Passow, 2014; Middelburg, J., 2019). Assim, a grande maioria da matéria orgânica exportada de águas próximas à superfície é convertida de volta em seus constituintes

inorgânicos por organismos heterotróficos, principalmente na picnoclina superior por meio da remineralização (Sarmiento & Gruber, 2006). Apesar de que apenas 4% da produção primária líquida é depositada no fundo do mar, a bomba biológica regula o CO_2 atmosférico e, portanto, o sistema climático (De la Rocha & Passow, 2007 e 2014).

A quantidade de matéria orgânica particulada (MOP) gerada na superfície dos oceanos é diretamente proporcional à produtividade primária, no entanto, a exportação para zonas mais profundas depende de outros processos (De la Rocha & Passow, 2007 e 2014). Existem dois processos principais que descrevem como a MOP pode ser exportada para o fundo dos oceanos: (I) o transporte pelo zooplâncton, conhecido como migrações verticais diurnas; e (II) assentamento gravitacional de agregados minerais (biogênicos e terrígenos), que atuam como lastro aumentando a velocidade de afundamento das partículas orgânicas (Honjo et al., 2008). Portanto, variações na entrada do material terrígeno e no comportamento do zooplâncton determinam a exportação da MOP para o fundo oceânico.

Além da entrada de partículas atmosféricas na superfície dos oceanos (Schlosser et al., 2014; Baker & Jickells, 2017), a dinâmica das correntes e contracorrentes no abastecimento de oxigênio (Karstensen et al., 2008; Brandt et al., 2015), e a dinâmica das massas de água nas camadas centrais/intermediárias (Gordon et al., 1992; Poole & Tomczak, 1999) e nas zonas de ressurgência são alguns dos processos que afetam significativamente o funcionamento da bomba biológica. Dentro desses processos, nas zonas dos oceanos onde o conteúdo de oxigênio dissolvido é limitado (ZMO) a dinâmica da MOP é diferente à encontrada nas zonas oxigenadas (Devol & Hartnett, 2001). Não há um limite convencionado em função do oxigênio dissolvido que defina uma ZMO. Alguns pesquisadores indicam duas classificações baseadas no teor de oxigênio dissolvido, onde ocorrem processos biogeoquímicos diferentes: condições hipóxicas, com valores aproximados a 60 μmol kg^{-1}, e condições subóxicas, com teores menores a 10 μmol kg^{-1} (Karstensen et al., 2008; Stramma et al., 2008).

O volume do oceano global ocupado pelas ZMO varia substancialmente. Estas encontram-se principalmente nas bordas lestes dos oceanos tropicais em áreas de alta produtividade, ocupando predominantemente as massas de água centrais e a camada superior das intermediárias (Karstensen et al., 2008). No oceano Atlântico, apesar do volume ocupado pelas ZMO ser baixo (5 % no Norte e 7 % no Sul), estas zonas representam um papel fundamental na eficiência da bomba biológica (Rasse & Dall'Olmo, 2019). Nestas zonas a redução do fluxo da MOP nas partículas que estão afundando é menor quando comparado com nas zonas oxigenadas (Roullier et al., 2014; Keil et al., 2016; Cavan et al., 2017; Engel et al., 2017). Portanto, visto que trabalhos prévios (Stramma et al., 2008; Passow and Carlson, 2012) indicam que nos últimos 50 anos as ZMO estão-se expandindo verticalmente, com uma tendência de diminuição de oxigênio dissolvido de 0,18 ± 0,004 μmol kg^{-1} ano^{-1} (Santos et al., 2016), é claro a importância de estudos e contribuições neste tema.

Uma ferramenta importante para o estudo da dinâmica da MOP dentro do oceano são os isótopos estáveis. O fracionamento isotópico do $\delta^{13}C_{COP}$ dentro da MOP depende dos parâmetros físico-químicos tais como temperatura, pCO_2, pH, disponibilidade de nutrientes, e fatores fisiológicos, portanto, as assinaturas isotópicas podem variam de acordo com a latitude nos oceanos (Rau et al., 1992; Lourey et al., 2004; Lara et al., 2010). Por exemplo, o fitoplâncton a 22°C possui um $\delta^{13}C$ em torno a -20 ‰, quanto que a 1°C torna-se mais negativo (-27 ‰). No caso do $\delta^{15}N_{NTP}$, este depende da fonte de nitrogênio usada para o crescimento do fitoplâncton e das condições fisiológicas (Wada et al., 1987), tendo sido usado como um proxy para a utilização de nitrato em água superficial (Laurey et al., 2003).

Alguns trabalhos pretéritos ressaltaram como é a relação da assinatura isotópica com os parâmetros físico-químicos nos oceanos. Por exemplo, altos valores dos nutrientes (principalmente do nitrato), altos valores de pCO_2, e baixas taxas de crescimento do fitoplâncton geram um maior fraccionamento isotópico (Jeffrey et al., 1983; Wada et al., 1987; Fisher, G., 1991). É por isto, que existem fortes variações nas assinaturas isotópicas nas frentes polares e subpolares. Além disso, as diferentes comunidades de fitoplâncton, podem afetar a assinatura isotópica. No caso das diatomáceas, as quais dependem da

razão silicato/nitrato, apresentam valores mais negativos nos valores de $\delta^{13}C$ (Lourey et al., 2004; Lara et al., 2010, Garzon et al., 2016, MacKenzie et al., 2019). Em profundidade, os valores isotópicos dependem dos compostos orgânicos que estão sendo consumidos, sendo os aminoácidos os mais facilmente consumíveis, deixando a MOP residual empobrecida no isótopo de C mais pesado (Jeffrey et al., 1983; Smith et al., 2002).

O consumo ou remineralização da MOP dá-se principalmente nas camadas centrais dos oceanos. Estas águas se formam por processos de subducção nos subtópicos, combinando o efeito do vento é a perda de calor na superfície dos oceanos (Tomczak and Godfrey, 1994). A formação destas águas envolve o ciclo sazonal da camada de mistura, onde aquela parcela de água resultante da camada de mistura entre um inverno e outro é subduzida seguindo a sua isopicnal de referência (Tomczak and Godfrey, 1994; Hazeleger and Drijfhout, 2006). Dentro das massas de águas centrais, as contribuições das águas modais são bastante relevantes, sendo estas, parcelas de água formadas pela interação oceano-atmosfera que possuem uma pequena variação nas sus propriedades tanto vertical quanto horizontalmente (Hanawa and Talley, 2001; Sato and Polito, 2014).

No Atlântico as águas centrais tem sido estudadas por vários pesquisadores, indicando, por exemplo, quais são os limites entre a Água Central do Atlântico Norte (ACAN) e a Água Central do Atlântico Sul (ACAS), e as principais correntes atuantes na região (Poole and Tomczak, 1999; Stramma and England, 1999). Quanto estes estudos se focam nas massas de água centrais em função de um grande rango de propriedades, as contribuições das águas modais às águas centrais ainda não é bem compreendida, incluída o aporte de as águas do Indico através das estrutura de mesoescala para o Atlântico (Santos et al., 2016; de Souza et al., 2018).

Especificamente no oceano Atlântico Tropical a dinâmica oceanográfica é bastante complexa. Existe uma grande interação oceano-atmosfera através da zona de convergência intertropical (ZCIT), um complicado sistema de correntes e contracorrentes, o encontro de duas massas de água (ACAN e ACAS), e a presença de duas ZMO. Apesar de vários autores terem usado os isótopos

estáveis da MOP para avaliar a dinâmica biogeoquímica em algumas áreas críticas do oceano, existem poucos trabalhos no oceano Atlântico Tropical focados na interação entre a MOP e os complexos processos oceanográficos que lá ocorrem.

Essa complexa dinâmica nesta região exerce um grande papel dentro do sistema climático através da exportação da MOP para o fundo do oceano. Além disso, é muito relevante conhecer como os processos físicos e os processos biogeoquímicos estão interagindo em relação às mudanças que está atravessando o oceano Atlântico, e, como essa dinâmica pode estar afetando a bomba biológica. Portanto, este trabalho foi focado no estudo da dinâmica e quantificação das massas de água centrais dentro do oceano Atlântico Tropical, assim como também o comportamento da MOP (junto com os seus isótopos estáveis, $\delta^{13}C_{COP}$ e $\delta^{15}N_{NTP}$) em função dos processos acima mencionados.

CAPÍTULO II:

Objetivos

2.1 Objetivo geral

Investigar a dinâmica da matéria orgânica particulada com base na sua distribuição isotópica de $\delta^{13}C$ e $\delta^{15}N$ e a sua relação com os parâmetros físico-químicos nas massas d'águas do oceano Atlântico Tropical oeste.

2.2 Objetivos específicos

- Quantificar as frações de mistura e a variabilidade temporal das diferentes águas modais subtropicais na camada de água central no oceano Atlântico Tropical.
- Caracterizar as variações verticais dos teores de carbono e nitrogênio na MOP e a sua composição isotópica ($\delta^{13}C$ e $\delta^{15}N$) na coluna d'água ao longo da secção latitudinal em 38°O desde o equador até 15°N.

- Avaliar, com base nos teores de C e N, a sua distribuição isotópica, e os parâmetros físico-químicos, se a MOP é afetada pela dinâmica oceanográfica presente no oceano Atlântico Tropical.

CAPÍTULO III:
Material e Métodos

Nesta secção será abordada o material e métodos utilizados para cada um dos manuscritos apresentados no capítulo IV por separado. Atingindo como o primeiro manuscrito o objetivo especifico I, e com o segundo manuscrito os subsequentes objetivos.

3.1 Manuscrito I

Neste primeiro manuscrito abordou-se a quantificação das frações de mistura e a variabilidade temporal, através da análise otimizada com parâmetros múltiplos (OMP), das diferentes águas modais subtropicais na camada de água central no oceano Atlântico Tropical.

3.1.1 Banco de dados e análise otimizada com parâmetros múltiplos (OMP)

Dados hidrográficos e químicos do *World Ocean Database 2018* (WOD18; Boyer et al., 2018; www.nodc.noaa.gov) foram usados para determinar a distribuição espacial das propriedades físico-químicas e para calcular as frações da mistura (%) das distintas variedades das águas subtropicais modais que contribuem à camada central do Atlântico Tropical. A área de estudo foi restrita

de 30°N a 30°S e 60°W a 10°E. Para isso, foram utilizados os seguintes parâmetros: a temperatura potencial, salinidade, oxigênio dissolvido, sílica dissolvida, nitrato e fosfato e vorticidade potencial. Assim, o conjunto de dados foi filtrado para considerar apenas os dados das estações que possuíam esses parâmetros. Foram utilizados apenas dados classificados como de boa qualidade pelos procedimentos de controle do WOD18.

Considerando o objetivo da análise, e evitando interferências causadas pela Água Tropical quente e salgada na fronteira entre as camadas superficiais e centrais, os primeiros 100 m da coluna de água não foram incluídos. Assim, a análise otimizada com parâmetros múltiplos (OMP) está focada na parte superior do oceano de 100 m a cerca de 1000 m de profundidade, uma camada que inclui as águas centrais dos oceanos Atlântico Sul e Norte, e a camada superior da Água Intermediaria Antártica (AIA). Para o uso da versão estendida da OMP os parâmetros semiconservativos (nutrientes e oxigênio) foram corrigidos utilizando as relações de remineralização propostas por Takahashi (1985) e depois modificadas por Anderson & Sarmiento (1994) para $O:NO_3^-:PO_4^{3-}$ (171:17:1), quanto que para $O:Si(OH)_4$ se utilizou a proposta por Poole e Tomczak (1999) com uma razão de 171:11.

3.1.2 Definição das águas tipo fonte e pesos dos parâmetros

Para determinar os índices termohalinos, foram utilizadas as regiões de formação para as variedades das águas subtropicais modais propostas por Sato & Polito (2014) para o hemisfério sul, e por Worthington (1959) e Siedler et al. (1987) para o hemisfério norte (Figura 1). Uma compilação de região de formação para AIA foi determinada com base em McCartney (1977), Hanawa & Talley (2001) e Holte et al. (2012). A região de formação utilizada para a *Subtropical Indian Mode Water* (STIMW) foi definida de acordo com Hanawa & Talley (2001). Assim, as águas tipo fontes utilizadas para representar às águas que contribuem à Água Central do Atlântico Sul (ACAS) foram a *Subtropical Mode Water of 18°C* ($STMW_{18}$), a *Subtropical Mode Water of 14*°C ($STMW_{14}$), a *Subtropical Mode Water of 12°C* ($STMW_{12}$) e a STIMW; enquanto que as que contribuem à Água Central do Atlântico Norte (ACAN) foram a *Eighteen Degree Water* (EDW) e *Madeira Mode Water* (MMW).

Uma etapa chave na análise de OMP é a determinação de um fator de ponderação para cada parâmetro utilizado na resolução das equações da matriz linear (Poole e Tomczak, 1999). Aqui, é usado conforme descrito por Tomczak & Large (1989), para calcular o peso para cada parâmetro j (Wj):

$$W_j = \frac{\sigma_j^2}{\delta_{j\,max}},$$

onde σ_j^2 é a variância de cada parâmetro "*j*", e $\delta_{j\,max}$ é a variância máxima associada ao mesmo parâmetro na região de formação da água tipo fonte. Se a coluna de água for bem representada pelas águas tipo fonte escolhidas, os resíduos são muito baixos e qualquer resultado com resíduos de conservação de massa superiores a 5% é descartado.

3.1.3 Quantificação das frações de mistura dentro dos vórtices de mesoescala

Uma análise geoespacial foi executada para avaliar a influência do oceano Índico sobre a termoclina do Atlântico através do vazamento das Agulhas. Assim, as frações das águas fontes calculadas na análise OMP, contendo a contribuição (%) de cada STMW, foram unidas espacialmente com três bancos de dados de identificação de vórtices diferentes: (i) o DT2.0exp de tempo retardado (Schlax & Chelton, 2016), (ii) os bancos de dados NRT3.0exp (Mason et al., 2014) quase em tempo real do produto AVISO + Mesoscale Eddy Trajectory Atlas (http://www.aviso.altimetry.fr/), e (iii) o banco de dados TOeddies desenvolvido por Laxenaire et al. (2018).

A junção espacial foi realizada no software QGIS 3.10 considerando o algoritmo "Unir atributos por localização". O tamanho de cada vórtice foi descrito por um círculo com uma área igual àquela delimitada pelo contorno de velocidade geostrófica máxima. Deve-se notar que esta abordagem é baseada em duas razões: primeiro, a área definida por este parâmetro reflete melhor as condições do núcleo dos vórtices e é menos distorcida por outros vórtices ao seu redor (Laxenaire et al., 2018) e, segundo, o banco de dados DT2.0exp não identifica o contorno mais externo dessas estruturas. Portanto, para manter a consistência dentro da análise, o parâmetro de contorno externo não foi usado.

3.2 Manuscrito II

3.2.1 Estratégia de amostragem

Este estudo foi conduzido em parceria com o projeto *Prediction and Research Moored Array in the Tropical Atlantic (PIRATA),* que é uma colaboração internacional entre os Estados Unidos de Norte America (NOAA), a França (Meteo-France**,** CNRS e IFREMER), e o Brasil (INPE and DHN). A amostragem foi realizada a bordo do RV Vital de Oliveira entre os dias 16 de outubro e 10 de novembro de 2018 em um transecto meridional (38 °O) do equador até 15°N (Pág. 78). Este cruzeiro abrangeu 14 estações com uma resolução espacial de cerca de um grau de latitude, tomando perfis de temperatura, salinidade, pressão e oxigênio dissolvido. Além disso, em 7 estações, amostras discretas de água do mar foram coletadas para análise química, incluindo nutrientes inorgânicos, carbono orgânico particulado (COP), nitrogênio particulado e seus isótopos estáveis ($\delta^{13}C_{COP}$, $\delta^{15}N_{NTP}$) usando um CTD / Carrossel equipado com 24 garrafas Niskin de doze litros.

3.2.2 Análises químicas e isotópicas

Amostras discretas de 100 mL para nutrientes inorgânicos foram coletadas e armazenadas em frascos de polietileno, sendo imediatamente congeladas a −20°C até serem analisadas. Para evitar possível contaminação e levando em consideração a baixa turbidez da água na região, as amostras não foram filtradas, utilizando-se, em compensação, uma amostra de água do mar não tratada como referência na hora de medir a absorbância, conforme recomendado por Hansen e Koroleff, (1999).

As garrafas Niskin foram agitadas antes de tomar as alíquotas de 2-3 L em envases de polipropileno de alta densidade, e este processos foi repetido para as alíquotas tomadas antes de fazer a filtragem a bordo em filtros GF/F Whatman de 25 mm de diâmetro, previamente calcinados à 450°C por 4h na *glove box*. Logo de realizar a filtração um pequeno volume (30 mL) de água ultrapura foi acrescentado para retirar os resíduos de sal. Cuidados foram tomados conforme recomendado no protocolo do GEOTRACES para o material particulado (Cutter et al., 2017; consultado em 20/08/2020,

https://www.geotraces.org/methods-cookbook/). Assim, as garrafas Niskin foram homogeneizadas suavemente antes da retirada das alíquotas, e o mesmo processo foi aplicado para as alíquotas antes da filtração, que era realizada em um sistema *glove box*. Finalmente, os filtros foram armazenados imediatamente a −20°C até a análise. Para a determinação dos isótopos estáveis $\delta^{13}C_{COP}$ e $\delta^{15}N_{NTP}$, teor de carbono e nitrogênio, os filtros foram secos a 60°C por 12h e completamente oxidados no analisador elementar por combustão em temperaturas acima de 1000°C sob O_2 puro. A composição isotópica de N_2 e CO_2 foi então analisada por espectrometria de massa (Thermo Scientific™ Delta V™ Isotope Ratio Mass Spectrometer).

CAPÍTULO IV:

Contribuições das águas modais nas camadas centrais do oceano Atlântico Tropical

Para a obtenção do título de Mestre pelo Programa de Pós-Graduação em oceanologia, é requerido que o discente realize a submissão de pelo menos um artigo cientifico como primeiro autor em periódico com corpo indexado. Desse modo, os resultados da pesquisa desenvolvida durante o período de mestrado e a discussão dos resultados serão apresentados em forma de artigos neste capítulo. O primeiro manuscrito, de autoria de Elias Azar, Andres Piñango, Mônica Wallner-Kersanach, e Rodrigo Kerr, é intitulado **"Source waters contribution to the tropical Atlantic central layer: new insights on the Indo-Atlantic exchanges"** e foi aceito para publicação no periódico **"Deep-Sea Research Part I"**.

Abstract

This study reveals the influence of the Subtropical Mode Water (STMW) varieties and their spatiotemporal variability on the upper thermocline of the tropical Atlantic Ocean. Optimum Multiparameter water mass analysis was applied using the hydrographic and chemical datasets available from the World Ocean Database 2018 and The Global Ocean Ship-Based Hydrographic Investigations Program. Eighteen Degree Water (EDW) and Madeira Mode Water (MMW), sourced in the northwest and northeast North Atlantic, respectively, contribute to the North Atlantic Central Water (NACW) layer, which follows the North Equatorial Current and setting up the limit with the South Atlantic Central Water (SACW) at about 10ºN. The contribution of the EDW to the NACW spreads at the surface layer (excluding the first 100 m) until the 26.6 kg m^{-3} isopycnal (~250 m). MMW contributes to denser levels of the upper layer, mainly between 26.8 and 27 kg m^{-3} (300 – 700 m). In the southern hemisphere, mode waters formed in the eastern South Atlantic ($STMW_{18}$) and along the edge of the subtropical front ($STMW_{12}$) were the main contributors to the surface and denser levels, respectively. The variety formed in the Brazil-Malvinas confluence ($STMW_{14}$) was restricted to the southwestern side of the South Atlantic gyre, while the Subtropical Indian Mode Water (STIMW; mode water advected from the Indian Ocean into the South Atlantic Ocean) influenced the SACW structure between 20°S and 30°S with an averaged mixing fraction of ~ 34% ± 20 %, mainly at isopycnals of 26.2 and 26.4 kg m^{-3} (100 – 400 m). The main source of the STIMW, the Agulhas eddies, act as an interocean exchanges structure that transport an average of 5.5 ± 3.2 Sv (1 Sv = 10^6 m^3 s^{-1}) of STIMW to the Atlantic, even after they have been altered by splitting and/or merging processes. In addition, a smaller contribution of ~ 20% of STIMW was associated with the North Brazil Current at ~ 350 m, showing the interhemispheric connection between the Indian Ocean to the upper branch of the Atlantic Meridional Overturning Circulation. Therefore, due to the previously reported increase of the Agulhas Leakage and the dynamic of the bifurcation of the southern Equatorial Current, the heat and salt fluxes to the northern hemisphere may likely increase in the following years.

Keywords: Agulhas eddies, Mesoscale eddies, Mixing processes, Mode water, OMP analysis, Thermocline, Upper ocean, Water masses, NACW, SACW.

1. Introduction

Mode waters have been highlighted by several authors since the beginning of oceanography studies (e.g., Worthington, 1958; Siedler et al., 1987; McCartney and Talley 1982, Gordon et al., 1987; Provost et al., 1999). Although recently, more attention has been given to their role in physical and biogeochemical processes and global climate issues (Fratantoni et al., 2013; Kelly and Dong 2013; Sato and Polito, 2014; de Souza et al., 2018). This term denotes a specific water mass layer characterised by a vertical and horizontal homogenous water (Hanawa and Talley, 2001), with slight variation in their physicochemical properties. Other well-defined characteristics are the relatively large geographical area occupied and minimum stratification presented by the mode waters. Thus, mode water is marked as a thermostad/pycnostad layer trapped between the seasonal and main thermoclines. Its formation is usually linked to the ocean and atmosphere interactions and changes, while mode water varieties are almost always identified near the warm side of ocean currents or in frontal zones in every ocean (Hanawa and Talley, 2001; Sato and Polito, 2014).

In the northern hemisphere, two main Subtropical Mode Water (STMW) varieties contribute to the central water layer of the North Atlantic Ocean (Figure 1): the North Atlantic Subtropical Mode Water (NASTMW), better known as the Eighteen Degree Water (EDW), and the Madeira Mode Water (MMW) (Worthington, 1958; Siedler et al., 1987; Fratantoni et al., 2013). The EDW has unique properties, such as its temperature of 18°C, its salinity of 36.5, and a potential density ($\sigma\theta$) of 26.5 kg m^{-3}. It is found throughout the northwestern part of the subtropical gyre as demonstrated by Worthington (1958), who also delimited its formation area (Figure 1). MMW is denser than the EDW and is associated with the warm side of the Azores Front (35ºN – 25ºW) and is found offshore of the coastal upwelling area, with temperatures varying between 16°C and 18°C and σθ ranging from 26.5 kg m–3 to 26.8 kg m–3. MMW is advected southwestward from its formation zone and joins the thermocline as part of the North Atlantic Central Water (NACW; Siedler et al., 1987; Hanawa and Talley, 2001).

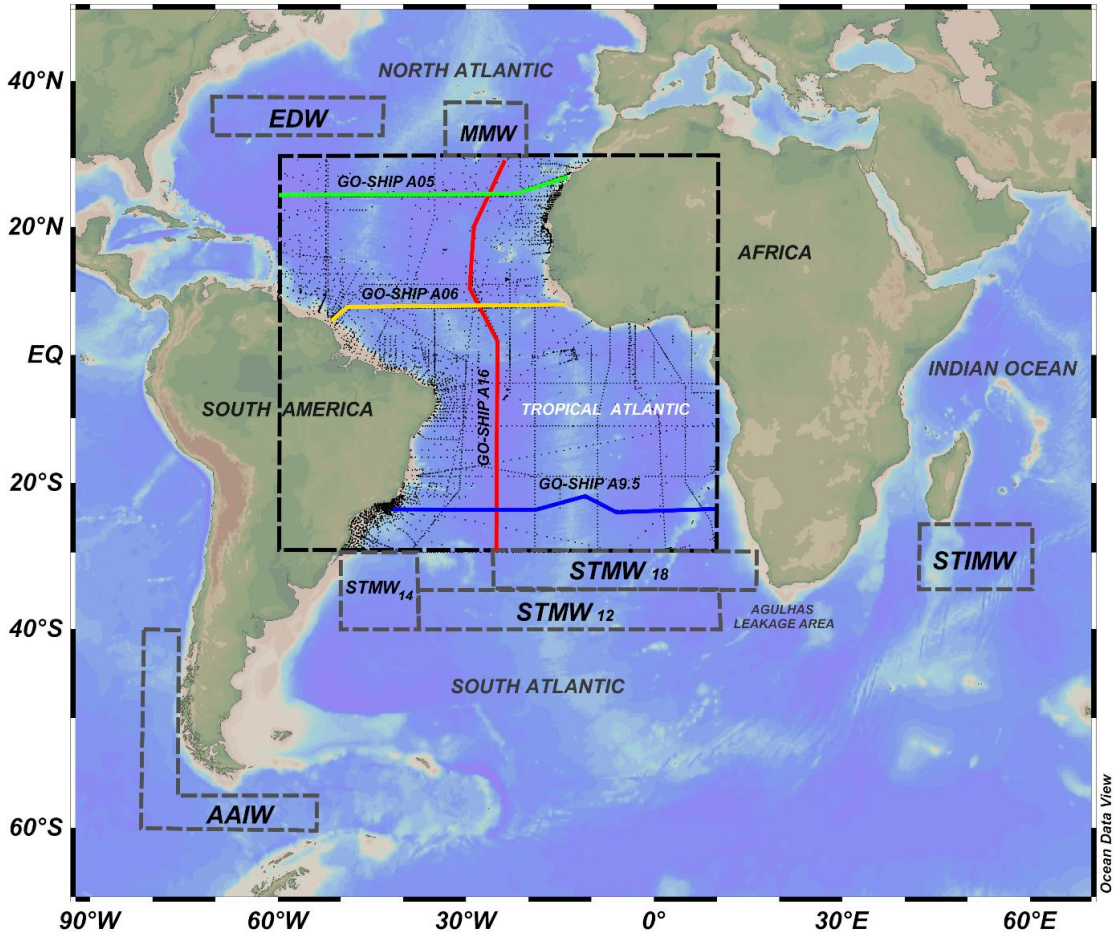

Figure 1. Map of the study region (dashed black square) and the source areas (dashed grey polygons) of the Subtropical Mode Water (STMW) varieties and Antarctic Intermediate Water (AAIW). The dots depict the hydrographic stations from the World Ocean Database 2018. STMW varieties are: Eighteen Degree Water (EDW), Madeira Mode Water (MMW), STMW of 18ºC ($STMW_{18}$), STMW of 14ºC ($STMW_{14}$), STMW of 12ºC ($STMW_{12}$), and Subtropical Indian Mode Water (STIMW). The red, green, yellow, and blue lines depict the GO-SHIP A16, A05, A06, and A9.5 repeated hydrographic sections, respectively.

In the southern hemisphere, three main STMW varieties are identified in the South Atlantic Ocean (Figure 1). These mode waters ventilate the thermocline in the subtropical cell, which was initially described by Provost et al. (1999). These STMW varieties have different σ_θ surfaces: the lightest is found with a pycnostad of 26.2 kg m^{-3}, while the other two occupy a layer of 26.5 kg m^{-3} and 26.7 kg m^{-3}. The nomenclature adopted to characterise these STMW varieties has been continuously changed by scientists in this field of study. To avoid

misunderstood and allow further comparison with previous studies, a table with the STMW nomenclatures and their respective source regions used by different authors is shown (Table 1). Here, we distinct the STMW varieties of the South Atlantic Ocean using the subscript indices relative to the thermostad layer temperature at their source areas (i.e., $STMW_{12}$ – formed along the edge of the subtropical front, STMW14 - formed in the Brazil-Malvinas confluence, and $STMW_{18}$ – formed in the eastern South Atlantic).

The structure and the mixture of the central layer in the Atlantic Ocean were unravelled by Poole and Tomczak (1999). These authors used three source water masses to determine the fraction of the mixture at the central layer, including one source water mass in the northern hemisphere and both, eastern and western, in the South Atlantic (Table 1). Besides, in the central layer, the definition of the southern STMW varieties was recently update using temperature and salinity profiles obtained through the Argo floats (Sato and Polito, 2014). Thus, studies based on this definition have improved the understanding of the unknown aspects of the structure of the Atlantic Ocean's thermocline (Santos et al., 2016; Souza et al., 2018). Nonetheless, the structure and the mixture of the thermocline in the tropical Atlantic in terms of the STMW contribution are still unclear.

In addition, previous investigations on the central layer of the Atlantic Ocean have pointed out the significant influence of water masses coming from the Indian Ocean (e.g., Poole and Tomczak, 1999; Stramma and England, 1999). This has been a subject of debate since the work proposed by Gordon et al. (1987), who presented further evidence based on chlorofluoromethanes-11 and oxygen, that about two thirds (~ 65%) of the Benguela Current thermocline transport is drawn from the Indian Ocean (Gordon et al., 1992). Thus, implying a critical impact on interocean exchanges of salt, heat, and other properties, which can significantly impact the Atlantic Meridional Overturning Circulation. Despite that, the role of the Indian Ocean water masses influencing and changing the characteristic properties in the South Atlantic Ocean is still a challenge and under debate (e.g., Souza et al., 2011; Casanova-Masjoan et al., 2017; Castellanos et al., 2017; Souza et al., 2018; Rühs et al., 2019).

Table 1. Water mass nomenclature, acronyms, and properties for the Subtropical Mode Water (STMW) varieties as defined by the references cited.

Acronym	Full name	Temperature (°C)	Salinity	σ (kg m^{-3})	Source region	Reference
NASTMW	North Atlantic Subtropical Mode Water	18	36.5	26.5	Western North Atlantic	Worthington (1958)
EDW	Eighteen Degree Water	18	36.5	26.5	Western North Atlantic	Kelly and Dong (2013) Fratantoni et al. (2013)
NACW	North Atlantic Central Water	6.99 - 13.90	34.94 - 35.89		High environmental variability	Poole and Tomczak (1999)
MMW	Madeira Mode Water	16 - 18	36.5 - 36.8	26.5-26.8	Easter North Atlantic	Siedler et al. (1987)
STMW1	Subtropical Mode Water	16 - 18	35.9 - 36.2	26.2	Northern of the BC overshoot (35°S)	Provost et al. (1999)
STMW2		14 - 16	35.5 - 35.9	26.5	Over the BC overshoot	
STMW3		12 - 14	35.2 - 35.5	26.7	Eastern flank of the BC overshoot	
WSACW	Western South Atlantic Central Water	6.55 - 16.27	34.40 - 35.69	----	Western South Atlantic (35°S)	Poole and Tomczak (1999)
ESACW	Eastern South Atlantic Central Water	5.96 - 14.41	34.41 - 35.30	----	Eastern South Atlantic (35°S)	
SASTMW1	South Atlantic Subtropical Mode Water	15 ± 0.9	35.6 ± 0.2	26.4 ± 0.1	Over the BC overshoot (centered at 35°S)	Sato and Polito (2014)
SASTMW2		16.7 ± 0.9	35.7 ± 0.2	26.1 ± 0.1	Eastern Atlantic (centered at 32.5°S)	
SASTMW3		13.2 ± 0.9	35.2 ± 0.2	26.5 ± 0.1	Eastern flank of the BC overshoot (centered at 37°S)	
$STMW_{18}$	Subtropical Mode Water	18 ± 0.56	35.80 ± 0.11	----	Eastern Atlantic	de Souza et al. (2018)
$STMW_{14}$		14 ± 0.53	35.40 ± 0.01	----	Over the BC overshoot	
$STMW_{12}$		12 ± 0.50	35.03 ± 0.14	----	Eastern flank of the BC overshoot	

The South Atlantic central layer has been reported to be sensitive to the process of ocean acidification (Salt et al., 2015), with acidification rates higher than those reported by surface and intermediate waters (Kitidis et al., 2017, Orselli et al., 2018; Carvalho-Borges et al., 2018; Orselli et al., 2019a). Furthermore, changes in the dissolved oxygen content has been decreasing within the central layer in both hemispheres, mainly through the vertical and horizontal expansion of the oxygen minimum zones (Stramma et al., 2008; Karstensen et al., 2015; Santos et al., 2016). Thus, the reported changes in physical and biogeochemical properties of the central layers in the Atlantic Ocean highlights the need for a better and detailed comprehension of their source water masses variability and changes. In this context, this study aims to quantify the contribution and underline the temporal variability of the STMW varieties influencing the total mixture on the central waters filling the tropical Atlantic's upper thermocline. In addition, the role of the Subtropical Indian Ocean Mode Water (STIMW) influencing the central water composition in the subtropical region of the South Atlantic Ocean is quantified.

2. oceanographic and biogeochemistry features of the tropical Atlantic Ocean

The ocean dynamics of the tropical Atlantic Ocean is regulated by a complex system of currents and countercurrents (Stramma and Schott, 1999). This specific region of the Atlantic Ocean is considered as an end-member of the subtropical cells, where water masses subducted in the subtropics are upwelled by the Ekman divergence at the equator and flow poleward in the surface layers (Hazeleger and Drijfhout, 2006). Western boundary currents, mesoscale eddies, and the complex structure of zonal currents complicate this circulation scheme in the tropical Atlantic. This system is characterised by an advanced mixture of the waters in the upper thermocline, evidenced by the smooth shape of the temperature-salinity diagram in the first hundreds of metres (Figure 2a). The NACW and the SACW occupy the same density range (Figure 2b) in the respective hemispheres, hence the tropical Atlantic Ocean, where these water masses cross, is density-compensated through a multitude of processes (water masses intrusions, filaments, and lenses) that shape the structure of the central

layer (Stramma and Schott, 1999; Stramma and England, 1999; Poole and Tomczak, 1999).

As this work is focused on the upper Atlantic thermocline, the properties and features of the upper layer, about 1000 m of the water column, are addressed (see Stramma and Schott, 1999 for further description). The surface layer of the tropical Atlantic is occupied by Tropical Water (TW), which has a highly seasonal variability (Figure 2a) and forms the surface mixed layer of the tropical Atlantic. The isopycnal surfaces at 25.8 and 26.2 kg m^{-3} mark the lower limit of the TW in the northern and southern hemisphere, respectively (Karstensen et al., 2008). The central water layer is formed by subduction processes at subtropic latitudes (Price, 2001). Within these regions, the influences of the STMW varieties become critical due to the atmosphere-ocean interactions, inducing waters to be subducted and advected away from their formation areas (Hanawa and Talley, 2001).

As previously mentioned, the NACW has two main STMW varieties that are responsible for the ventilation of the upper thermocline of the northern subtropical cell (Worthington, 1958; Siedler et al., 1987; Fratantoni et al., 2013). The EDW is formed in an area of very high surface heat loss to the atmosphere, and it is advected southward out of the Gulf Stream Extension region, filling the western subtropical gyre (Worthington, 1958; Hanawa and Talley, 2001). Meanwhile, on the eastern side of the North Atlantic, the MMW, which is slightly denser than EDW, is found at increased depths and displaced to the west and southwest during the year after its formation by wintertime convection. Furthermore, it shows a horizontal extension of at least 500 km and accounts for 15-20% of the total central water formation in the corresponding density range as obtained from tracer studies in the North Atlantic gyre (Siedler et al., 1987). The southern limit of the NACW is defined by the Cape Verde Frontal Zone at about 15º N (Lozier et al., 1995).

SACW is the predominant water mass in the tropical Atlantic and has three main STMW varieties that contribute to the thermocline (Provost et al., 1999; Sato and Polito, 2014). The $STMW_{18}$ (Table 1) occupies a broad area from the eastern side of the basin and reaches as far as 55°W. This STMW dominates the first 200

m spreading across all the South Atlantic Ocean, and its formation area is placed on the eastern side of the Atlantic basin (Figure 1) centred at 2.8°W and 32.4°S (Sato and Polito, 2014; Souza et al., 2018). The $STMW_{14}$ is dominant at 36.8°W and 36.2°S in the Brazil Current recirculation gyre, and the region affected by the southern excursions of the Brazil Current fronts with a mean potential density of 26.4 ± 0.1 kg m^{-3}. Its presence is mostly concentrated west of 25°W and becomes quantitatively important below 25°S (Souza et al., 2018). The denser $STMW_{12}$ (26.5 ± 0.1 kg m^{-3}) is formed along the South Atlantic Subtropical Front and the southern edge of the subtropical gyre (Sato and Polito, 2014). It is mainly concentrated at the layer between 200 m and 500 m.

Besides the three STMW formed in the South Atlantic Ocean that contribute to the upper thermocline, there is an important interocean exchange of heat and salt throughout the Agulhas Leakage (Gordon et al., 1987; Gordon et al., 1992; Schouten et al., 2000; Souza et al., 2011). Many authors have highlighted the critical impact of this contribution from the Indian Ocean to the Atlantic's thermocline, but quantities are still under debate. This is mainly because of the similarities in the physical and chemical properties of the subtropical waters in the Indian and Atlantic oceans that make it difficult to separate one from another properly (Poole and Tomczak, 1999; Souza et al., 2011; Casanova-Masjoan et al., 2017; de Souza et al., 2018; Rühs et al., 2019).

On the other hand, setting aside the spatial distribution of the potential temperature and salinity, the distribution of the biogeochemical parameters is less obviously correlated with the distribution of the central waters from the North and South Atlantic Ocean as mentioned above (Figure 3). In the tropical Atlantic, there are two important regions known as the oxygen minimum zones, which are related to the nutrient distribution cycle: the eastern tropical North Atlantic (centred at 12ºN and 20ºW) and eastern tropical South Atlantic (centred at 10ºS and 7ºE). These zones are characterised by displaying a dissolved oxygen concentration less than 100 µmol kg^{-1} (Figure 3-c) and are a consequence of a combination of weak ocean ventilation, which supplies oxygen, and respiration, which consumes oxygen (Karstensen et al., 2008).

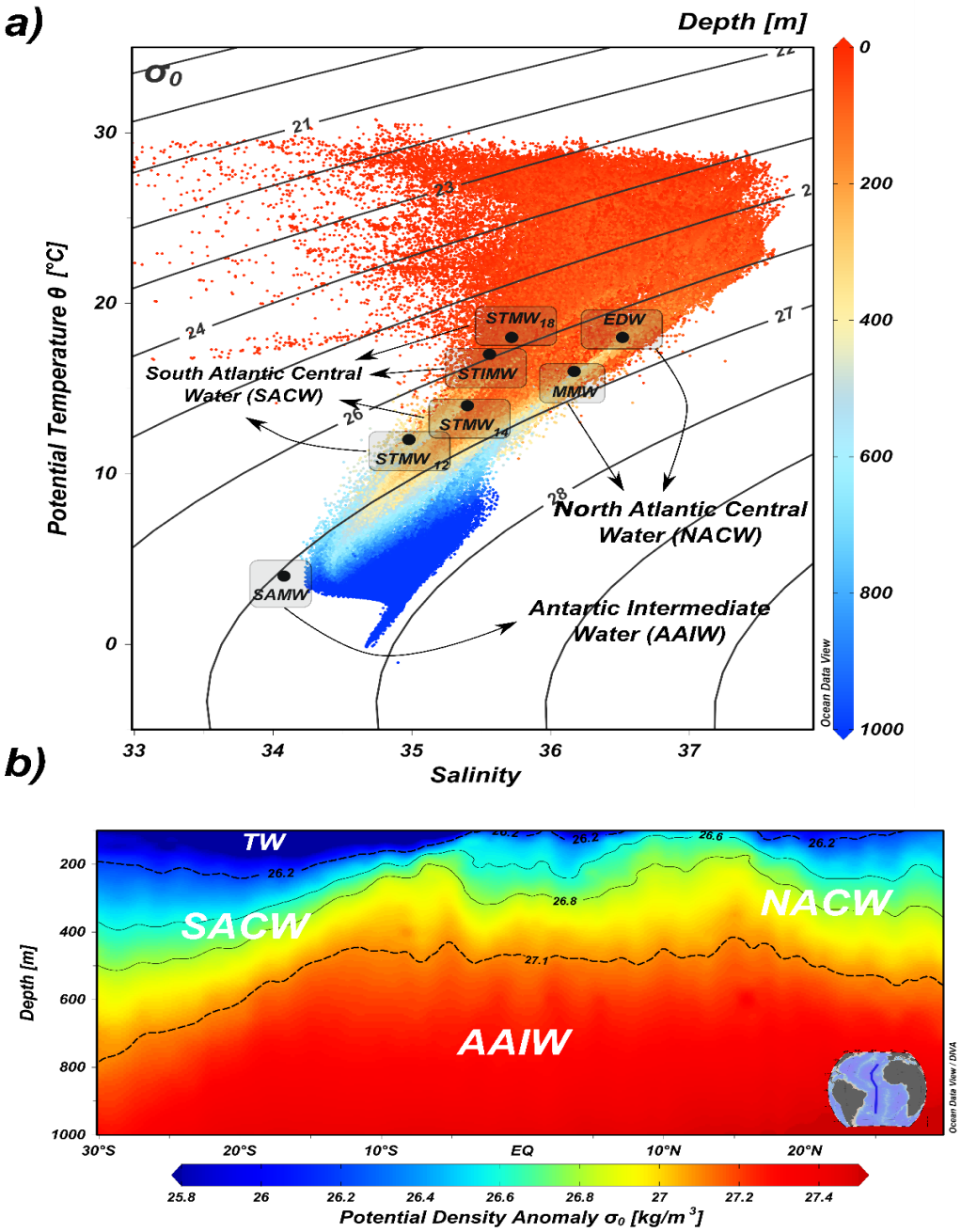

Figure 1. Upper layer structure in the Atlantic Ocean. Potential temperature-salinity diagram of the upper ocean on the tropical Atlantic showing the thermohaline indexes of the source water types used in this work (a). The colour scale in (a) depicts the water depth in metres. Antarctic Intermediate Water (AAIW), Eighteen Degree Water (EDW), Madeira Mode Water (MMW), Subtropical Mode Water (STMW) of 18ºC ($STMW_{18}$), STMW of 14ºC ($STMW_{14}$), STMW of 12ºC ($STMW_{12}$), and Subtropical Indian Mode Water (STIMW). Vertical distribution of the isopycnals along the GO-SHIP A16 hydrographic section (b). The 26.2 and 27.1 kg m^{-3} isopycnals are shown by dashed lines, depicting the

boundaries between Tropical Water (TW), the central layer, and the AAIW, which were defined by Stramma and England (1999) and Karstensen et al. (2008).

These zones have been the subject of interest for several authors (Karstensen et al., 2008; Stramma et al., 2008; Karstensen et al., 2015; Santos et al., 2016) leading to the conclusion that these zones are expanding owing to warming trends found in the intermediate-depth, and their position depends upon upwelling patterns. These patterns control the surface water's biological productivity and complex nutrient cycles. Overall, the concentration of the nutrients within these regions is high (Figure 3d-f), due to the upwelled water from deeper zones with high nutrient concentrations, and the intense remineralisation within the thermocline.

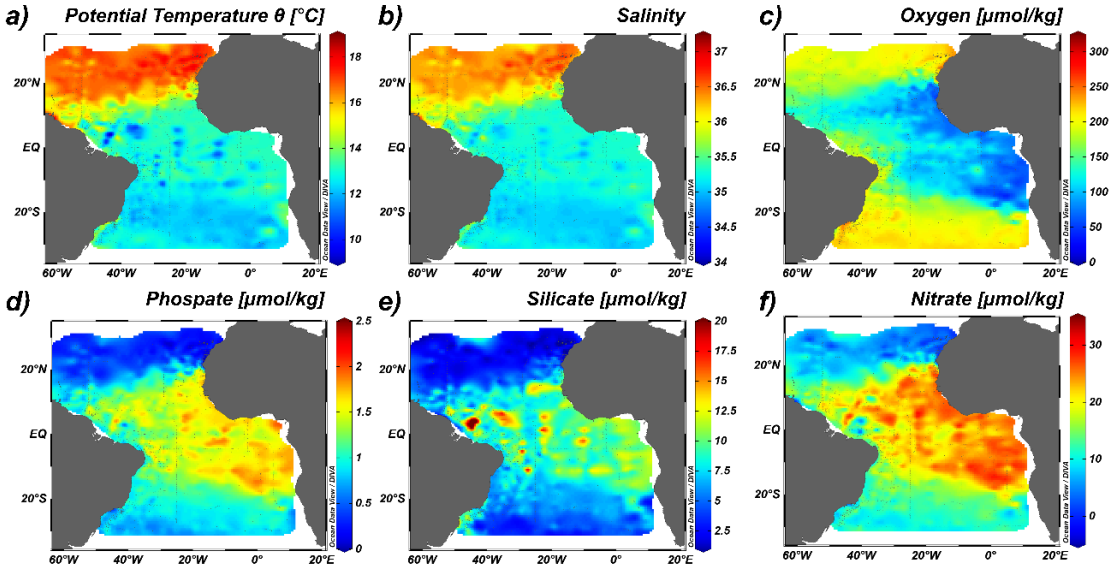

Figure 2. Physical-chemical properties at the 26.6 kg m^{-3} isopycnal in the tropical Atlantic Ocean. Potential temperature (θ, a), salinity (b), dissolved oxygen (c), and dissolved nutrients content (d-f), as indicated (data from the WOD18; Boyer et al., 2018; www.nodc.noaa.gov).

3. Data and methodology

3.3 Data set and GO-SHIP sections

Hydrographic and chemical data from the World Ocean Database 2018 (WOD18; Boyer et al., 2018; www.nodc.noaa.gov) were used to determine the spatial distribution of the physical-chemical properties and to calculate the mixing

fractions (%) of the distinct STMW varieties (i.e., the source water masses) that contribute to the central layer in the study region. This was restricted from 30°N to 30°S and 60°W to 10°E (black dashed square in Figure 1). Potential temperature, salinity, dissolved oxygen, silicic acid, nitrate and phosphate contents, and potential vorticity (PV; Eq. 1) were the parameters used. Thus, the data set was filtered to only consider the data from stations that have these parameters. Only data classified as good quality by the control procedures of the WOD18 were used.

The PV parameter was determined as:

$$PV = \pm \frac{f}{\rho_0} \frac{d\sigma_\theta}{dz}, \qquad (1)$$

where f is the planetary vorticity, ρ_0 is the mean seawater density, σ_θ is the potential density, and the positive/negative sign is for the northern/southern hemisphere, respectively.

Considering the purpose of the analysis, and avoiding interference caused by the warm and salty TW at the boundary between surface and central layers, the first 100 m of the water column was not included (Poole and Tomczak, 1999; Souza et al., 2018). This is because of the high variability of property exchanges at the surface mixed layer. Thus, the analysis is focused on the upper ocean from 100 m to roughly 1000 m, a layer that includes the central waters from the South and North Atlantic oceans, and the upper layer of the AAIW (Stramma and England, 1999).

The repeated sections of the Global Ocean Ship-based Hydrographic Investigations Program (GO-SHIP) obtained from the Carbon Hydrographic Data Office (CCHDO, http://cchdo.ucsd.edu) were used to assess the temporal variability of the contribution of the STMW varieties influencing the tropical Atlantic's upper thermocline. The GO-SHIP sections are temporally distributed as follows: three zonal sections corresponding to A05 at 24.5 °N in 1992, 1998, 2004, and 2011; A06 at 7.5 ºN in 1993 and 2010; A9.5 at 25 °S in 2009 and 2018; and the meridional section of A16 in 1993, 2003-2005, and 2013-2014. The

sections used are depicted in Figure 1, and the same good quality control procedures were applied.

3.4 Optimum multiparameter analysis and source water type indexes

The optimum multiparameter (OMP) water mass mixing analysis has been a powerful tool to determine the relative fractions of the mixture of distinct water masses, in both, regional and oceanic scales. This method was first proposed by Tomczak (1981) as an alternative and improved method for the classical temperature-salinity diagram. Later, Mackas et al. (1987) and Tomczak and Large (1989) made significant improvements to the original multiparameter method. It is an inverse model based on solving linear water mass mixing equations to find the relative contribution of each source water type (SWT) that best reproduces the observed data, while the residuals are minimised by applying the least-squares method (e.g., Ferreira and Kerr, 2017).

The basic assumption of OMP analysis is that a linear relationship exists between the parameters (Tomczak, 1981; Poole and Tomczak, 1999), and this allows a water mass to be fully represented by a combination of different SWT. The sum of the contributions should be 100%, and negative contributions are not allowed because they have no physical meaning, obeying the law of mass conservation. The method is summarised in Eq. (2) and has been applied by several authors (e.g. Klein and Tomczak, 1994; Poole and Tomczak, 1999; Larqué et al., 1997; Kerr et al., 2009a; Kerr et al., 2009b; Santos et al., 2016; Ferreira and Kerr, 2017; Souza et al., 2018 among others).

$$\mathrm{Gx} - \mathrm{d} = \mathrm{R}, \qquad (2)$$

where G is a matrix with the property values of each SWT (Table 2), x is a vector of the calculated contributions for each SWT, d is a vector of the observed data, and R is the residual value.

Conservative parameters as potential temperature (θ) and salinity (S) have been successfully and more traditionally used in the OMP analysis owing to their conservative characteristics. On the contrary, semi-conservative parameters (dissolved oxygen-DO, phosphate-PO_4^{3-}, nitrate-NO_3^-, and silicic acid-$Si(OH)_4$) modify their concentrations as the water masses evolve owing to biogeochemical

processes, such as remineralisation, respiration, and hydrothermal processes (Redfield et al., 1963; Takahashi, 1985; Anderson and Sarmiento, 1994). Corrections for this behaviour could be completed by applying the nutrient ratios, which allow the utilization of oxygen involved in the remineralisation of nutrients to be numerically corrected. Hence, this study used the nutrient ratio proposed by Takahashi (1985) and then modified by Anderson and Sarmiento (1994) for DO: NO_3^- : PO_4^{3-}, while the ratio found by Poole and Tomczak (1999) was used for DO: $Si(OH)_4$ (Table 2).

3.5 Source Water Type definition and parameters weight

The first step in the OMP analysis process is to represent the water masses by a combination of distinct SWT that represents the mixing in the study region. To achieve this, it is necessary to investigate the SWT properties in the water mass source area (i.e., considering their pure form before mixing). To determine the SWT indices, the southern STMW source regions (see Figure 1) identified by Sato and Polito (2014) and northern STMW source regions identified by Worthington (1959) and Siedler et al. (1987) are considered here. A compilation of source areas for AAIW was determined based on McCartney (1977), Hanawa and Talley (2001), and Holte et al. (2012). The STIMW source area in the Indian Ocean was defined following Hanawa and Talley (2001). Thus, the SWT used to represent the source water masses that contribute to the SACW are $STMW_{18}$, $STMW_{14}$, $STMW_{12}$, and STIMW (Figure 1 and Table 2), while the source contributors for the NACW are the EDW and MMW. The AAIW is represented by the SWT index that characterises the SAMW.

A key step in the OMP analysis is the determination of a weighting factor for each conservative and semi-conservative parameter in the resolution of the linear array equations (Poole and Tomczak, 1999). Here, Eq. 3 is used, as described by Tomczak and Large (1989), to calculate the weight for each parameter j (W_j):

$$W_j = \frac{\sigma_j^2}{\delta_{j\,max}}, \qquad (3)$$

where σ_j^2 is the variance of each parameter j among all the SWT, and $\delta_{j\,max}$ is the maximum variance that is associated with the same parameter in the source water mass region. If the water column is well represented by the SWT chosen, the residuals are very low, and any result with mass conservation residuals higher than 5% is discarded. The temporal variability of the source water mass properties was reduced by using several years of data to determine the SWT index.

Table 2. Source Water Type (SWT) indexes and corresponding standard deviations, parameter weights, and Redfield ratio defined for this study. Values were defined by investigating the hydrographical parameters of the mode water layer in their respective source areas (see Figure 1). The values of potential vorticity (PV) were multiplied by 10^8, as recommended by the OMP manual. See the text for water masses and SWT acronyms.

Water mass	SWT	θ (ºC)	S	DO (µmol/kg)	PO_4^{3-} (µmol/kg)	NO_3^- (µmol/kg)	$Si(OH)_4$ (µmol/kg)	PV (10^8 ms^{-1})	σ (kgm^{-3})
NACW	EDW	18 ± *0.15*	36.52 ± *0.11*	210.48 ± 13.54	0.17 ± *0.14*	3.13 ± *1.43*	1.53 ± *1.53*	0.01 ± *0.03*	26.5 ± *0.1*
	MMW	16 ± *0.57*	36.17 ± *0.09*	225.84 ± 14.66	0.22 ± *0.25*	2.85 ± *1.59*	1.35 ± *2.72*	0.03 ± *0.04*	26.7 ± *0.1*
SACW	$STMW_{18}$	18 ± *0.56*	35.72 ± *0.14*	233.21 ± 12.41	0.18 ± *0.10*	0.51 ± *1.42*	1.79 ± *1.53*	–0.06 ± *0.04*	25.8 ± *0.1*
	$STMW_{12}$	12 ± *0.57*	34.98 ± *0.18*	241.74 ± 12.81	0.71 ± *0.09*	8.48 ± *1.76*	2.72 ± *0.83*	-0.03 ± *0.04*	26.6 ± *0.1*
	$STMW_{14}$	14 ± *0.33*	35.40 ± *0.19*	224.82 ± *14.42*	0.59 ± *0.12*	7.35 ± *1.82*	3.62 ± *2.96*	–0.02 ± *0.03*	26.5 ± *0.1*
	STIMW	17 ± *0.28*	35.56 ± *0.05*	227.94 ± 10.99	0.27 ± *0.07*	1.86 ± *1.05*	3.05 ± *1.03*	–0.05 ± *0.05*	26.0 ± *0.1*
AAIW	SAMW	4 ± *0.15*	34.08 ± *0.09*	307.76 ± 9.96	1.69 ± *0.21*	22.52 ± *2.73*	9.81 ± *4.49*	–0.03 ± *0.04*	27.1 ± *0.1*
	Weight	76.5	17.7	4.7	4.9	7.7	0.4	0.1	-
	Redfield ratio	-	-	-171	1	17	11	-	-

3.6 OMP sensitivity tests and data representation

Sensitivity tests were performed using the standard deviation of the conservative parameters (Table 1) calculated in their formation regions (Figure 1). This test consisted of analysing the same dataset by adding and subtracting the standard deviation to infer changes in fractions of contribution related to

changes in the choice of SWTs used. It has been successfull conducted by several studies (e.g., Kerr et al. 2009a, Dotto et al. 2016, Ferreira and Kerr, 2017; Souza et al. 2018). Concerning this, the run conducted by subtracting the standard deviation gave an unexpected and ambiguous result (not shown). This result displayed a water mass contribution where it was not logical, providing incorrect contributions of the STMW varieties in the study area. The similarity of some of the SWT indexes (Table 2) is likely the reason for these ambiguous results. Therefore, with the run performed adding the standard deviation, the error of the analysis is expected to be around 12 % for EDW, 9 % for MMW and $STMW_{18}$, 1 % for $STMW_{14}$, 14 % for $STMW_{12}$, 10 % for STIMW, and 4 % for AAIW.

Data interpolation using the "oce" package (Kelley and Richards, 2019) for R software (R Core Team, 2019) with the "Unesco" method was applied because of the different vertical resolutions of the data available for each year evaluated. A vertical interpolation resolution of 20 m from 100 to 1000 m, while 0.25º was the horizontal resolution used here. The GO-SHIP A16 transect between 1993 and 1995 lacks nutrient data from the equator to 30°S, so data from the GO-SHIP transect A17 from this same period was added to the data for this zone. The results are expressed as anomalies of the source water masses contribution, which are calculated either by the difference between the contribution of each year and the average contribution of the evaluated years (i.e., when the occupation was greater than 2 years) or by subtracting the recent to the older year (i.e., when only two years were sampled). The SWT and the parameters used for each section are listed in Table 3. Most of the figures are completed using Ocean Data View software (Schlitzer, 2019).

3.7 Matching the mesoscale eddies and STMW mixing fractions

A geospatial analysis was executed to assess the influence of the Indian Ocean to the Atlantic thermocline through the Agulhas leakage. Thus, the source water mixing fractions from the OMP analysis, containing the contribution (%) of each STMW, were spatially joined with three different eddy identification databases: (i) the delayed-time DT2.0exp (Schlax & Chelton, 2016), (ii) the near-real-time NRT3.0exp (Mason et al., 2014) databases from the AVISO+ Mesoscale

Eddy Trajectory Atlas Product (http://www.aviso.altimetry.fr/), and (iii) the TOeddies database developed by Laxenaire et al. (2018).

Table 3. Dataset, water mass mixing scheme, and parameters used in each of the OMP applications. Parameters were salinity (S), potential temperature (θ), dissolved oxygen (DO), nitrate (NO^{3-}), phosphate ($PO4^{3-}$), silicate ($Si(OH)_4$), and potential vorticity (PV).

Data set	Water mass mixing scheme	Parameters
WOD18	EDM + MMW + $STMW_{18}$ + $STMW_{14}$ + $STMW_{12}$ + STIMW + AAIW	S, θ, DO, NO_3^-, PO_4^{3-}, $Si(OH)_4$, PV
GO-SHIP A16	EDM + MMW + $STMW_{18}$ + $STMW_{14}$ + $STMW_{12}$ + STIMW + AAIW	S, θ, DO, NO_3^-, PO_4^{3-}, $Si(OH)_4$, PV
GO-SHIP A9.5	$STMW_{18}$ + $STMW_{14}$ + $STMW_{12}$ + STIMW + AAIW	S, θ, DO, NO_3^-, PO_4^{3-}, $Si(OH)_4$, PV
GO-SHIP A05	EDW + MMW + AAIW	S, θ, DO, NO_3^-, PO_4^{3-}, $Si(OH)_4$, PV
GO-SHIP A06	EDW + MMW + $STMW_{18}$ + $STMW_{12}$ + AAIW	S, θ, DO, NO_3^-, PO_4^{3-}, $Si(OH)_4$, PV

DT2.0exp is a database generated by altimetric observations from two satellites that use sea level anomalies (SLA) for the identification of eddies following the algorithm proposed by Schlax & Chelton (2016). On the other hand, the NRT3.0exp and the TOeddies databases rely on observations from all available satellites and identify eddies using the algorithm of Mason et al. (2014) and Laxenaire et al. (2018), respectively, based on absolute dynamic topography (ADT).

The spatial joint was made using the QGIS 3.10 software considering the "*Join attributes by location*" algorithm. The size of each eddy was described by a circle with an area equal to that enclosed by the contour of maximum circum-average geostrophic speed. It should be noted that this approach is based on two reasons: first, the area defined by this outline better reflects the conditions of the eddies' core and is less distorted by other eddies around it (Laxenaire et al., 2018) and second, the DT2.0exp database does not identify the outermost contour of

these structures. To maintain the consistency within the analysis, the outermost contour parameter was not used.

The DT2.0exp database was used to identify the eddies between 1993 and 2017, while the NRT3.0exp database was used to identify the eddies after 1st January 2018. The TOeddies database was used as an independent data source for comparison and to differentiate the anticyclonic eddies belonging to the Agulhas network from other anticyclonic eddies in the study area in the period between 2000 and 2016. After processing, the data from DT2.0exp and NRT3.0exp were merged into one dataset (hereafter referred to as AVISOme). Both AVISOme and TOeddies products were filtered by sampling date to obtain the hydrographic stations from WOD18 and GO-SHIP repeat sections that were inside an eddy at the moment of its sampling. Then, the total matches were filtered again to keep only the hydrographic stations that have the STIMW contribution in the mixture (layer warmer than 9°C).

Based on the mean contribution of the STIMW found with the geospatial analysis, it was possible to calculate the amount of water that entered the Atlantic Ocean through the Agulhas leakage (i.e., advected from the Indian Ocean). This simple calculation (Eq. 4) is based on the assumption that the input of the Indian Ocean waters mainly flow through the Benguela Current (BC). A stationary state was assumed with a mean value of 16.1 Sv, in the layer warmer than 9ºC ($V_{BC>9ºC}$), as the water mass volume transported by this current (Gordon et al., 1992). Then, the average STIMW volume transported (V_{STIMW}), considering the averaged values of the STIMW contribution attained (X_{STIM}), was calculated.

$$V_{STIMW} = X_{STIMW}\, V_{BC>9^{\circ}C} \qquad (4)$$

4 Results

4.1 *North Atlantic Central Water (NACW)*

The two main STMW varieties that contribute to the NACW are the EDW and the MMW. The contribution of these STMW varieties is restricted to northern latitudes greater than 10ºN (Figure 4), following the North Equatorial Current, where the values displayed are greater than 20%. The EDW's influence is confined to the subsurface, occupying the first metres of NACW in the water

column. The contribution values of EDW are higher at low depths (Figure 4a-b and f) reaching as much as 100%, while at deeper zones, its contribution decreased substantially. Besides, its spatial distribution is not uniform, displaying a greater contribution in the western part of the basin at lower latitudes (~10-15ºN).

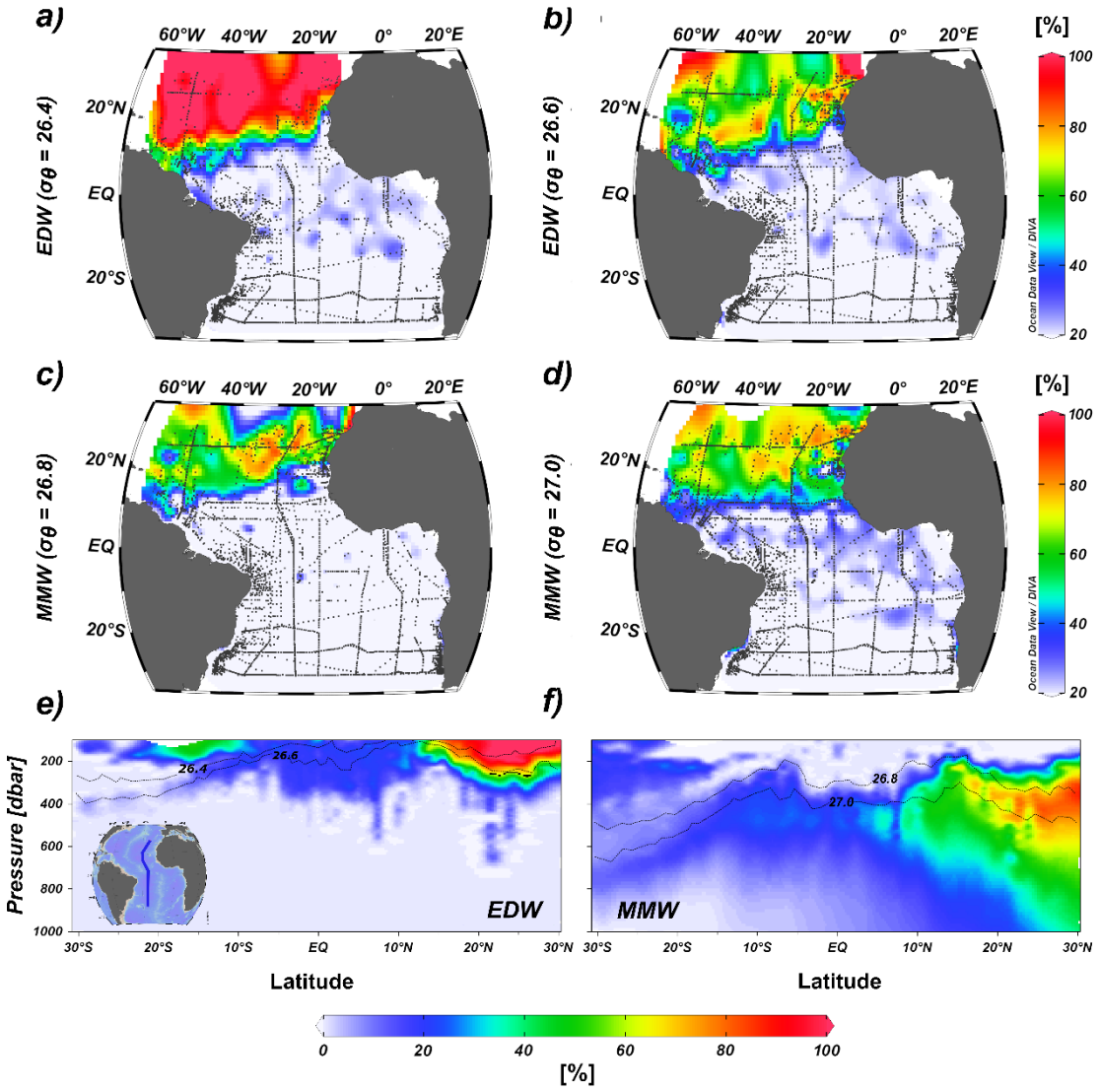

Figure 3. Spatial (a-d) and vertical (e-f) fractions of the mixture of the Subtropical Mode Water varieties contributing to the North Atlantic Central Water. Eighteen Degree Water (EDW) at 26.4 kg m^{-3} (a) and 26.6 kg m^{-3} (b) isopycnals. Madeira Mode Water (MMW) at the 26.8 kg m^{-3} (c) and 27.0 kg m^{-3} (d) isopycnals. Vertical distribution in a meridional transect from 30ºN to 30ºS (see inset panel in f), considering the contribution of MMW (e) and EDW (f).

The contribution of MMW to the mixture displays a more symmetric behaviour reaching roughly the same values in both western and eastern boundaries (Figure 4c-d). Its maximum influence within the thermocline is defined by the 26.8 and 27.0 kg m^{-3} isopycnals, with values around 80%. Deeper than 600 m, its contribution decreases quickly (40%-50%) at the latitude of 10ºN, while at higher latitudes (30ºN) its contribution remains high (Figure 4e).

4.2 *South Atlantic Central Water (SACW)*

The SACW is mainly composed by contributions of STMW18 and STMW12 in the tropical Atlantic (Figure 5). STMW14 does not show a relevant contribution throughout the entire study region. This water mass has been reported to contribute to higher subtropical latitudes (26–40ºS) and west of 20ºW. Therefore, in the analysis of the southern section (GO-SHIP A9.5), its influence on the thermocline is clearly seen (Figure S1). The contribution of STMW18 is confined to surface levels and widely distributed, mainly occupying the northern part of the southern subtropical gyre north of 20ºN and the equatorial zone (Figure 4a). Its distribution follows the Benguela Current, then joining the South Equatorial Current and feeding the main currents and countercurrent near the equator. Moreover, this STMW variety is one of the main contributors to the upwelling areas along the coastal regions of Africa (Figure 5a-b). The influences of $STMW_{18}$ become negligible (< 30%) at isopycnals higher than 26.4 kg m–3 (Figure 4e).

The influences of $STMW_{12}$, which is formed near the South Atlantic Subtropical Front (Figure 1), is more restricted to the southern part of the subtropical gyre (Figure 5c), reaching a mixing fraction greater than 80% in the zonal band of latitudes higher than 15ºS. This behaviour is described in the southern part of the isopycnal of 26.6 kg m–3, which is from 400 m deep in the south (30ºS) to 200 m at the equator. However, the contribution of $STMW_{12}$ is widely distributed at the isopycnal of 26.8 kg m–3 (Figure 5d), displaying a mixing fraction close to 50% in the entire South Atlantic basin. Therefore, $STMW_{12}$ displays a decreasing meridional contribution, showing a thick layer (200 – 700 m) at the south and becoming thinner as it moves northward (200 – 400 m; Figure 5f).

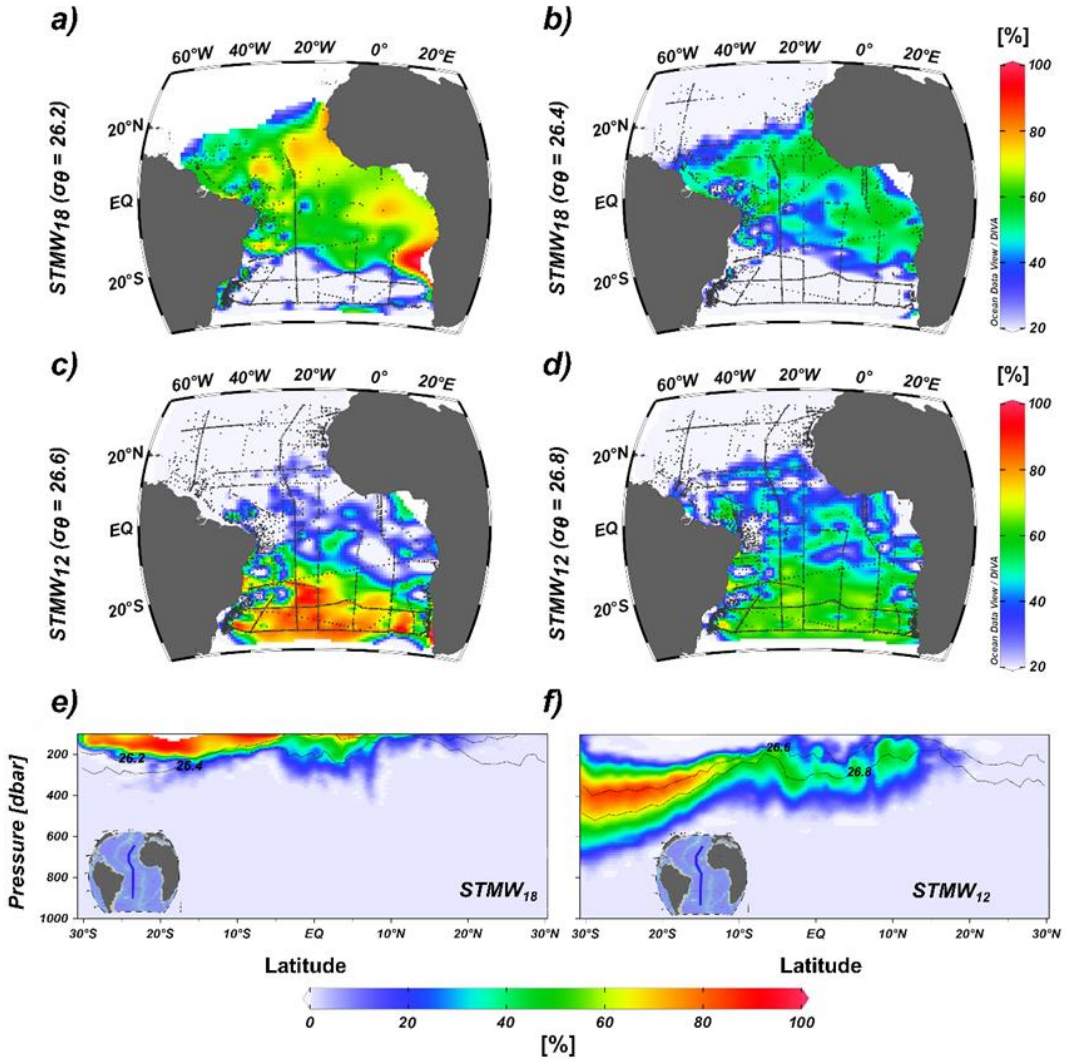

Figure 4. Spatial (a-d) and vertical (e-f) fractions of the mixture of the Subtropical Mode Water (STMW) varieties contributing to the South Atlantic Central Water. $STMW_{18}$ at 26.2 kg m^{-3} (a) and 26.4 kg m^{-3} (b) isopycnals. $STMW_{12}$ at the 26.6 kg m^{-3} (c) and 26.8 kg m^{-3} (d) isopycnals. Vertical distribution in a meridional transect from 30ºN to 30ºS (see inset panels in e and f), considering the contribution of $STMW_{18}$ (e) and $STMW_{12}$ (f).

4.2.1 Subtropical Indian Mode Water (STIMW)

STIMW is an important water mass contributing to the zonal band spanning from 30ºS to 20ºS (Figure 6). It shows high mixing fraction greater than 40% in this region, where its influence is restricted to the isopycnal range of 26.2

and 26.4 kg m^{-3} (Figure 6a-c). At greater depths (> 400 m), STIMW becomes negligible in the contribution to the thermocline's waters, but it is possible to recognise a small contribution to the water masses following the North Brazil Current (Figure 6d). Its spatial distribution is not uniform throughout the zone, displaying a mixing fraction greater than 80%, in the vicinity of Cape Town (Africa) and lower values close to the coast of Brazil (western side). Thus, indicating the origin and the pathway of this water mass through the South Atlantic Ocean. Furthermore, this STMW variety displays an isopycnal displacement, deepening its contribution as it moves from the eastern to the western side of the South Atlantic (Figure 6f).

4.3 Antarctic Intermediate Water (AAIW)

AAIW is the denser water mass considered in the analysis (Table 2), and only its upper level is investigated here. Its distribution is wide-spreading reaching as far as 20ºN with a significant contribution (Figure S2). This water mass starts to be defined at the 27.1 kg m^{-3} isopycnal (Stramma and England, 1999), but its contribution becomes important at lower depths (Figure S2a). For instance, near the equator, around 40% of the AAIW contribution takes place at the 26.8 kg m^{-3} isopycnal(~ 300 m). On the contrary, at greater depths (> 700 m), the AAIW influence displays a mixing fraction of roughly 100% (Figure S2b-d), mainly in the southern hemisphere. Beyond 20ºN its distribution decreased, which is likely due to mixing with MMW advected from the North Equatorial Current.

4.4 Temporal variability of the STMW varieties

The water mass anomalies showed no clear changes in the contribution percentages over the assessed years (Figures S3 and S4). To accurately assess the temporal changes, only the values of the water mass fractions anomalies in the source water mass core (i.e., EDW > 60%), were used. Their frequency distributions were observed for each year for the GO-SHIP repeated sections A16 and A05 (Figure 7). Thus, it was focused on the frequency distribution rather than absolute values, since some of the averaged source water mass anomalies are close to the reported error. The EDW shows a small displacement of the frequency distribution to positive values from 1993 to 2013 for section A16 (Figure 7a). However, considering section A05, there are no clear changes observed

between 1993 and 2011, although a relatively higher contribution is observed for 1998 (Figure 7a). Likewise, when comparing the difference for the EDW contribution between 2010 and 1993, a relative increase is observed (section A06, Figure S5). The denser MMW shows no significant changes in the frequency anomalies distribution, which are centred around 0%, but lower contributions for 2003 and 2004 are recorded for sections A16 and A05, respectively. Nonetheless, MMW showed a lower contribution in 2010 for section A06 when comparing to 1993 (Figure S5).

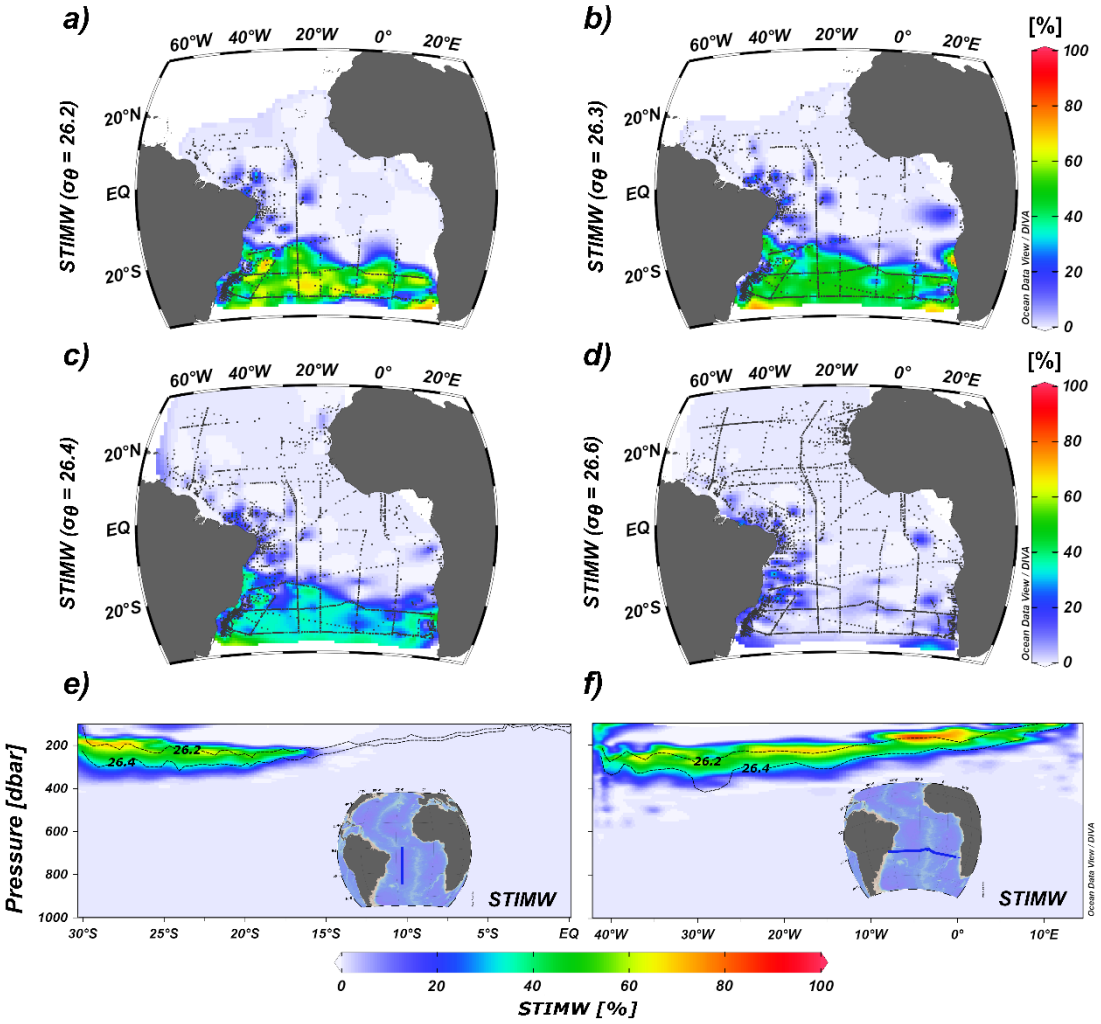

Figure 5. Spatial (a-d) and vertical (e-f) fractions of the mixture of the Subtropical Indian Mode Water (STIMW) contributing to the South Atlantic Central Water at the 26.2 kg m^{-3} (a), 26.3 kg m^{-3} (b), 26.4 kg m^{-3} (c), and 26.6 kg m^{-3} (d) isopycnals. Vertical distribution in a meridional transect from the Equator to 30ºS (e; see inset panel) and zonal transect at 24ºS (f; see inset panel), considering the contribution of STIMW.

In the southern hemisphere, the mixing scheme contributing to the SACW layer is more complex, with more than two STMW varieties contributing to the central layer. The lightest variety ($STMW_{18}$) shows a higher contribution in 2013 for section A16 marked by the displacement toward positive values of the frequency distribution of the water mass anomalies (Figure 7b). These results are supported by the higher contribution found in 2010 and 2018 for sections A06 and A9.5 (Figure S5 and S1). $STMW_{14}$ shows a small increase (~ 10%) in the contribution comparing 2018 to 2009 in section A9.5 (Figure S1). The denser $STMW_{12}$ displays no significant changes but exhibits a positive displacement in 2003 for section A16 (Figure 7b). Likewise, the results for sections A06 and A9.5 (2010 and 2018) exhibited a small negative contribution in the mass fraction of $STMW_{12}$ (Figure S5 and S1). For STIMW, the amplitude of the distribution is the highest of the varieties, even showing a bimodal distribution (Figure 7b), making it difficult to define a clear pattern in its temporal variability. Finally, the AAIW contribution showed no significant changes in its contribution (Figure 7c).

4.5 Mesoscale structures and the STIMW contribution to the South Atlantic

The match-up results allowed the identification of 171 hydrographic stations sampled inside 58 eddies identified using the AVISOme database from 1993 to 2019, and 55 eddies using the TOeddies database from 1993 to 2017 in the South Atlantic basin (Figure 8a-b, Table 4). Thus, three different outcomes are reported: (i) all eddies identified (cyclonic and anticyclonic) that were matched with the same date of hydrographic sampling (Figure 8a-b), including those north of 20ºS, which has a small STIMW influence; (ii) the cyclonic and anticyclonic eddies identified that have an STIMW influence, and (iii) the anticyclonic eddies exclusively sourced from the Agulhas system (Figure 9b, Laxenaire et al., 2018).

Considering all the eddies sampled and the entire thermocline (100-1000 m), the main source water masses contributing to the mixture in the central layer of the South Atlantic are AAIW, $STMW_{12}$, $STMW_{14}$, and STIMW with roughly 39%, 37%, 11%, and 10%, respectively for both databases (Figure 8). To obtain a more suitable averaged contribution of the STIMW inside the eddies identified, the results of the main source water masses present in the layer warmer than 9°C (Figure 8) are shown. Considering this water layer, the main contributors to the

mixture are $STMW_{12}$ (~45%), STIMW (~34%), and $STMW_{14}$ (~18%). Although most of the observations were sampled in anticyclonic eddies (Table 4), there are no significant differences in the STIMW contribution when split between cyclonic (~ 32%) and anticyclonic (~ 34%) eddies. This is also true when only the anticyclonic eddies derived from the Agulhas Current retroflexion zone are considered (~ 34%, Figure 8a-b).

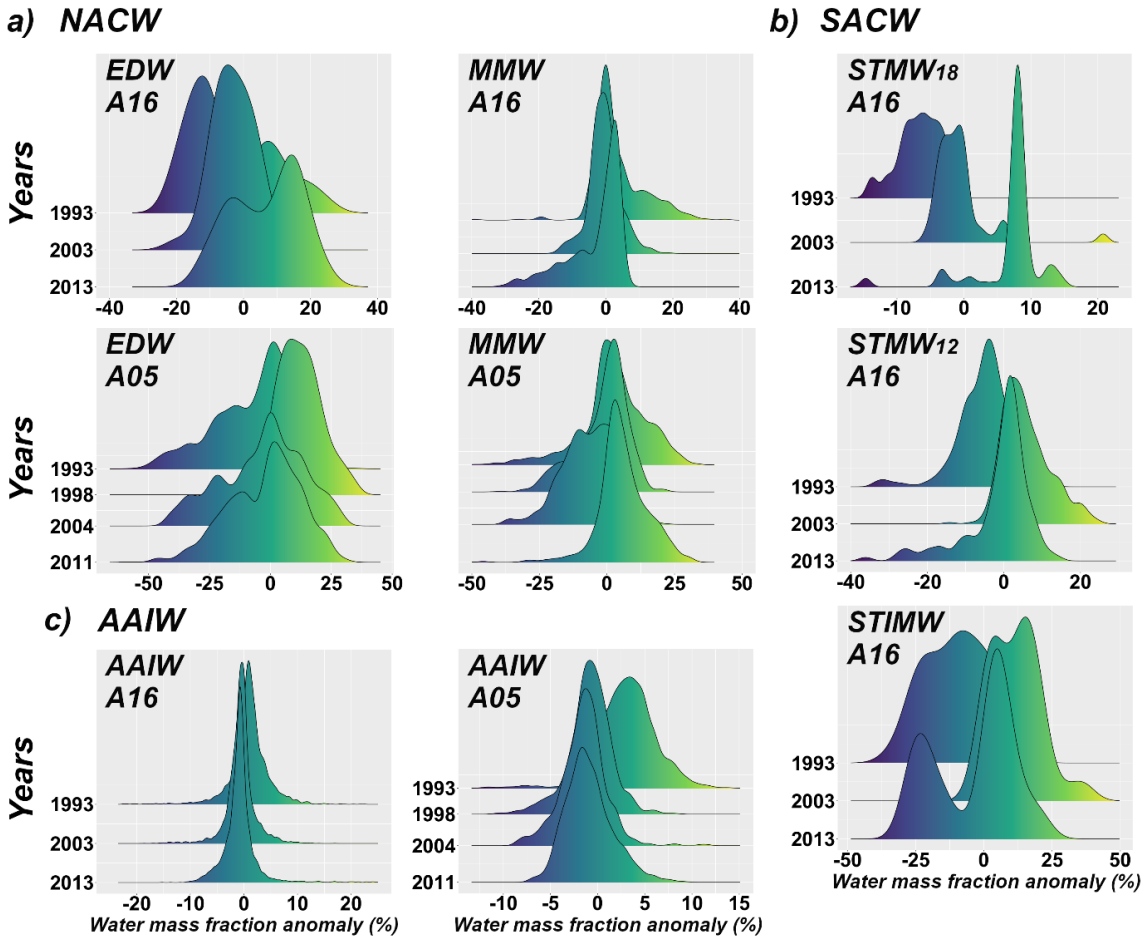

Figure 6. Frequency distribution of the source water mass fraction anomaly (i.e., % difference of the source water mass contribution between a specific year and then averaged for all the occupations) in the core contribution (i.e., > 60%) of the source water masses composing the (a) North Atlantic Central Water (NACW), (b) the South Atlantic Central Water (SACW), and (c) the Antarctic Intermediate Water (AAIW) for GO-SHIP hydrographic repeated sections A16 and A05. The source water masses acronyms are: Eighteen Degree Water (EDW), Madeira Mode Water (MMW), Subtropical Mode Water (STMW) of 18ºC ($STMW_{18}$),

STMW of 12ºC ($STMW_{12}$), and Subtropical Indian Mode Water (STIMW). For the STIMW, the core was defined as a contribution > 40%.

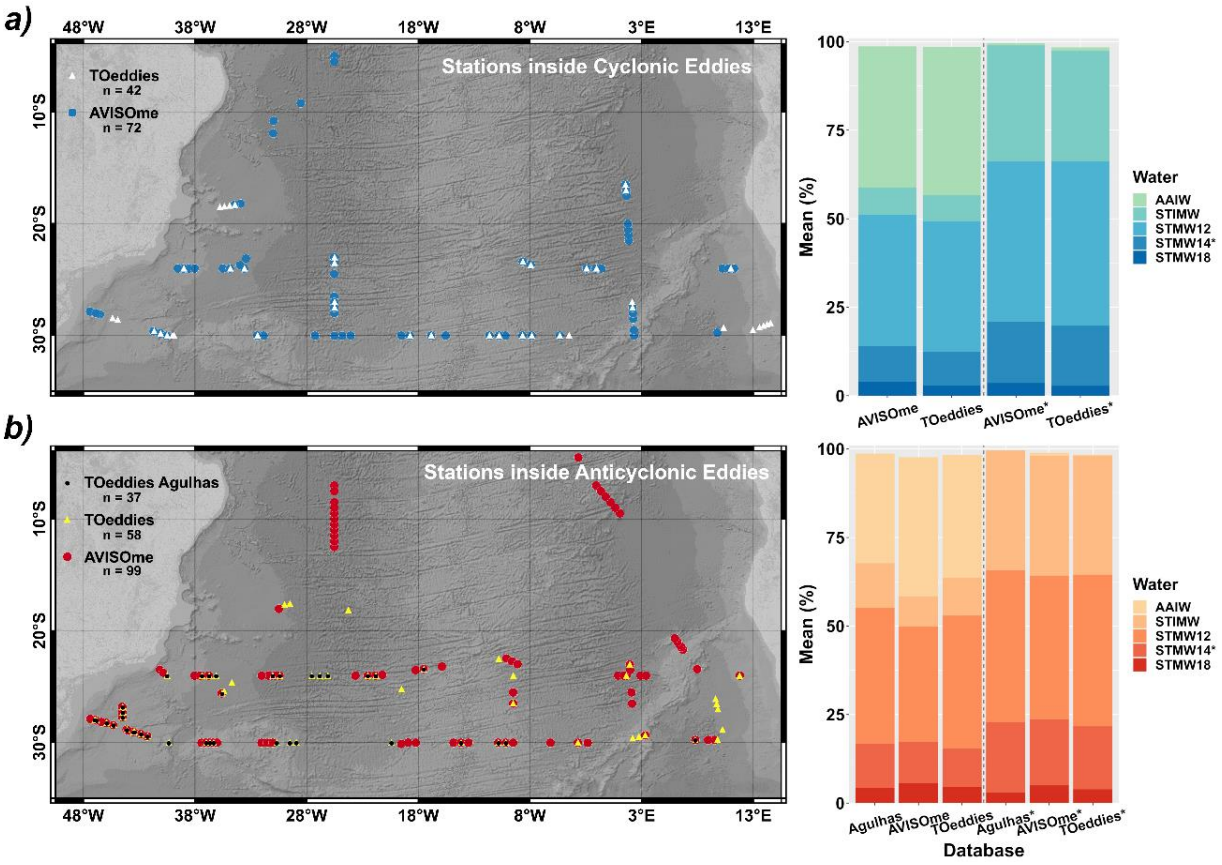

Figure 7. Hydrographic stations sampled under ocean (a) cyclonic (blue dots and white triangles) and (b) anticyclonic (red dots and yellow triangles) eddies. The Agulhas eddies in (b) are marked by black dots. The averaged contribution of Subtropical Mode Water (STMW) varieties for (a) cyclonic and (b) anticyclonic eddies is depicted by the vertical bars in the right panels. Data from the AVISO+ Mesoscale Eddy Trajectory Atlas Product (http://www.aviso.altimetry.fr/), both DT2.0exp and NRT3.0exp were merged into AVISOme representing data from 1993 to 2019 (blue and red dots). Agulhas eddies were recognised using the TOeddies database (black dots) developed by Laxenaire et al. (2018). In the right panels, database names represent the entire thermocline (100 – 1000 m), while those with an asterisk represent only the layer warmer than 9ºC (~100 – 400 m). The acronyms represent as follows: Antarctic Intermediate Water (AAIW), STMW of 18ºC ($STMW_{18}$), STMW of 14ºC ($STMW_{14}$), STMW of 12ºC ($STMW_{12}$), and Subtropical Indian Mode Water (STIMW). The contribution of the $STMW_{14}$ is

assumed from the values attained for Madeira Mode Water within this region, where the analysis mistook these two mode water varieties (see section 5.2).

Table 4. Values found by geospatial analysis. “Join attributes by location” algorithm in QGIS 3.10 was used between the source water fractions of the mixture from the OMP analysis and two different databases of eddies trajectories: the AVISOme (1993 – 2019) represents the merge between DT2.0exp and NRT3.0exp data from the AVISO+ Mesoscale Eddy Trajectory Atlas Product (http://www.aviso.altimetry.fr/). TOeddies (1993 – 2017) and Agulhas TOeddies (2000 – 2016) are based on Laxenaire et al. (2018). * Represents the results in the central layer warmer than 9ºC (~ 100 – 400 m) where the STIMW influence is noticeable.

Parameter	**AVISOme**	**AVISOme***	**TOeddies**	**TOeddies***	**Agulhas TOeddies**	**Agulhas TOeddies***
Total number of stations in the suitable time	1015	1015	903	903	549	549
Number of stations inside an eddy	171	130	100	94	37	37
Number of stations inside cyclonic eddies	72	57	42	39	-----	-----
Number of stations inside anticyclonic eddies	99	73	58	55	37	37
Total number of discrete samples	2621	650	1755	490	656	243
Number of discrete samples inside cyclonic eddies	1145	272	800	188	-----	-----
Number of discrete samples inside anticyclonic eddies	1476	378	955	302	656	243
Total number of eddies identified	70	58	58	55	-----	-----
Number of cyclonic eddies	28	24	21	20	-----	-----
Number of anticyclonic eddies	42	34	37	35	20	20

5 Discussion

5.1 On the influence of the STMW varieties on the central layer in the tropical Atlantic

The contribution of the STMW varieties to the central layer reveals a detailed picture of how the thermocline in the tropical Atlantic is composed (Figures 4-7 and 9). The vertical and spatial distribution of the NACW and SACW is well marked by their sources. The EDW and MMW are restricted to northern latitudes (Figure 4), while the $STMW_{18}$ and $STMW_{12}$, which are the main contributors in the southern hemisphere, can contribute up to 20ºN (Figure 5). These results indicate that northern STMW varieties are less transported by both the Guiana Undercurrent and the North Equatorial Undercurrent, so the Guinea Dome is filled by southern STMW varieties likely fed by the northern South Equatorial Current. Thus, the boundary between the NACW and SACW in the tropical Atlantic follows the North Equatorial Current (Figures 4 and 9), which displays an oblique behaviour from northeast to southwest (Stramma and England, 1999). On the eastern side of the North Atlantic, this boundary is settled at 20ºN as suggested by previous studies (e.g., Poole and Tomczak, 1999). At this latitude, the influence of the recirculation around the Guinea Dome is dominated by contributions from $STMW_{18}$ and $STMW_{12}$, which inhibit the southward displacement of the NACW to southern latitudes. This feature is evident for both EDW and MMW until the 27.0 kg m^{-3} isopycnal. At greater depths, the denser MMW contributes to southern latitudes (Figures 4d), suggesting that the Guinea Dome's influence reaches up to approximately 500 m (27.0 kg m^{-3}).

$STMW_{18}$ is the lighter source water mass that contributes to the SACW (Figures 5 and 9), this variety is displaced from its formation region through the Benguela Current and the southern South Equatorial Current (Stramma and England, 1999; de Souza et al., 2018). At shallower isopycnals (26.2 and 26.4 kg m^{-3}) it feeds mainly the North Brazil Current following the bifurcation of the southern South Equatorial Current (Figure 5a-b). Thus, this path feeds the Angola Gyre and the main zonal currents and countercurrents at the equator. On the other hand, the denser $STMW_{12}$ is the major contributor at the isopycnals greater

than 26.4 kg m^{-3} (Figure 5c-d), being distributed by the southern Equatorial Current and the Brazil Current into the subtropical gyre at 26.6 kg m^{-3} (~400 m). At higher isopycnals (~26.8 kg m^{-3}), its contribution appears north of the bifurcation of the southern Equatorial Current, reaching as far as 15ºN (Figure 5f), contributing to the lower branch of the North Brazil Current and the zonal equatorial currents. Hence, at these depths it is mixed with the contribution of the MMW. These results bring new evidence on the source water mass contribution in the SACW, enhancing the comprehension of the ocean circulation patterns in the tropical Atlantic previously described by Peterson and Stramma (1991) and Stramma and Schott (1999). Furthermore, we broaden the spatial distribution obtained by de Souza et al. (2018), who reported the influence of $STMW_{18}$ until 20ºS in the South Atlantic Ocean.

These results update previous studies that investigated the central layer of the Atlantic Ocean (Tomcak, 1981, Poole and Tomczak, 1999; Stramma and England, 1999; Stramma and Schott, 1999; Souza et al., 2018). For instance, Poole and Tomczak (1999) noticed that the distribution of the NACW at a lower depth of 300 m was obscured by high mass conservation residuals, while in the model used in this work it was possible to determine the contribution at any depth (Figure 4) in the NACW. In the southern hemisphere, they showed that WSACW (equivalent to a combination of $STMW_{18}$ and $STMW_{14}$) dominates the entire South Atlantic basin at 300 m with little contribution from ESACW (equivalent to $STMW_{12}$). Nonetheless, in the refined approach taken, it is revealed that the main source water contributor is $STMW_{12}$ formed along the Subtropical Front (Figure 1). Another key difference is the contribution of STIMW to the South Atlantic, which is revealed to be an important feature (Figure 6). These differences can be explained by the different definitions of the SWT. Poole and Tomczak (1999) divided the Atlantic's thermocline into three main water masses (Table 1) with two SWT defining each. The authors did not consider the contribution of AAIW to the mixture, while the refined approach used incorporates not only it but also includes the sources related to the STMW varieties that feed the South Atlantic central layer.

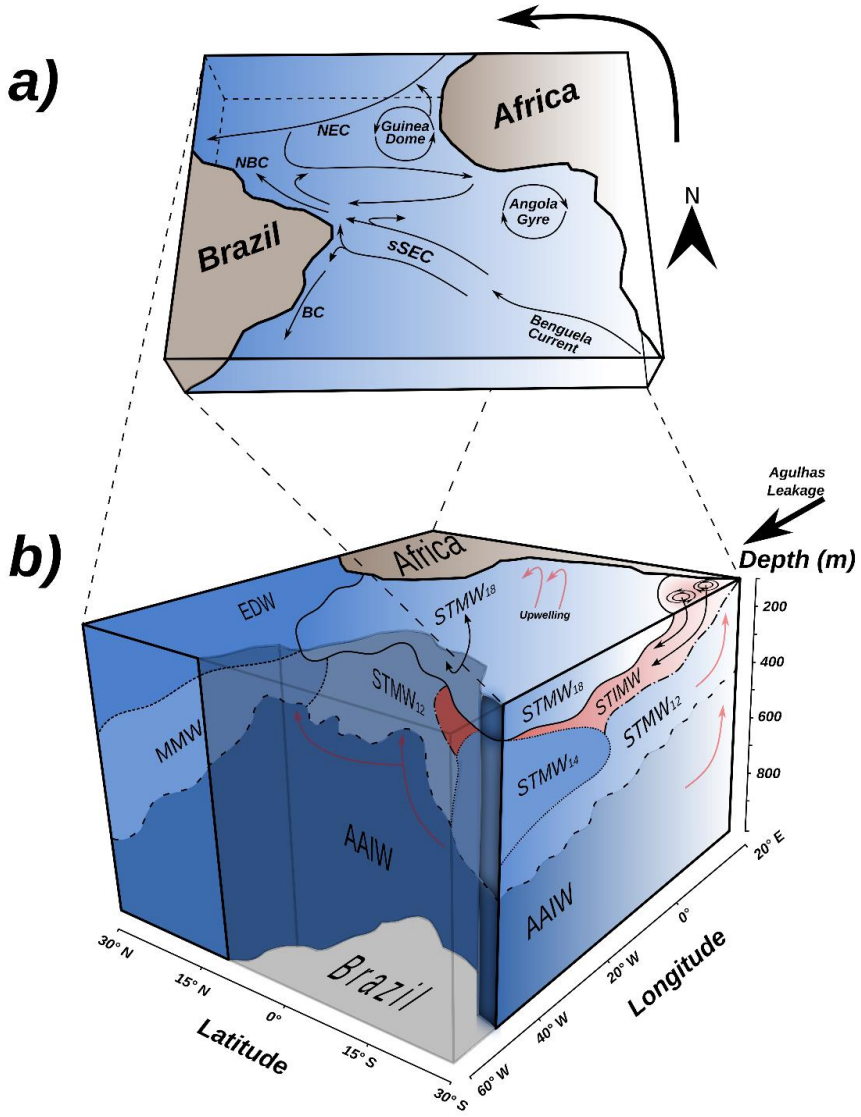

Figure 8. Schematic representation of the main ocean currents, spatial and vertical contribution of the different Subtropical Mode Water (STMW) varieties to the central layer (100 to 1000 m) of the tropical Atlantic. Main ocean currents in the study region are the North Brazil Current (NBC), North Equatorial Current (NEC), Brazil Current (BC), southern South Equatorial Current (sSEC), and Benguela Current (a). The thick arrow in (a) depicts the rotation view for panel (b). The source water masses are: Antarctic Intermediate Water (AAIW), Eighteen Degree Water (EDW), Madeira Mode Water (MMW), Subtropical Mode Water (STMW) of 18ºC ($STMW_{18}$), STMW of 14ºC ($STMW_{14}$), STMW of 12ºC ($STMW_{12}$), and Subtropical Indian Mode Water (STIMW). From bottom to top, the limits of STMW varieties are defined by lines: spaced dashed line for AAIW,

dotted line for $STMW_{14}$, dotted and dashed for $STMW_{12}$, dashed line for MMW, and full line for $STMW_{18}$ (EDW is limited by $STMW_{18}$ and MMW). Red arrows depict the upwelling zones, and the shaded area represents the continent.

The results do not show the contribution of the $STMW_{14}$ variety (formed at the Brazil-Malvinas Confluence), which becomes important at latitudes greater than 25ºS according to Sato and Polito (2014) and Souza et al. (2018). Instead, at this latitude, the contribution of MMW was found, which is considered unlikely and unrealistic. A similar error has been found by previous works (e.g., Poole and Tomczak, 1999; Souza et al., 2018), obtaining a misleading distribution or mistaken water masses. The closeness of the indexes used here to characterise the parameters that identify the SWT of $STMW_{14}$ and MMW is likely the reason for this behaviour. Therefore, even using the semiconservative water mass tracers here, is it not possible to decouple the contributions between $STMW_{14}$ and MMW on the southwestern side of the South Atlantic Ocean, which become a challenge for further studies.

5.2 On the temporal changes of the STMW varieties on the central layer in the tropical Atlantic

The temporal variability of the STMW varieties influencing the NACW and SACW composition depends on the coupled interaction of the atmosphere and the ocean (Yasuda and Kitamura, 2003). This variability is mainly associated with oceanic heat advection and air-sea heat fluxes, changes in the stratification in the western boundary currents, and the variability of the mesoscale activity, which can influence both the volume and longevity of STMW (Karstensen and Quadfasel, 2002; Qiu and Cheng, 2006; Fernandez et al., 2017). Thus, their temporal variability displays a large annual variability. Recent studies show water masses decadal variability related to the El Niño-Southern Oscillation (ENSO) cycle as well (Vanegas et al., 1998; Tsubouchi et al., 2007; Li, 2012; Fernandez et al., 2017). Based on the availability of the periods sampled with a quasi-decadal resolution, only a few inferences can be made on this topic (Figure 7). Thus, in the following discussion, three different processes that could affect the variability of the STMW varieties are explored: (i) changes in the conservative

properties, (ii) an increased/decreased rate of water mass formation and advection, and (iii) the mesoscale influence.

The increase in the conservative properties (like warming processes) in the upper layer could affect the OMP analysis to distinguish the source waters mixing fractions (Tomczak, 1981), mainly considering the lightest water masses (EDW and $STMW_{18}$). Warming in the ocean layer from 75 m to 700 m was estimated to be 0.015ºC per decade from 1971 to 2010 (Rhein et al., 2013). This value is within the standard deviation of the temperature index used here (Table 2), considering the sensitivity analysis performed. Besides that, previous work on STMW in the southwestern Pacific Ocean showed no trend in its properties from 1984 to 2014 (Fernandez et al., 2017). Thus, it is unlikely that the increased reported changes in the contribution of the lightest STMW varieties (Figures 7a-b) are related to ocean surface warming for both SACW and NACW.

Recently, based on a high-resolution numerical 3D Lagrangian trajectory model, Li (2012) suggested that the rate of subduction in the mode waters in the southwestern Pacific Ocean is closely linked to the El Niño-Southern Oscillation (ENSO) cycle. This model was supported by new data that spans 1984 to 2014 in the same area, where the heat content of the STMW layer is anticorrelated with inventories, particularly during the ENSO years, suggesting that large volumes of STMW are coincident with cooler conditions in the prior winter and less oceanic heat storage (Figure 12 in Fernandez et al., 2017). In the specific case of the Atlantic Ocean, there is evidence that sea surface temperature is negatively correlated with the ENSO phase in the Pacific Ocean (Ham et al., 2013; Rey et al., 2015). In that sense, despite the temporal resolution being limited in this work, the results are in agreement with those found by Fernandez et al. (2017). Positive anomalies were found in 1998 for the EDW (Figure 7a) and in 2010 for $STMW_{18}$ (Figure S4), those years are characterised by the ENSO influence as shown by the bi-monthly Multivariate El Niño/Southern Oscillation index (Figure S5, MEI.v2; https://www.esrl.noaa.gov/psd/enso/mei/, last data from November 4th, 2019). In the years around 1993 and 2003 frequency distribution anomalies (Figure 7) were found close to zero, not matching with the ENSO cycle, but close to those reported in Figure 12 by Fernandez et al. (2017) in the southwestern Pacific.

Thus, as previously reported, the STMW inventories could be likely associated with the ENSO influence, but more studies are still needed in the Atlantic Ocean to assess this issue.

The contribution of $STMW_{14}$, $STMW_{12}$, and STIMW do not display a clear increase or decrease in the core contribution in the evaluated years, even exhibiting a bimodal distribution for the STIMW (Figure 7b). The influence of STIMW on the Atlantic Ocean is mainly associated with mesoscale activity through the Agulhas eddies (Gordon, 1985; Duncombe, 1991). Moreover, these three water masses occupy narrow range of isopycnal levels, and for that reason, they could respond to the mesoscale variability and display a complex pattern in their temporal changes. It is important to bear in mind that the absolute values of the water mass anomalies are close to the reported error. Therefore, even though the interpretation is focused on the frequency distribution rather than the absolute values, further investigations based on a higher resolution ocean model or a dataset with a higher frequency of sampling for the central layer of the oceans are still needed to fully comprehend the temporal variability and changes in the STMW varieties contribution.

5.3 On the influence of the STIMW on the SACW

The results in this study show the higher influence of the STIMW (contribution > 80%) in the subtropical latitudes extends from 20ºS to 30ºS (Figure 6), which is characterised by an averaged contribution of 34% ± 20%. Moreover, its vertical distribution within this region is characterised by an oblique downward distribution (Figure 6f) and is associated with the isopycnal northwestward displacement of the eddies (Richardson, 2007; Azevedo and Mata, 2010). Likewise, the main contributors to SACW in the zonal band from 20°S to 30°S that occupy the same isopycnals levels of STIMW are $STMW_{12}$ and $STMW_{14}$ (Figure 8 and 9). These results suggest that waters coming from the Indian Ocean are isopycnally mixed mainly with the mode water varieties formed along the Subtropical Front ($STMW_{12}$) and to a lesser extent with mode waters formed at the Brazil-Malvinas Confluence ($STMW_{14}$).

Here, the source waters mixing fractions supported the refined SACW mixing scheme in the thermocline layer within this key interhemispheric and

interocean zone (Figure 9) for a better comprehension of the upper branch of the Atlantic Meridional Overturning Circulation. For instance, Gordon et al. (1992) proposed that the Benguela Current is a mixture of 60-65% Indian waters and 35-40% SACW based on chlorofluoromethane-11, but did not show the contribution of each source water mass. Likewise, Souza et al. (2018) proposed that the STIMW is mixed with $STMW_{12}$ in the 300-600 m layer, but because of OMP limitations, they were not able to evaluate the $STMW_{14}$ contribution. Recently, Laxenaire et al. (2019) show how a huge eddy from the Agulhas leakage displays a double core of STMW features. They found that the properties fall in the range of $STMW_{18}$ and $STMW_{12}$, and other eddies that they compared fall in the range of $STMW_{14}$. In that sense, as $STMW_{18}$ and STIMW have a similar temperature, salinity, and dissolved oxygen, but differ considering the concentration of the dissolved nutrients (Table 2, Poole and Tomczak, 1999), it is likely that the properties found by Laxenaire et al. (2019) in their eddy analysis refers to STIMW and not $STIMW_{18}$.

The Indian water influence on the Atlantic Ocean is mainly associated with mesoscale structures through the Agulhas eddies, which are formed in the Agulhas retroflexion and shed into the Atlantic through the Agulhas leakage (Gordon, 1985; Duncombe, 1991; Biastoch et al., 2009). The results here show no significant difference in the STIMW contribution regarding the eddies' rotation type (Figure 8). Thus, although the initial source of the STIMW is thought to be the Agulhas eddies (anticyclonic), the evolution of these eddies could generate other structures (cyclonic or anticyclonic) with an equal contribution of that water mass variety to the SACW. The new mesoscale structure could be generated by processes like merging or splitting that act along the evolution of the initial eddy (Hall and Lutjeharms, 2011). In order to prove that the main contribution of STIMW is mainly due to the mesoscale structure, further analysis was carried out. This further analysis involved coupling the eddies database and the contribution found for this variety in the repeated (2009 and 2018) GO-SHIP section A9.5 (Figure S7). The results show that the distribution of the STIMW matches with the eddies sampled during the sea voyage (GO-SHIP A9.5) in the respective years. Therefore, it could be taken as evidence that the main source of Indian waters is linked to the presence of mesoscale structures.

Concerning the volume of Indian waters that come into the South Atlantic, many studies have been carried out based on satellite data and to a lesser extent hydrographic data, which allows the mesoscale structures entering to the South Atlantic to be identified (e.g. Gordon et al., 1992; Richardson, 2007; Dencausse et al., 2010; Souza et al., 2011). Here, it was possible to obtain an average estimate of 5.5 ± 3.2 Sv entering the South Atlantic through the Agulhas eddies from 2000 to 2017. The volume of Indian waters transported into the South Atlantic reported by previous studies is in agreement with the estimate in this work. For instance, Richardson (2007) estimated an annual eddy volume transport of 10-13 Sv using a ratio of 8.25 eddies/year combining float and drifter data with altimetry, but he used a high number of eddies per year compared with others authors (e.g. Dencausse et al., 2010). Dencausse et al. (2010) used sea surface height data to calculate the volume transported by the Agulhas eddies between 1992 to 2006. They obtained an initial value of 8.5 Sv near the Agulhas Current Retroflexion and 1.4 Sv in the northwestern Cape Basin. Finally, Souza et al. (2011) coupled vertical profile data from the ARGO floats program and satellite sea surface height data to reconstruct all eddies shed by the Agulhas retroflexion between 2005 and 2008, attaining a volume of 9 ± 8 Sv and a meridional heat flux across the eddies' paths of 0.062 ± 0.012 PW. Therefore, although the estimate is based on a simple calculation, it is in the range calculated by the mentioned authors and can be suitable to describe the global mean value of the Indian Ocean influence on the South Atlantic's thermocline.

5.4 Implications in the large scale-ocean circulation

The Atlantic Meridional Overturning Circulation (AMOC) is strongly linked to the deep convection of North Atlantic Deep Water (NADW) (Reid, 1996; Gordon, 1996) in the North Atlantic Ocean, which trigger the deep branch of the AMOC. An important aspect of the NADW formation is the salt content in the thermocline waters coming from the southern hemisphere by the shallow branch of the AMOC (Gordon, 1986; Tomczak and Godfrey, 1994; Biastoch et al., 2009). Thus, the salt balance in the Atlantic Ocean has been proposed as one of the main factors controlling the strength of the AMOC (Weijer et al., 2001). Here, we found a contribution of ~ 20% of the STIMW associated to the transport carried out by the North Brazil Current at ~ 350 m (Figure 6). The mixing fraction of

STIMW composing the SACW is thought to be distributed by the translation of the Agulhas eddies along the Agulhas Corridor in the South Atlantic Ocean (Guerra et al., 2018). Therefore, this contribution is first distributed by the Benguela Current, which then feeds the southern South Equatorial Current, and finally the latter is bifurcated into the Brazil Current (southward) and the North Brazil Undercurrent/North Brazil Current (northward) (Peterson and Stramma, 1991; da Silveira et al., 1994; Stramma and England, 1999).

Our results evidence that the Indian Ocean waters influence the upper branch of the AMOC in the South Atlantic Ocean, thus highlighting both an interocean and interhemispheric water exchanges. This becomes relevant considering a climate scenario that both the Agulhas Leakage is increasing due to a poleward shift in the westerlies (Biastoch et al., 2009) and the latitude of the southern South Equatorial Current bifurcation changing southward (Marcello et al., 2018). The position of the current bifurcation controls the path of the heat and salt exchanges either to the south (via Brazil Current) or to the north (via North Brazil Undercurrent/North Brazil Current) (Rodrigues et al., 2007; Marcello et al., 2018), being a key parameter in the strength of the AMOC (Ballalai et al., 2019). This latitude varies according to the local wind stress curl, which is related to the Intertropical Convergence Zone. Thus, as the current bifurcation moves south (north) the North Brazil Current transport increase (decrease) and the Brazil Current transport decrease (increase) (Rodrigues et al., 2006; Marcello et al., 2018). Therefore, based on that and the results presented here, we can infer that the heat and salt fluxes to the northern hemisphere may likely increase in the following years.

Additionally, as the Indian Ocean waters influence both interocean and interhemispheric exchanges, as shown here, regional changes in the ocean carbon cycle may be linked to this issue. Orselli et al. (2019a) showed that the Agulhas eddies are efficient mesoscales structures to capture atmospheric CO_2 towards the ocean, even considering their anticyclonic nature. In addition, Orselli et al. (2019b) revealed that the Agullhas eddies have 23% more anthropogenic carbon content than the surrounding waters in the South Atlantic. Therefore, the Agulhas Leakage plays a key component not only in the AMOC (affecting ~ 10%

its strength, Weijer et al., 2001), but also in changing the biogeochemistry of the South Atlantic Ocean (e.g. Lehahn et al., 2011; Carvalho et al. 2019; Orselli et al., 2019a, b). For that reason, additional studies are encouraged to fully comprehend the coupled influence of the increasing contribution of Indian Ocean waters into the South Atlantic Ocean and further transport to the north, and its biogeochemical impact.

6 Summary and Conclusion

Here, the source water contribution (i.e. STMW varieties) of NACW and SACW in the tropical Atlantic was successfully revealed. In addition, new evidence of the influence of the Indian Ocean waters, through the mesoscale activity, was show to contribute to the mixing fractions composing the SACW. In the northern hemisphere, the contribution of EDW is confined to the upper levels of the NACW. Its spatial distribution follows the North Equatorial Current, and its contribution is mainly restricted at the 26.6 kg m^{-3} isopycnal. The MMW contributes to deeper levels (27.0 kg m^{-3}) of NACW, and for that reason, the eastern limit between NACW and SACW is placed at 10ºN at these depths.

The central layer structure in the southern hemisphere is relatively more complex due to several STMW varieties involved in the mixture. Overall, the main contributors for the SACW layers are the $STMW_{18}$, which is superficially distributed by the Benguela Current and the southern South Equatorial Current, and the $STMW_{12}$ restricted to the southern part of the subtropical gyre. Furthermore, $STMW_{12}$ is the main contributor at the isopycnals greater than 26.4 kg m^{-3}, and it is mixed with $STMW_{14}$ and STIMW in the zonal region spanning from 20ºS to 30ºS. Within this zone, the influence of STIMW is important as the contribution to the mixture is up to 80%, and displays an oblique downward distribution associated with the isopycnal northwestward displacement of the eddies. Based on these results, the mixture scheme of the main STMW varieties in the SACW is revealed, expanding and supporting previous studies in this regard.

It is shown that the source of the STIMW, influencing the SACW composition in the South Atlantic Ocean, is likely associated to the Agulhas eddies shed by the Agulhas retroflexion zone. These results are consistent and

supported by the detection of 58 eddies using the AVISOme database (from 1993 to 2019) and 55 eddies from TOeddies (from 1993 to 2017), sampled by oceanographic surveys investigated here. Based on that, the main source water masses contributing to the central layer warmer than 9ºC into the South Atlantic eddies are $STMW_{12}$ (~ 45%), STIMW (~ 34%), and $STMW_{14}$ (~ 18%). The same mixing scheme is verified by the Agulhas anticyclonic eddies, with minor changes in the magnitude of the mode waters contribution. There is no significant difference between cyclonic and anticyclonic eddies regarding STIMW contribution. For that reason, it is thought that the evolution of the initial Agulhas eddies can generate other mesoscale structures with a similar contribution of that water mass variety on the SACW layer. Moreover, it was possible to attain a rough mean estimate of 5.5 ± 3.2 Sv entering into the South Atlantic from 1993 to 2017, taking into account only the Agulhas eddies and assuming that they are transported mainly by the Benguela Current.

The temporal variability of the STMW varieties assessed in this study for the tropical Atlantic displayed similar patterns as those composing the central waters in the southwestern Pacific Ocean. For that reason, ENSO cycles are thought to be linked to the STMW inventories not only in the Pacific Ocean, but also in the Atlantic Ocean. On the other hand, as the STIMW, $STMW_{14}$, and $STMW_{12}$ occupy a narrow range of isopycnal levels (mainly in the 200-500 m layer) in the South Atlantic Ocean, the changes in their contribution to the SACW could be responding to the intensity and changes of the mesoscale variability (i.e., eddy split/merge, power of the mixing processes, etc.). This complicate the pattern in their temporal changes because the interplay between the boundaries of the ocean interior itself and the ocean-atmosphere exchanges.

Finally, the results are summarised into a schematic figure of the water masses structure of the central layer in the tropical Atlantic, splitting the NACW and SACW in their source waters (Figure 9). The novel evidence of the STIMW influence into the South and North Atlantic Oceans, along with the increase in the Agulhas Leakage, and the southward displacement of the latitude of the southern Equatorial Current bifurcation proposed by previous work, may likely increase the heat and salt fluxes to the northern hemisphere. Despite some authors has

suggested ~10% as the effect of the Agulhas Leakage in the strength of the AMOC, the real effect in the climate system is still poorly understood. Therefore, further studies using better spatiotemporal resolution, such as offered by the biogeochemical Argo floats and other instrumentations, along with the outcomes of new climate and ocean models are encouraged to be used to further investigate the Indo-Atlantic connection and its link to global climate-driven issues.

Supplementary Material:

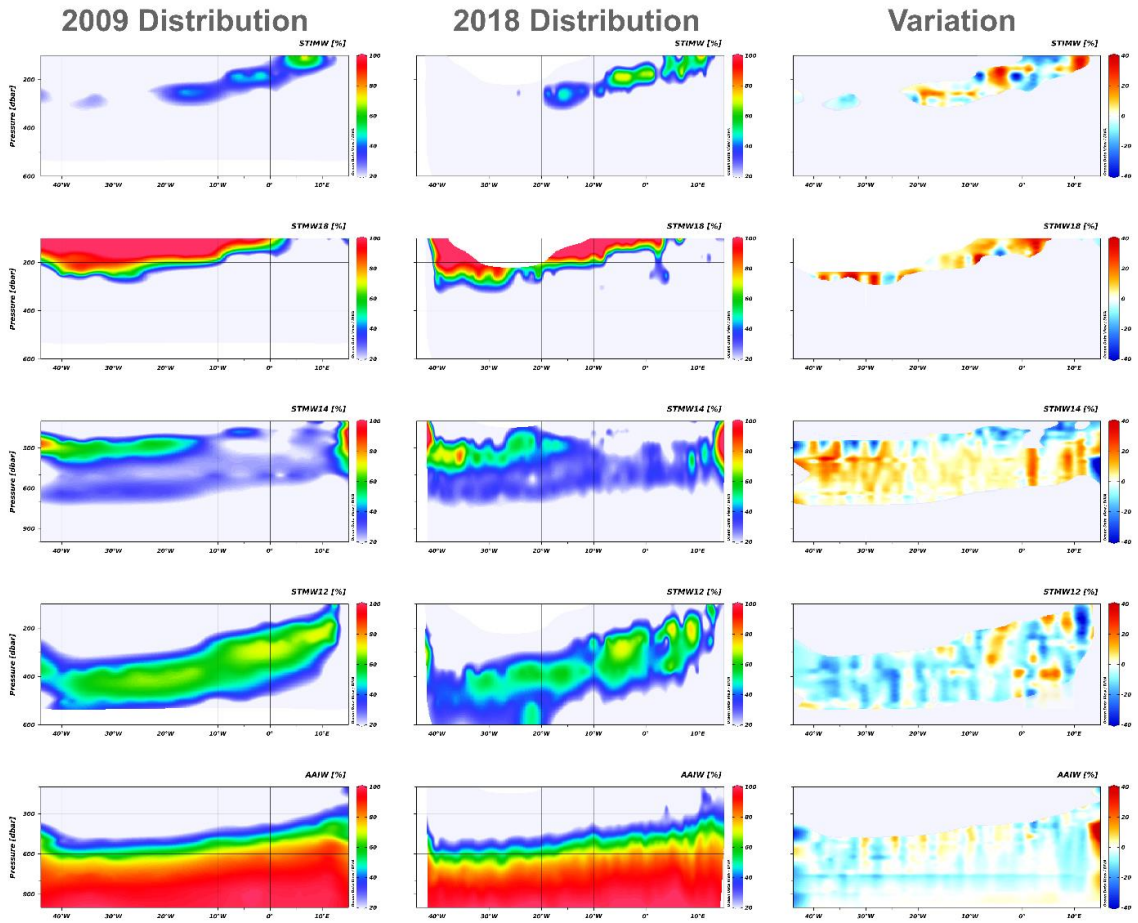

Figure S1. Anomalies of the contribution (i.e., difference between the % of the recent year and the old year) to the central layer mixture considering the Subtropical Mode Water (STMW) varieties and Antarctic Intermediate Water (AAIW) for GO-SHIP A9.5 repeated hydrographic section occupied in 2009 and 2018. STMW varieties contributing to SACW are $STMW_{18}$, $STMW_{14}$, $STMW_{12}$, and STIMW.

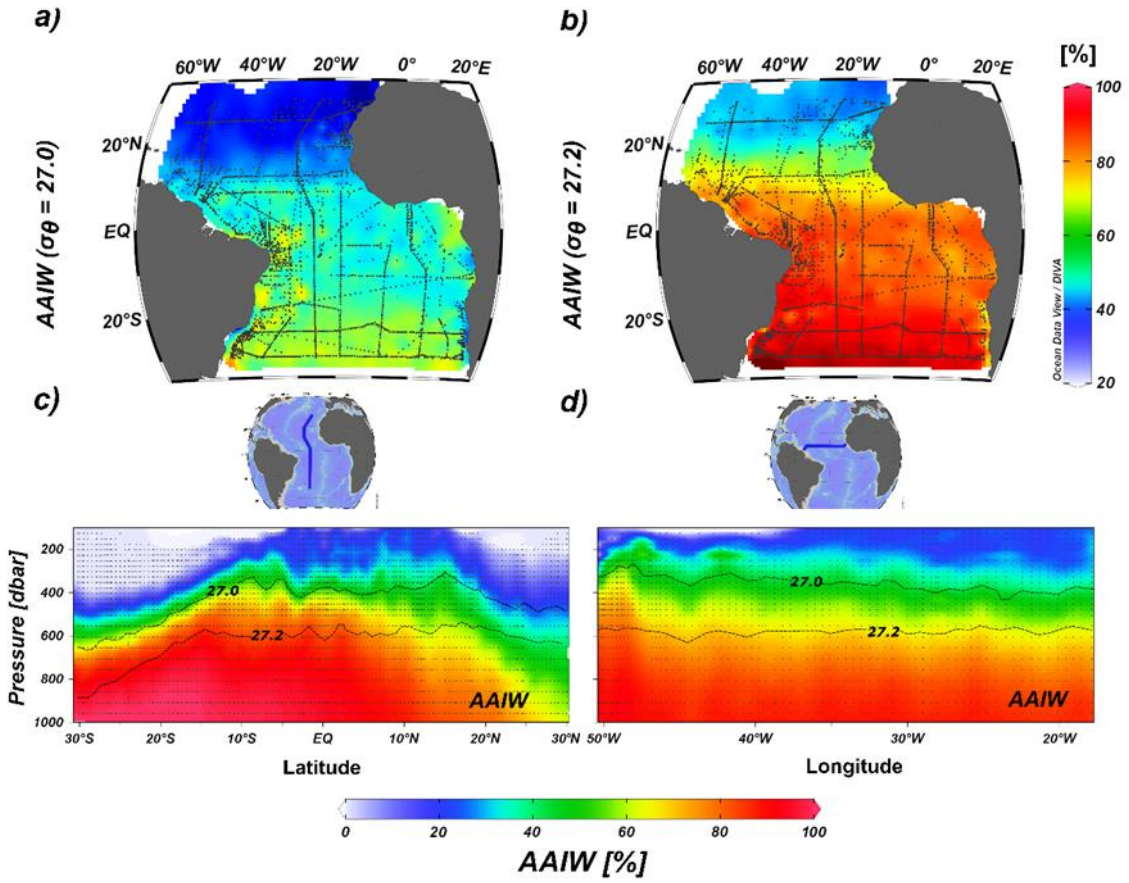

Figure S2. Spatial (a-b) and vertical (c-d) distribution of the Antarctic Intermediate Water (AAIW) in the tropical Atlantic at isopycnals of 27.0 kg m^{-3} (a) and 27.2 kg m^{-3} (b). Vertical distribution in a meridional transect from 30ºN to 30ºS (e; see upper panel) and zonal transect at 7.5ºN (f; see upper panel), considering the contribution of AAIW.

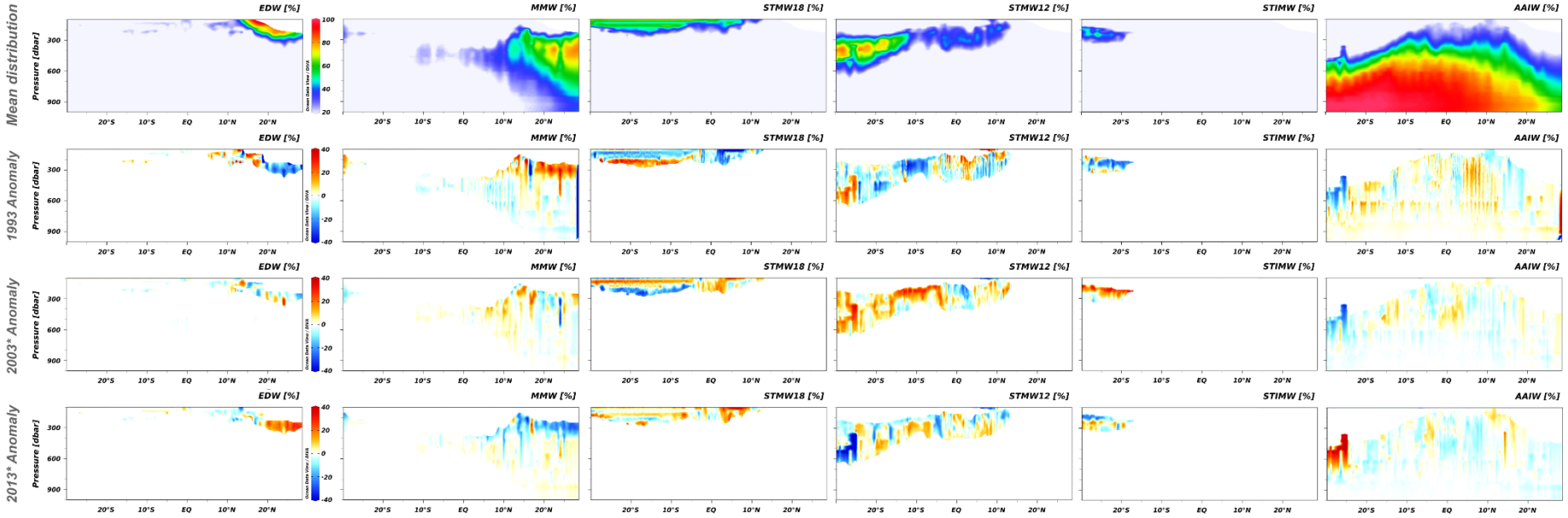

Figure S3. Anomalies of the contribution (i.e., difference between the % of a specific year and the average for all the occupations) to the central layer mixture considering the Subtropical Mode Water (STMW) varieties, Subtropical Indian Mode Water (STIMW), and Antarctic Intermediate Water (AAIW) for GO-SHIP A16 repeated hydrographic section occupied in 1993, 2003, and 2013. STMW varieties contributing to NACW are Eighteen Degree Water (EDW) and Madeira Mode Water (MMW), while STMW varieties contributing to SACW are $STMW_{18}$, $STMW_{12}$ and STIMW.

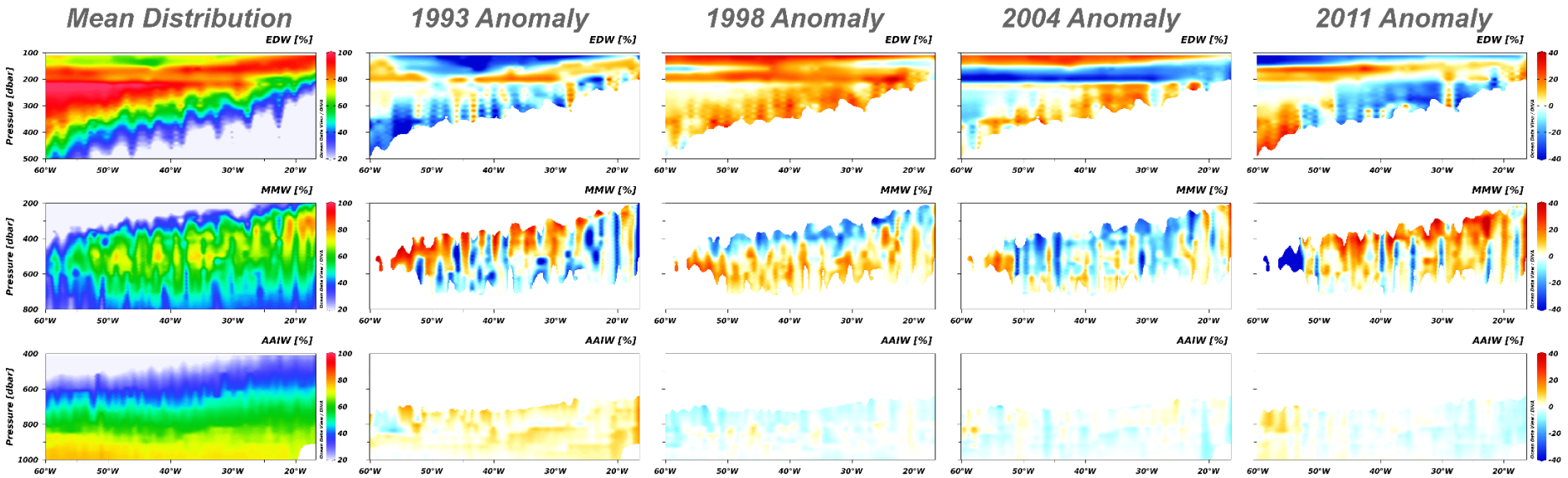

Figure S4. Anomalies of the contribution (i.e., difference between the % of a specific year and the average for all the occupations) to the central layer mixture considering the Subtropical Mode Water (STMW) varieties and Antarctic Intermediate Water (AAIW) for GO-SHIP A05 repeated hydrographic section occupied in 1993, 1998, 2004 and 2011. STMW varieties contributing to NACW are Eighteen Degree Water (EDW) and Madeira Mode Water (MMW).

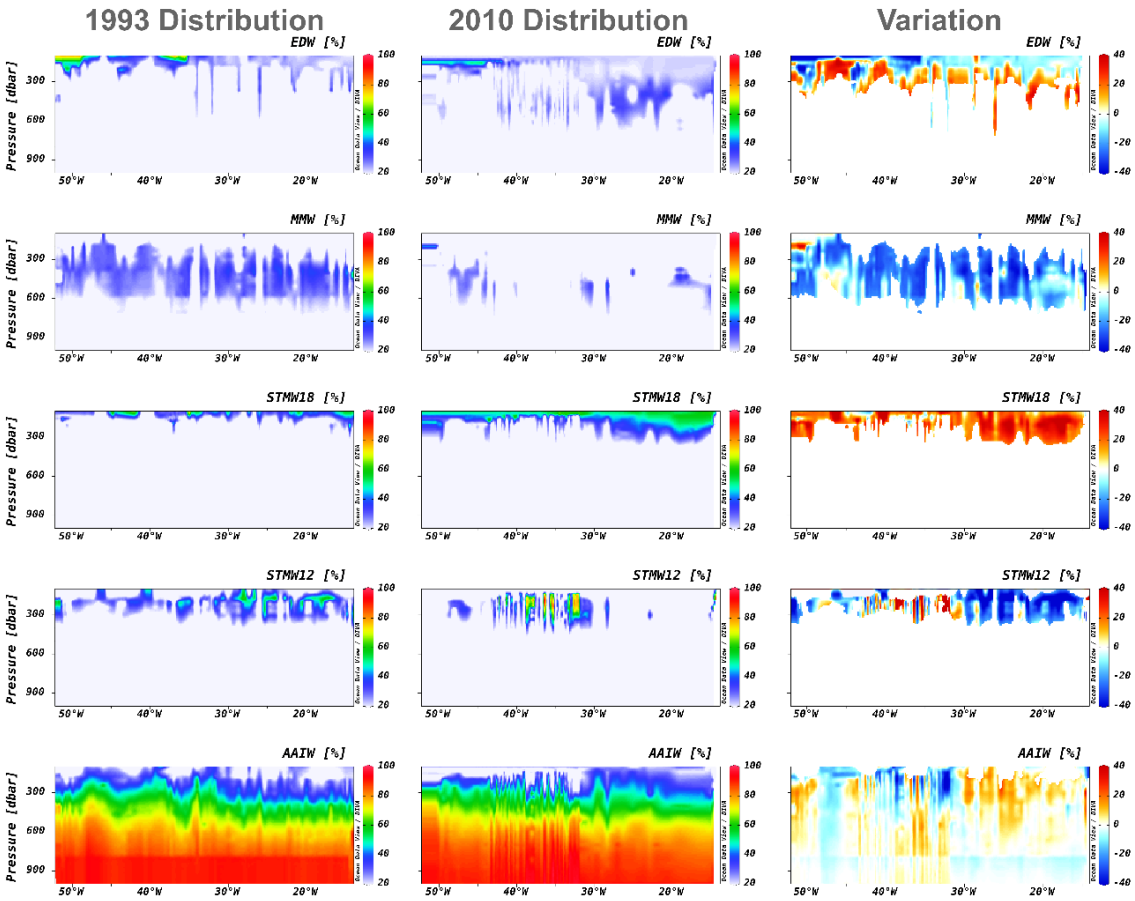

Figure S5. Anomalies of the contribution (i.e., difference between the % of the recent year and the old year) to the central layer mixture considering the Subtropical Mode Water (STMW) varieties and Antarctic Intermediate Water (AAIW) for GO-SHIP A06 repeated hydrographic section occupied in 1993 and 2010. STMW varieties contributing to NACW are Eighteen Degree Water (EDW) and Madeira Mode Water (MMW), while STMW varieties contributing to SACW are $STMW_{18}$, and $STMW_{12}$.

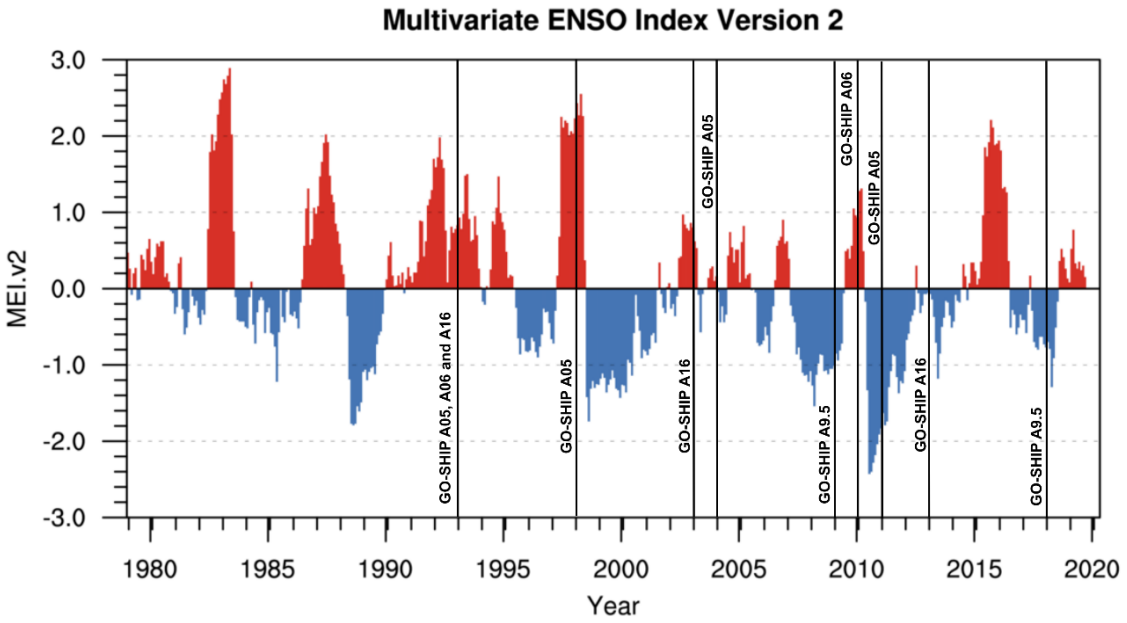

Figure S6. The bi-monthly Multivariate El Niño/Southern Oscillation (ENSO) index (MEI.v2) from 1980 to 2019 along with the GO-SHIP repeated sections used in this study. (https://www.esrl.noaa.gov/psd/enso/mei/, last data from November 4th 2019).

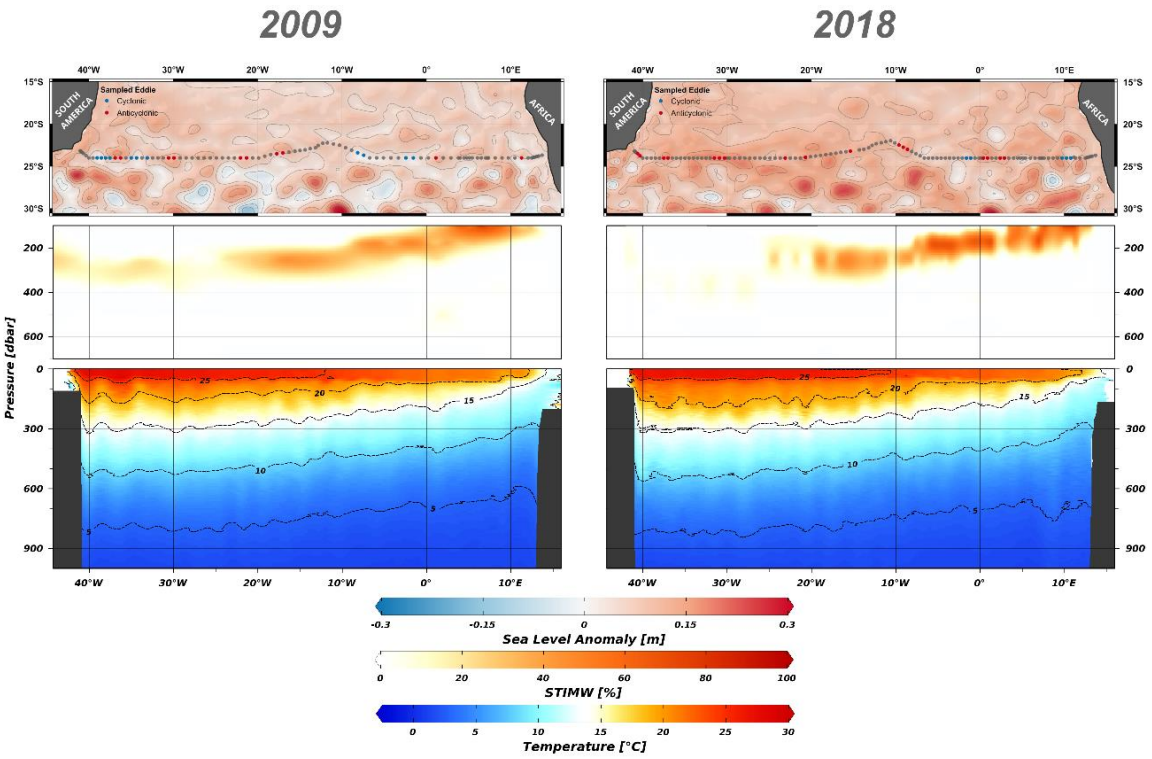

Figure S7. Mean surface sea level anomaly for March/April 2009 and for March/April 2018 along with WOCE 9.5 hydrographic stations, the contribution of the Subtropical Indian Mode Water (STIMW) for their respective year found in this study, and the temperature profile for each survey. Red dots depict hydrographic stations inside anticyclonic eddies at the moment of sampling, while blue dots depict hydrographic stations inside cyclonic eddies.

CAPÍTULO IV:

Caracterização isotópica da MOP no oceano Atlântico Tropical Oeste

O segundo manuscrito, de autoria de Elias Azar, Andres Piñango, Gabriela Martins, Thayná Peterle, Eunice da Costa Machado, Carlos Eduardo de Rezende, Maria da Graça Baumgarten, e Mônica Wallner-Kersanach, é intitulado **"$\delta^{13}C$ and $\delta^{15}N$ composition of particulate organic matter in the tropical Atlantic: evidence of low remineralization in the oxygen minimum zone"**, e será submetido para publicação no periódico **"Journal of Marine Systems"**.

Abstract

The tropical north Atlantic Ocean is characterized by two main oceanographic features such as the Ekman divergence and the presence of an oxygen minimum zone (OMZ). These characteristics affect the physical and biogeochemical processes in the ocean, such as the efficiency of the biological carbon pump. Recent studies have suggested the reduction in the remineralization rates and lesser attenuation fluxes in the OMZs comparing to well-oxygenated waters. Despite that, the effect of the hypoxic condition on the isotopic distribution in the sinking POM is still poorly understood. In this work, is characterized the POM by its organic carbon (POC) and nitrogen (TPN) content and the $\delta^{13}C_{POC}$ and $\delta^{15}N_{TPN}$ signatures in a meridional transect (38°W) from the equator to 15°N. A strong influence of the Ekman divergence was found in the latitude range of 5°- 10°N due to the influence of the intertropical convergence zone (ITZC), subsurface isopycnals were almost 200 m shallower in this region. POC (~ 4 µmol L^{-1}) and TPN (~ 0.2 µmol L^{-1}) were higher in the subsurface at 8°N and the $\delta^{13}C_{POC}$ (-25 ‰) was relative heavier than those southern, suggesting that the ballast effect due to terrigenous particles coming from aeolian input, enhance the sinking velocities of the POM. The same patter in POM and $\delta^{13}C_{POC}$ was found in the OMZ and just beneath it. In this case, it was likely associated with changes in zooplankton behaviour owing to poor oxygen concentration. The C:N ratio increase with deep, which indicates the preferable consumption of the organic nitrogen compound. The multiple regression model explains 66 % of $\delta^{13}C_{POC}$ variance using POC, phosphate, and TPN as independent variables, being the latter the most significant. Thus, the $\delta^{13}C_{POC}$ of the remaining POM is sensitive to the consumption of the labile nitrogen organic compound, and it is influenced by the ITZC and the OMZ.

Keywords: Particulate Organic Matter, Oxygen Minimum Zone, Carbon and Nitrogen Isotopes, Biological Carbon Pump.

1. Introduction

The biological pump is a set of complex mechanisms that constantly transport large amounts of particulate organic carbon (POC) and biominerals (i.e., $CaCO_3$), from the surface's ocean toward its interior (Volk and Hoffert, 1985; Honjo et al., 2008). It begins near the surface, where dissolved inorganic material (i.e., CO_2, nitrate, phosphate, and silicate) are transformed into organic matter (carbohydrates, lipids, and proteins) and biominerals (silica and calcium carbonate) by phytoplankton through photosynthesis (Falkowski et al., 1998, De la Rocha and Passow, 2014). The net primary production account for 50 Pg C y^{-1} (1 Pg or 1 Gt is 10^{15} g) of which 10 Pg C y^{-1} is exported (from the euphotic zone) and 2 Pg C y^{-1} reach the seafloor (De la Rocha and Passow, 2014; Middelburg, J., 2019). Thus, most of the organic matter exported from near-surface waters is converted back into its inorganic constituents by heterotrophic organisms in the upper pycnocline through remineralization (Sarmiento and Gruber, 2006). Despite only 4% of the net primary production is deposited at the seafloor, the biological pump regulates the atmospheric CO_2 and, therefore, the climate system (De la Rocha and Passow, 2007 and 2014).

Ocean regions with low oxygen concentration play a key role in the flux of POC to the deep ocean. These regions are known as oxygen minimum zones (OMZs). There is no oxygen threshold that defines the OMZ but generally is considered the value around 60 µmol kg^{-1} in oxygen content for the upper limit (Karstensen et al., 2008; Stramma et al., 2008). The volume of the global ocean occupied by an OMZ varies substantially, in the North Pacific represents about 40% of the volume, while in the South Pacific drops to 13%. These estimations are using 90 µmol kg^{-1} as an upper bound for OMZ oxygen concentration for ocean densities lighter than the potential density ($\sigma_{\theta)} < 27.2$ kg m^{-3} (Karstensen et al., 2008). Likewise, the values for the North and South Atlantic are even smaller with 5% and 7%, respectively. It has been recognized that the OMZs reduces less efficiently the POC fluxes related to oxygen-rich waters (e.g $O_2 >$ 120 µmol kg^{-1}, Devol & Hartnett, 2001; Van Mooy et al., 2002; Roullier et al., 2014; Keil et al., 2016; Cavan et al., 2017; Engel et al., 2017; Rasse and Dall'Olmo, 2019). Thus, despite these OMZs represent a small volume of the global ocean, they impact the efficiency of the biological carbon pump, and as

these zones are expanding, they will become key areas to understand the amount of POC that is exported to the deep ocean (Stramma et al., 2008; Passow and Carlson, 2012; Santos et al., 2016; Cavan et al., 2017; Hahn et al., 2017; Schmidtko et al., 2017).

Several hypotheses have arisen regarding the effect of the OMZs in the POC fluxes (Cavan et al., 2017). These include changes in the zooplankton behavior, sinking material are more refractory, preferential consumption of nitrogen-rich organic matter, and a low oxidation rate of sinking particles by microbes (Devol & Hartnett, 2001; Van Mooy et al., 2002; Keil et al., 2016). Cavan et al. (2017) indicate that vertical migration of zooplankton is inhibited due to the lower oxygen concentration, and up to 70% of the POC remineralization inside the OMZs is owing to microbial degradation. Nonetheless, this effect in the less POC flux attenuation is seen in large sinking particles (i.e. >100 μm), but in a recent study, the small particles (<100 μm) show attenuation rates equivalent or significantly higher in the OMZs relative to well-oxygenated waters in the North Atlantic (Rasse and Dall'Olmo, 2019). This finding highlights that more information about the processes controlling the fluxes of small and large particles is needed to understand the role of OMZs in the biological pump.

Several studies have been carried out to assess the biogeochemical dynamics of the particulate organic matter (POM) in the ocean based on stable isotopes (e.g. $\delta^{13}C_{POC}$ and $\delta^{15}N_{TPN}$; Jeffrey et al., 1983; Wada et al., 1987; Fisher, G., 1991; Smith et al., 2002; Lourey et al., 2004; Lara et al., 2010; Landrum et al., 2011; Garzon et al., 2016; MacKenzie et al., 2019). The isotopic signature of the $\delta^{13}C_{POC}$ depends on the physicochemical parameters such as temperature, partial pressure of CO_2 (pCO_2), pH, nutrient availability and physiological factors (i.e. growth rate), thus printing different isotopic values along latitudes (Rau et al., 1992; Lourey et al., 2004; Lara et al., 2010). Otherwise, $\delta^{15}N_{TPN}$ depends on the nitrogen source used for phytoplankton growth, and physiological conditions (Wada et al., 1987), and has been used as a proxy for surface water nitrate utilization (Laurey et al., 2003). Once POM begins to degrade, the isotopic signature change depending on the compounds that are being oxidized (i.e.

carbohydrates and proteins), and this has been used successfully to evaluate processes within the C and N cycle in the ocean.

Despite several authors have used stable isotopes in the POM to assess the biogeochemical dynamics in some critical areas of the ocean (e.g. Wada et al., 1987; Fisher, G., 1991; Smith et al., 2002; Lourey et al., 2004; Lara et al., 201; MacKenzie et al., 2019) few works are focused on the effect of the oxygen minimum layer on the stable isotope ($\delta^{13}C_{POC}$ and $\delta^{15}N_{TPN}$) of the sinking particles. Therefore, as part of the partnership project between Brazil and the National oceanographic Administration (NOAA): *Prediction and Research Moored Array in the Tropical Atlantic* (PIRATA), this work will be focused in the effect of the oxygen minimum layer in the POM dynamics in the northern tropical Atlantic based on $\delta^{13}C_{POC}$ and $\delta^{15}N_{TPN.}$ Besides, the possible effect of the oceanographic features (i.e. equatorial Ekman upwelling and the intertropical convergence zone) in the POM dynamics will be addressed.

2. Study Area: the north-western tropical Atlantic Ocean

This study is focused on the northern part of the tropical Atlantic (Fig. 1): where the ocean dynamics is regulated by a complex system of currents and countercurrents (Stramma and Schott, 1999). This region is considered as an end-member of the subtropical cells, where water masses subducted in the subtropics are upwelled by the Ekman divergence at the equator and flow poleward in the surface layers (Hazeleger and Drijfhout, 2006). In term of water masses, it is a complex region where the North Atlantic Central Water (NACW) and the South Atlantic Central Water (SACW) cross, while their distributions are density-compensated through a multitude of processes (Stramma and Schott, 1999; Stramma and England, 1999; Poole and Tomczak, 1999). Besides, subtropical mode waters formed in the subtropical fronts have important contributions to the central layer as showed by Azar et al. 2020, even indicating the influence of the Indian water to the Atlantic Ocean. Beneath this layer, denser but less saline water denoted by the Antarctic Intermediate Water (AAIW) is flowing northward. Therefore, the main thermocline is composed by the central layer and the upper part of the AAIW (Stramma and England, 1999; Stramma and Schott, 1999). At deeper levels (neutral isopycnal of 27.7 kg m^{-3}), flowing

southward, is the saltier and more oxygenated North Atlantic Deep Water (NADW), and moving northward, the Antarctic Bottom Water (AABW), which is in contact with the seafloor and cannot flows beyond the Mid Atlantic Ridge (Stramma and England, 1999; Ferreira and Kerr, 2017).

One important feature of the tropical North Atlantic is the intense and seasonal air-sea interaction. The timing and characteristics of the seasonal evolution of the location of the Intertropical Convergence Zone (ITCZ) and the sea surface temperature depend on coupled dynamics and land-sea contrasts (Stramma and Schott, 1999). The ITCZ displaced to the North (~ 10°N) in August and to the South (~ Eq-1°S) in February. The evolution and the position of the ITCZ define some physical (i.e. sea surface salinity and temperature) and biogeochemical (i.e. dissolve Fe, Al, Mn, and other micronutrients) characteristics in the upper ocean (Barrett et al., 2012; Schlosser et al., 2014; Baker and Jickells, 2017). Thus, it has been proposed that this supply of micronutrient through atmospheric deposition, set the distribution of diazotrophic *Trichodesmium spp.*, which are responsible for N_2 fixation, and the corresponding phosphorous depletion in surface waters (Schlosser et al., 2014).

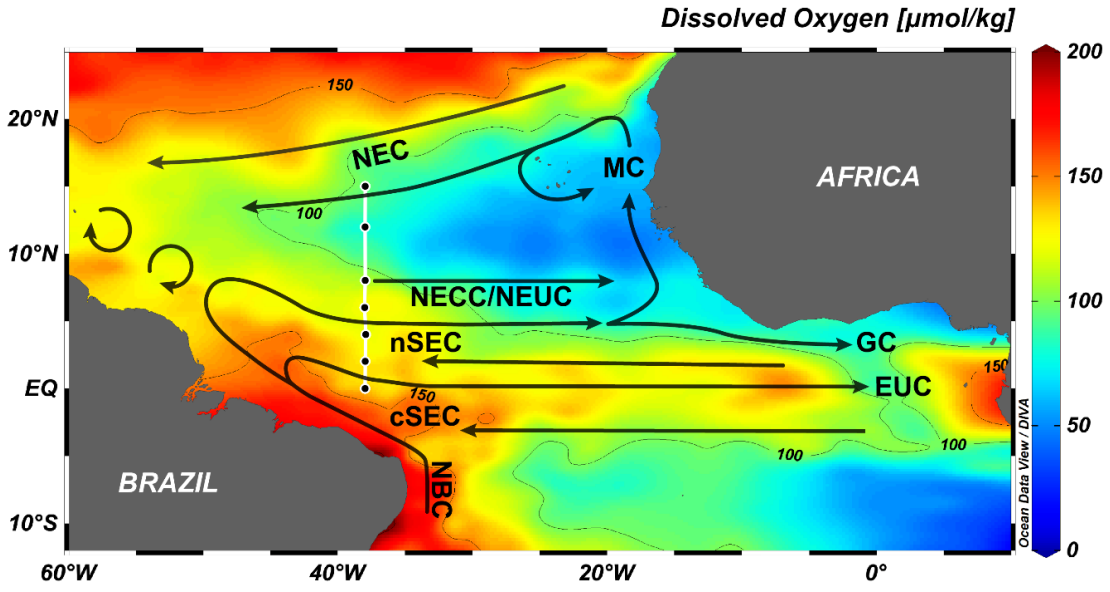

Figure 1. Oxygen concentration (µmol kg−1) in the tropical Atlantic at σ_θ = 27.1 kg m^{-3} as obtained from World Ocean Database 2018 (WOD18; Boyer et al., 2018; www.nodc.noaa.gov) with the main current system (Brandt et al., 2015) and the cruise (black line) imposed. The main currents (black arrows) are the

North Equatorial Current (NEC), the Mauritania Current (MC), the northern and central branches of the South Equatorial Current (nSEC and cSEC), the North Equatorial Countercurrent (NECC), the Guinea Current (GC), the North Brazil Current (NBC), the North Equatorial undercurrent (NEUC), and the Equatorial Undercurrent (EUC).

In the tropical Atlantic, there are two OMZs where the oxygen content is lesser than 60 μmol kg^{-1} (Karstensen et al., 2008; Stramma et al., 2008; Brandt et al., 2015). These are located on the eastern tropical North Atlantic (centered at 12ºN and 20ºW) and the eastern tropical South Atlantic (centered at 10ºS and 7ºE), marked as weakly ventilated shadow zones of the thermocline, as a consequence of the minimal replenishment of oxygenated waters (Luyten et al., 1983). Besides, the oxygen consumption within these regions is enhanced by the complex cycling of nutrients (Helly and Levin, 2004). These physical and biogeochemical factors control the supply and consumption of the oxygen content, which in recent decades has presented a substantial imbalance (e.g. 10% of the oxygen consumption had not been balanced by ventilation, Brandt et al., 2015). Thus, during the last 60 years, the oxygen concentration has decreased and vertically expanded between 300 to 700 m on these regions (Stramma et al., 2008; Santos et al., 2016; Hahn et al., 2017).

According to Stramma et al. (2005), the oxygen minimum in the eastern tropical North Atlantic is located at 400–500 m close to the isopycnal of 27.1 kg m^{-3} representing the water mass boundary between central water masses and the AAIW. The lowest oxygen values found (less than 50 μmol kg^{-1}) were located between 10.5°N and 12.5°N near 400 m depth. Hence, the OMZ in the North Atlantic exhibits oxygen concentration in the hypoxic range (Stramma et al., 2008).

3. Material and Methods

3.1 Sampling strategy

This study was conducted as part of the project titled Prediction and Research Moored Array in the Tropical Atlantic (PIRATA), which is an international collaborative between the United States of America (NOAA), France

(Meteo-France**,** CNRS e IFREMER), and Brazil (INPE and DHN). The sampling was carried out on board of the RV *Vital de Oliveira* between the 16th October and the 10th November 2018 in a meridional transect (38°W) from the Equator to 15°N (Fig. 1). This cruise embraced 14 oceanographic stations with a spatial resolution of about one degree of latitude, taking profiles of temperature, salinity, pressure, and dissolved oxygen. Additionally, in 7 oceanographic stations, discrete seawater samples were collected for chemical analysis including dissolved inorganic nutrients, particulate organic carbon (POC), particulate nitrogen, and their stable isotopes ($\delta^{13}C_{POC}$ and $\delta^{15}N_{TPN}$, respectively) using a CTD/Carrousel equipped with 24 twelve-litter Niskin bottles.

3.2 Chemical and isotopes analysis

Discrete samples of 100 mL for inorganic nutrients were taken and stored in plastic bottles, and immediately frozen at −20 °C until the samples were analyzed. To avoid possible contamination and considering the low turbidity in the region, samples were not filtrated but compensated using an untreated seawater sample as a reference as recommended by Hansen and Koroleff, (1999). Nitrate + nitrite, silicate, and phosphate were determined according to seawater standard manual methods by colorimetry with a detection limit of 0,4 µmol L^{-1}, 0,06 µmol $L^{-1,}$ and 0,03 µmol L^{-1}, respectively (Hansen and Koroleff, 1999).

Mostly 2-3 L aliquots were filtered on board through GF/F filters of 25 mm diameter to sampled the MOP in the water column (Whatman, pre-combusted at 450 °C, 4 h). Cautions were taken as recommended in the GEOTRACES protocols (Cutter et al., 2017; last seen on 08/20/2020, https://www.geotraces.org/methods-cookbook/) for the particulate material. Thus, Niskin bottles were gentle mixing before taking the aliquots, and the same process was applied for aliquots before filtration, which was carried out in a glove box. Finally, filters were immediately stored at -20 °C until analysis. Elemental and isotopes analysis were carried out with Thermo Scientific Delta V Advantage coupled to a Flash 2000 elemental analyzer. Inorganic carbon was removed by putting the filters under concentrated HCl vapor for a 24h period. For determination of stable $\delta^{13}C_{POC}$ and $\delta^{15}N_{TPN}$ isotopes, carbon and nitrogen

content, filters were dried at 60 °C for 12-h and completely oxidized in the elemental analyzer by combustion at temperatures above 1000 °C under pure O_2. The isotope composition of N_2 and CO_2 was then analyzed by mass spectrometry. Detection limit found for POC was 0.04 % and 0.02 % for TPN. Results relative to the Pee Dee Belemnite (PDB) and atmospheric N_2 standards, for carbon and nitrogen isotopes, respectively, according to Peterson and Fry (1987) and are expressed in part per mile (‰) related to the value of the standard as follow:

$$\delta\ (‰) = ((R_{sample} / R_{standard})\ - 1)\ * 1000$$

where *R* is equal to $^{13}C/^{12}C$ or $^{15}N/^{13}N$, both, in the sample and the standard.

3.3 Data Correction by Crossover Analysis

A crossover analysis (Lauvset and Tanhua, 2015) was applied to evaluate the consistency of the data (oxygen and nutrients) with previous cruises. This analysis allows an on-going and post-cruise data adjustment by comparing it with previous measurements near the assessed region. Comparison is made in the deep part of the water column (typically > 1500 m), where most of the parameters (i.e. salinity, oxygen, and nutrients) exhibit minors changes in the short temporal scale. The result is referred to as the offset, which is the mean weighted difference between several stations on two different cruises. This offset can be defined either as additive (i.e. salinity) or multiplicative (oxygen and nutrients) difference between the cruise being analysed and the referenced cruise. Thus, the parameters' profiles of the stations in the two cruises (separated for a defined radius) are interpolated and compared with the "running-cluster" routine (Tanhua et al. 2010). Therefore, the offset calculated for each parameter (assuming the reference cruise as the correct value) could be applied to adjust the data; for more detail see Lauvset and Tanhua (2015).

Here, the reference cruises were taken from the GLODAP.V2 data set (Olsen et al., 2016). The maximum radius used to compare was 3° and the depth was set to a minimum of 2000 m. It was possible to compare salinity and dissolved oxygen with 15 cruises, and dissolved inorganic nutrients with 5 cruises. Only oxygen and nutrient data displayed an offset, and for that reason,

these parameters were adjusted. Likewise, it was applied a data vertical interpolation using the "oce" package (Kelley and Richards, 2019) for R software (R Core Team, 2019) with the "Unesco" method. Two different vertical resolution was used, 50 m (from the surface to 1000 m) and 200 m (from 1000 m to 6000 m). The definition of the mixed layer depth (MLD) is based on potential density criterion (Lukas and Lindstrom, 1991), which determines the depth as where potential density varies in 0.1 kg m^{-3} compare to surface density. For graphical representation, most of the figures were completed using the freely available Ocean Data View® software (Schlitzer, 2019).

4. Results

4.1 Hydrographic setting and properties

Salinity varied from 34.50, associated with the fresh Antarctic Intermediate Water (AAIW), to 39.60 at the surface (Fig. 2a). In case of sea surface salinity, minimum values (~ 35.2) were found between 5°N and 10°N comparing to the highest values (~ 38) for both sides, southern and northern. Within this latitude, in the upper layer (thermocline) neutral density surfaces and isotherms become shallower (Fig. 2a-b). Likewise, the maximum value of the monthly accumulated precipitation in October 2018 was placed at this latitude (Fig. 2c). The mixed surface layer was shallow along the section, but displaying its lowest values (~ 15 m) between 5°N and 10°N. Otherwise, chlorophyll reaches its maximum (1.3 mg m^{-3}) between this latitude (Fig. 2d), being these values at the lowest depths. Thus, within the section, latitude range 5 - 10°N displayed specific hydrographic characteristics, where the ITCZ was placed during sampling.

4.2 Biogeochemical parameters

The main biogeochemical characteristics found are listed in table S1. Dissolved oxygen varies from 54.39 µmol kg^{-1} to 263.80 µmol kg^{-1}, displaying its minimum at 400m (Fig. 3). This core of minimum dissolved oxygen content is nearby the western limit of the Eastern Tropical North Atlantic OMZ (Fig. 1), which has been expanding in the last decades (Stramma et al., 2008). Thus, water column in the 300 - 600 m layer and 11-13°N (38°W) is characterized by values of oxygen lower than 75 µmol kg^{-1}. Phosphate, nitrate, and silicate are distributed

following water mass distribution, displaying the highest values in the pycnocline (i.e. 300 – 1000 m, Fig. 3). In surface water, phosphate and silicate exhibit little higher concentration in the range of 6 - 10°N compared to the rest of the surface waters, suggesting aeolian input. The relationship found for dissolved inorganic N:P was 14.50 (n = 55, $p < 10^{-12}$) in the entire section, very close to that reported by previous in the global ocean (i.e. 16 ± 1; Anderson and Sarmiento, 1994).

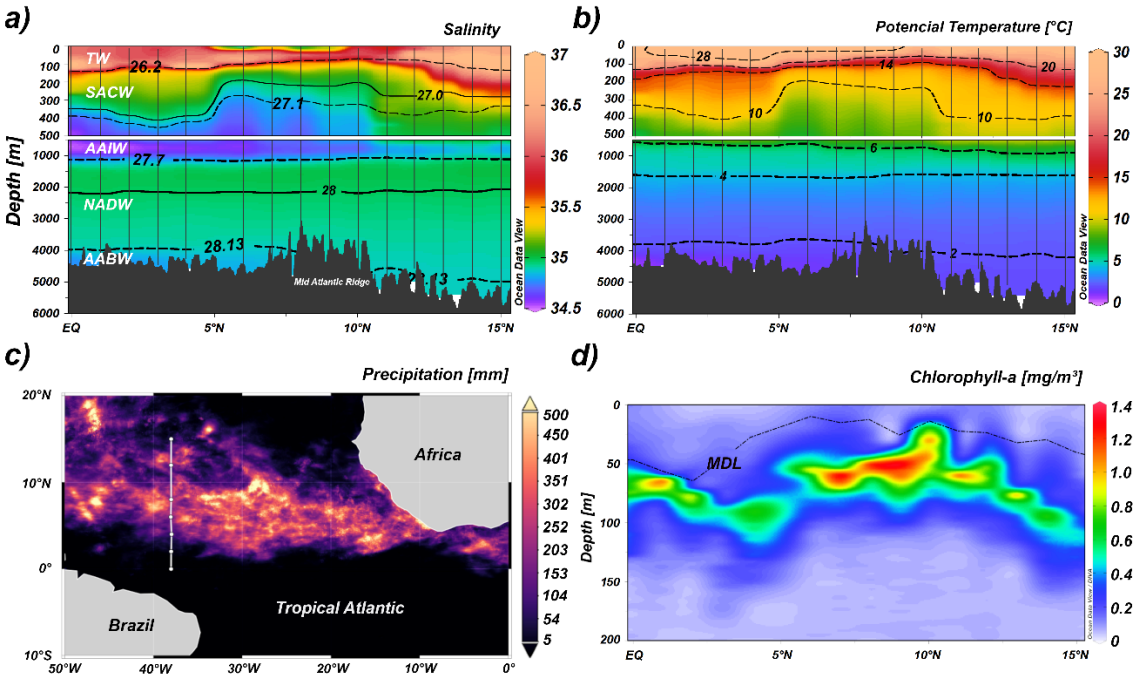

Figure 2. Hydrographic properties. Salinity (a), temperature (b), monthly accumulated precipitation for October 2018 (c), and Chlorophyll-a (d) in the meridional transect carried out in the tropical Atlantic. Dashed (water mass limits) and solid lines in (a) represent the neutral density (kg m^{-3}); the acronyms are as follows: Tropical Water (TW), South Atlantic Central Water (SACW), Antarctic Intermediate Water (AAIW), North Atlantic Deep Water (NADW), and Antarctic Bottom Water (AABW). Data on the monthly accumulated precipitation for October 2018 (c) was taken from NASA (https://giovanni.gsfc.nasa.gov/giovanni/). The mixed depth layer (MDL, d) was calculated following Lukas and Lindstrom, 1991.

POC and TPN overall decrease as depth increase in the region (Fig. 4). POC values agree with previous studies in the region (e.g. Jeffrey et al., 1983), and three main characteristics in the POC (0.98 – 5.19 µmol L^{-1}) distribution are

recognized: (i) higher surface values southernmost than northern, (ii) high values (~ 4 µmol L^{-1}) in the subsurface at 6 – 10°N and (iii) high values (~ 5 µmol L^{-1}) at depths greater than 1000 m at 11 – 13°N. Likewise, TPN (0.06 – 0.71 µmol L^{-1}) displays a similar behaviour, with values between 6°N and 10°N at the subsurface are not as high as for POC (Fig. 4). Overall, the atomic C:N ratio in the POM decrease as depth increase (Fig. 4d), but despite that, the atomic C:N relationship found for the entire region was 6.54 ($n = 54$, $p < 10^{-16}$) close to the Redfield ratio (i.e. 6.63, Redfield et al., 1963).

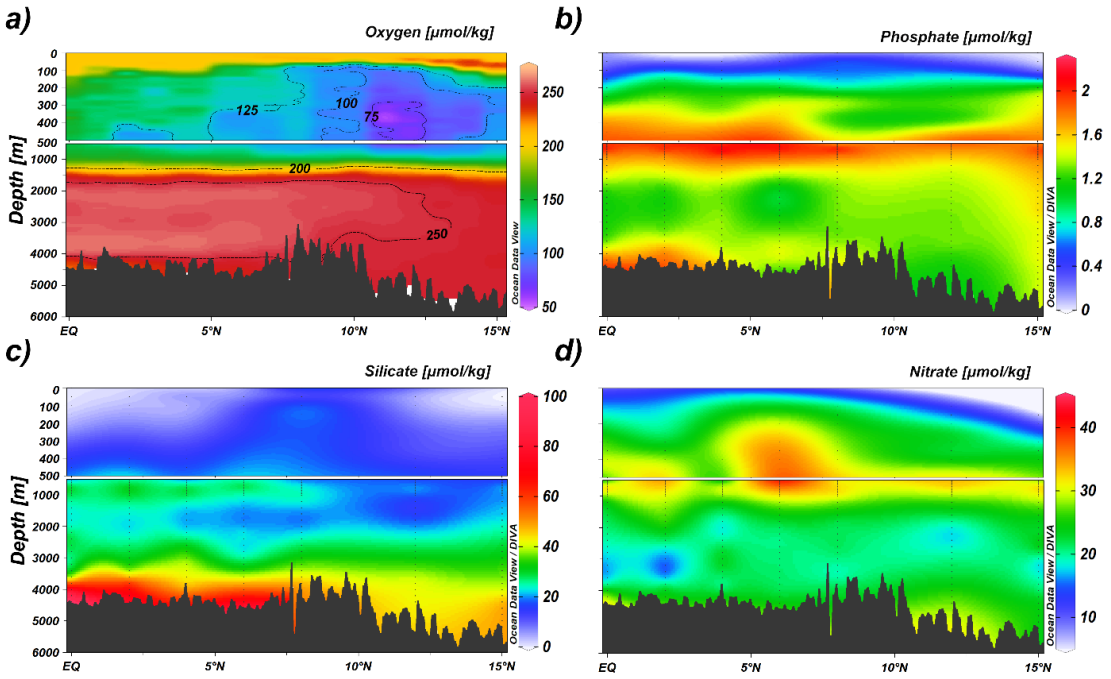

Figure 3. Biogeochemical properties obtained for the PIRATA cruise in October of 2018. Dissolve oxygen (a), phosphate (b), silicate (d), and nitrate (d).

Surface $\delta^{13}C_{POC}$ values vary around -22 ‰ (Table S1), while in the water column the $\delta^{13}C_{POC}$ becomes lighter as depth increase (Fig. 4). Values in latitudes higher than 7°N are a little heavier (~ -25.5 ‰) than those southern (~ -28 ‰), and beneath the oxygen-poor region (12°N) values are even close to -24 ‰. On the other hand, surface $\delta^{15}N_{TPN}$ values vary between 1 ‰ and 2 ‰ (Table S1, Fig. 4), but overall, $\delta^{15}N_{TPN}$ varies from 0.68 ‰, within the core of minimum oxygen content in the station at 12 °N, to 6.76 ‰ in the deepest sample of the same station.

5. Discussion

5.1 Hydrographic conditions

Significant differences in physical-chemical properties (i.e. temperature, salinity, and oxygen) were observed along the survey (Fig. 2 and 3). Sea surface temperature (SST) and salinity (SSS) in this section respond to the air-sea interactions through the ITCZ. The low-pressure system of the ITCZ is characterized by a highly relative humid air (Philander et al., 1996; Schlosser et al., 2014), which was placed between 5°N and 10°N in the survey (data not shown), making the atmosphere warmer, and, therefore, displaying the highest SST (Fig. 2b). Likewise, the intense precipitation (represented by the monthly accumulated precipitation, Fig. 2c) over evaporation, explains the minimum SSS observed in the ITCZ latitude range (5° - 10°N). This air-sea interaction also affects the SACW and AAIW distribution. The Ekman divergence generated by the ITCZ, makes deeper waters comes to a lower depth (Hazeleger and Drijfhout, 2006), raising the thermocline, the MDL and the biological productivity (represented by chlorophyll) to shallower depths (Fig.2d). On the other hand, the oxygen content responds to a complex balance of consumption and supply. Beyond 10°N (100 – 1000 m), there is no lateral oxygen supply by an eastward current (Fig. 1), which is generally associated with elevated oxygen content (Brandt et al., 2015), turning this area poor in oxygen.

5.2 POM and isotope variability

POC and TPN correlated significantly in the entire section ($r = 0.90$, $n = 54$, $p < 0.001$, Fig. 5), indicating that most of PN is in the organic form (PON). Individual values are lower than higher latitudes (e.g Lara et al., 2010; Barrera et al., 2017; Huang et al., 2018), indicating the relatively low production in surface waters in this area. The linear function to describe POC and TPN covariance was *POC = 6,50*TPN + 1.24,* very close to the encountered for the global ocean (POC = 6.17*PON + 1.24; Huang et al., 2018). In surface waters the C:N was determined by primary production (values closer to the Redfield ratio) as several studies suggest (e.g. Honjo et al., 2008; De la Rocha and Passow, 2014).

Otherwise, the vertical C:N variation has been debated for several authors (e.g Anderson and Sarmiento, 1994; Canva et al., 2017; Huang et al., 2018), indicating that the depth dependence of C:N ratio in global data is weak (Huang et al., 2018). In contrast, our results along with previous studies (Engel et al., 2017), show important vertical variations (Fig. 4). This vertical variation is likely associated with preferential consumption of nitrogen organic compounds, mainly amino acids.

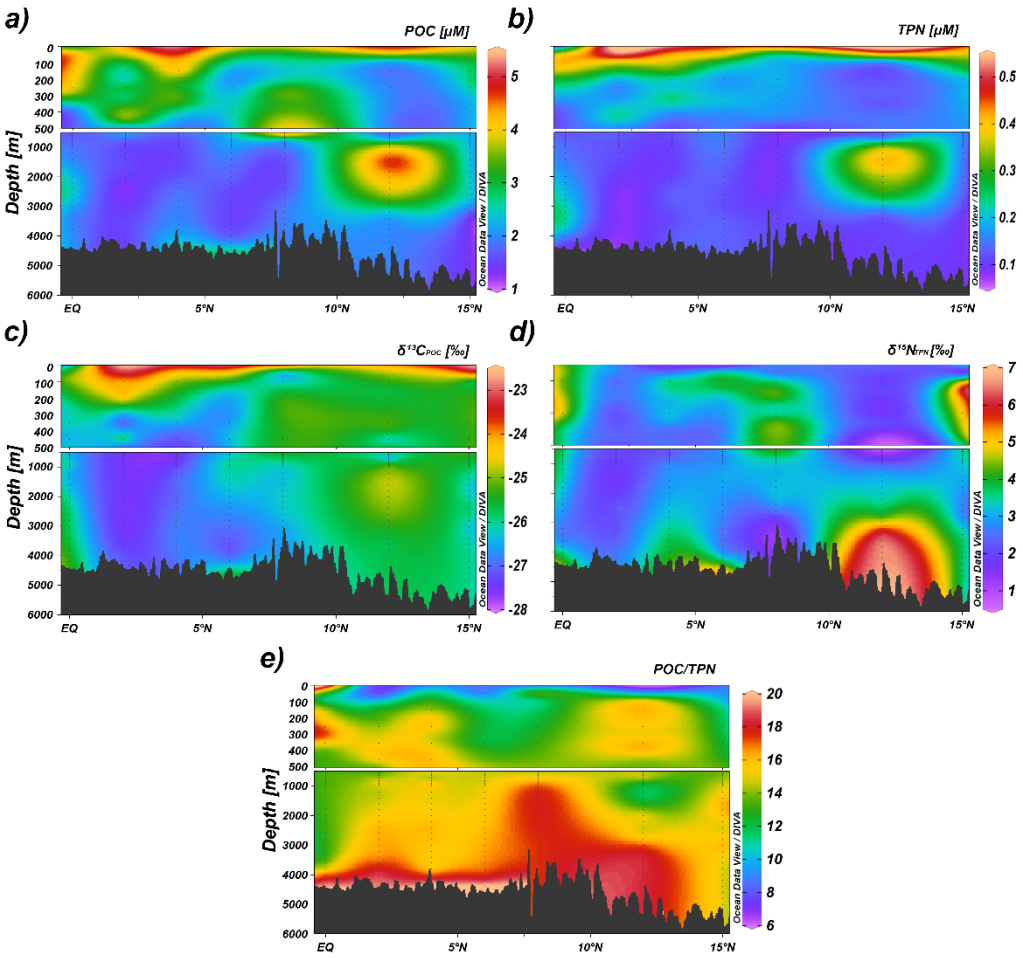

Figure 4. Particulate matter content and their isotope ratios along the meridional transect. Particulate organic carbon (a), total particulate nitrogen (b), $\delta^{13}C_{POC}$ (c), $\delta^{15}N_{TPN}$ (d), and the C:N ratio in the particulate organic matter (f).

Surface $\delta^{13}C_{POC}$ values found along the transect are similar to those reported by previous studies for low or mid-latitudes (e.g. Degens, E., 1969;

Jeffrey et al., 1983; Fischer et al., 1996), but heavier than those found in surface water at higher latitudes (e.g Lourey et al., 2004; Lara et al., 2010). This variance is due to the different properties (i.e. temperature, pCO_2, nutrients availability, among others) and ecosystems found on the ocean's surface (Rau et al., 1992; Lourey et al., 2004; Lara et al., 2010). Otherwise, surface $\delta^{15}N_{TPN}$ values were close to those reported at the subtropical North Atlantic (i.e. about 32°N, Landrum et al., 2011) and those found in the sediment traps within the tropical and subtropical Atlantic (Holmes et al., 2003).

$\delta^{13}C_{POC}$ shows a mid-correlation with POC ($r = 0.68$, $n = 54$, $p < 0.001$, Fig. 5), but a higher correlation with TPN ($r = 0.80$, $n = 54$, $p < 0.001$, Fig. 5), which suggest that the isotopic values in the POM ($\delta^{13}C_{POC}$) are sensitive to nitrogen organic consumption, since the particulate hydrolysable amino acids compound are the most labile components in the POM (Engel et al., 2017). $\delta^{13}C_{POC}$ also display, but in this case, negative mid-correlation with C:N and phosphate ($r = -0.63$, $n = 54$, $p < 0.001$, Fig. 5). This supports that $\delta^{13}C_{POC}$ values are likely associated with the organic matter that is easily consumed.

The $\delta^{13}C$ values of the manly biochemical components of marine phytoplankton were proposed by Degens, (1969). He indicated that each component (i.e. proteins, total carbohydrates, lipids) has different values of $\delta^{13}C$, depending on the isotopic fractionation efficiency at the moment of formation during photosynthesis, making the $\delta^{13}C$ values of the living marine plankton (between -19 ‰ and -23‰). Based on that, proteins and carbohydrates are isotopically heavier than lipids, therefore, as POM is consumed along its pathway to deeper waters, labile compounds such as proteins are preferentially degraded compared to the more refractory lipids (Eadie and Jeffrey, 1973), leaving the remaining POM isotopically lighter. This has been proposed by several authors (Eadie et al., 1978; Jeffrey et al., 1983; Lourey et al., 2004), thus, our results can be explained taking this into account.

Otherwise, $\delta^{15}N_{TPN}$ shows no correlation with any physical-chemical parameters. Based on the available data, it is no possible to make a consistent interpretation, corroborating the complexity of the nitrogen cycle and highlighting the need of further studies to its better comprehension.

5.2.1 OMZ and ITCZ influence

Previous studies have demonstrated the potential reduction in remineralization rates of the POM within OMZ (i.e. less attenuation in the POM fluxes, Devol & Hartnett, 2001; Van Mooy et al., 2002; Roullier et al., 2014; Engel et al., 2017; Cavan et al., 2017; Rasse and Dall'Olmo, 2019). This less attenuation has different biogeochemical implications based on the oxygen content (Van Mooy et al., 2002; Roullier et al., 2014; Engel et al., 2017), i.e Pacific OMZ (suboxic < 5 µmol kg^{-1} O_2) and Atlantic OMZ (Hypoxic ~ 60 – 120 µmol kg^{-1} O_2). As mentioned above, the cruise crosses the limit of the Eastern Tropical North Atlantic OMZ, where the values of dissolved oxygen were lesser than 100 µmol kg^{-1} in the latitude range of 10°N – 14°N (Fig. 2). At this latitude, just beneath the OMZ (~ 1000 – 2000 m) high values of POC and TPN (similar to those at the surface) were found (Fig. 4). This indicates a complex coupling between the production and export of the POM within this zone and likely reduces remineralization rates inside the OMZ. For instance, Engel et al. (2017) found that transparent exopolymer particles exhibited a higher export efficiency than other components (in the tropical Atlantic). They could be affected by several processes like new production, abiotically or by bacteria, during solubilization and degradation of sinking particles; or capture of transparent exopolymer by sinking aggregates; among other processes. More recently, Rasse and Dall'Olmo (2019) found a permanent layer of small particles, presumably linked to microbial communities, which can play a critical role in the attenuation of POM fluxes (i.e. reducing remineralization rates and exporting more POM to deeper zones).

$\delta^{13}C_{POC}$ vertical values northern than 10° N were isotopically heavier than those found southern. This suggests, and is taken as strong evidence, that in this area remineralization rates are lesser compare to southern oxygenated waters, having in mind that the more efficient the POM is consumed, the more isotopically lighter is the POC remaining in the water column. The decrease in remineralization in the POM inside this OMZ is rather complex, but it has been recently proposed that changes in the zooplankton behaviour have a critical impact on this subject (Canva et al., 2017). Since zooplankton could fragment roughly half of the fast-sinking particles, of which more than 30 percent may be

released as suspended and slowly sinking matter to be consumed by microbes (Giering et al., 2014). Thus, the reduce daytime depth of the diel vertical migrators and the low resident populations within the oxygen-poor areas (Canva et al., 2017) have a critical impact on the remineralization of the sinking POM.

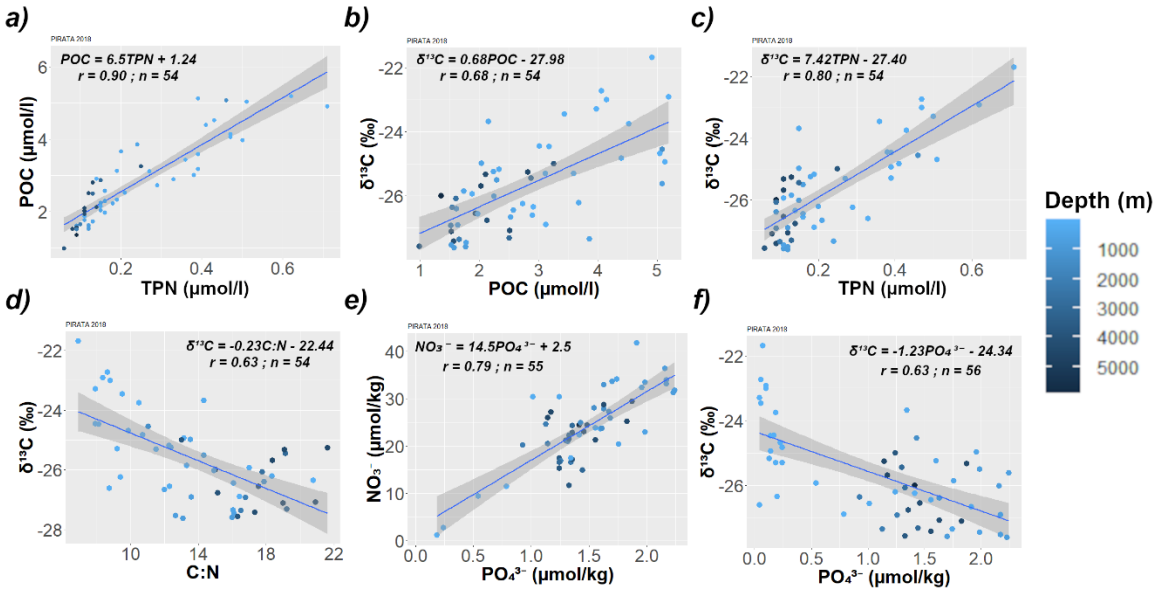

Figure 5. Main linear regressions of the biogeochemical parameters analyzed (a-f). The color scale depicts the depth at which the samples were taken. The shaded areas indicate the confidence interval (95 %) of each regression. Equation of each regression can be observed inside panels.

The position of the ITCZ also affects the distribution and the efficiency of the biological pump and the $\delta^{13}C_{POC}$ values. Along the transect the position of the ITCZ was marked by the band of maximum precipitation (Fig. 2) and the relative humid air (data not show), thus, placing it in the latitude range between 5°N and 10°N. Inside this range, specifically at 8°N in the 250 – 600 m layer, it was found high POC and low remineralization level exhibited by $\delta^{13}C_{POC}$ values (Fig. 4), and higher values of silicate and phosphate in the surface. It is well known that the particles coming from the Sahara dust are rapidly scavenged by the intense precipitation within this band (Schlosser et al., 2014). Once the particles are in the ocean, they could act as ballast and to increase the POM sinking velocity (Honjo et al., 2008; De la rocha and Passow, 2014) raising the POC at deeper waters. Previous studies have found pulses of small particles linked to the elevated precipitations and low wind stress, i.e. influenced by the ITCZ (e.g.

Barrett et al., 2012; Schlosser et al., 2014; Rasse and Dall'Olmo, 2019), showing the importance of this feature in the efficiency of the biological pump.

5.3 Main drivers of $\delta^{13}C_{POC}$ variability

Isotopic fractionation during marine phytoplankton's photosynthesis depends on several variables such as temperature, pCO_2, pH, and physiological factors (i.e. growth rate, Degens, 1969; Rau et al., 1992, Lourey et al., 2004; Lara et al., 2010). Based on that, many authors have been tried to found the best relationship and fit between surface $\delta^{13}C_{POC}$ and physicochemical variables in different latitudes and ecosystems (Rau et al., 1991 and 1992; Lara et al., 2010; Barrera et al., 2017).

In this work, as the aim was vertical $\delta^{13}C_{POC}$ variation, and no significant SST variation were registered, it was carried out a multiple regression model with the main variable affecting the isotopic values in the entire section (Fig. 6). The outcome explains the 66% of the variance using phosphate, POC, and TPN as independent variables, being the latter the most significant ($p < 0.001$) within the model. This supports that the consumption of nitrogen organic compounds in the sinking organic particles in the thermocline is controlling the $\delta^{13}C_{POC}$ values in the remaining POM. Besides, environmental features like the dust deposition along the ITCZ, which increase the ballast effect in the sinking POM, also constitute an important effect in the distribution of the $\delta^{13}C_{POC}$, since the ITCZ position is dynamic along the year. Lastly, the OMZ influence on the $\delta^{13}C_{POC}$ has to be considered when the POM system is studied in the tropical ocean, since the reduction in the remineralization rates (i.e. lesser flux attenuation), likely associated to zooplankton behaviour, is critical.

6. **Conclusion**

The hydrographic properties (i.e. temperature, salinity, oxygen, and nutrients) and sinking POM (and $\delta^{13}C_{POC}$) in the tropical Atlantic showed an integrated complex scheme involving the air-sea interactions through the low-pressure system of the ITCZ, the oceanographic current system that maintains the OMZ, and the consumption of the POM. Two main effects of the ITCZ were evidenced, (i) the Ekman divergence at the equator, raising the isopycnals

roughly 200 m in the 5°-10°N latitude, making shallower (and higher) the maximum chlorophyll values; and (ii) The input of terrigenous particles from the Sahara dust, which likely enhance the ballast effect on the POM, increasing the sinking velocity, and reducing the possibility of the POM being consumed (greater values of $\delta^{13}C_{POC}$).

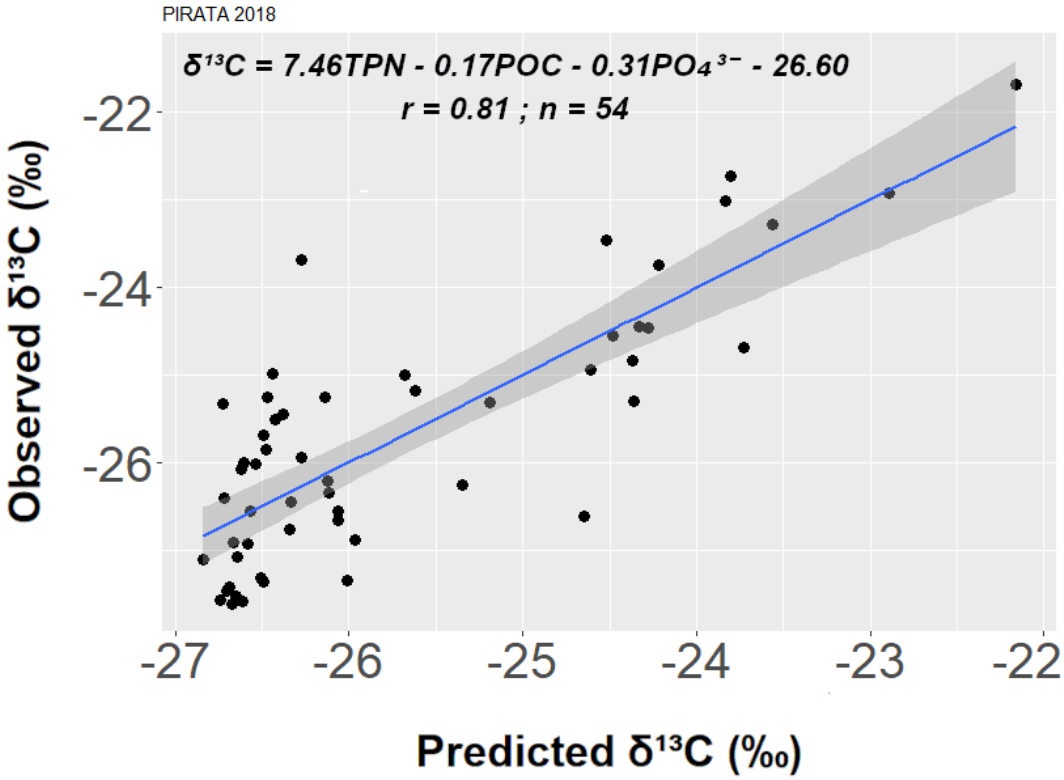

Figure 6. Relationship of the measured $\delta^{13}C$ in particulate organic matter vs. predicted $\delta^{13}C$ values from a multiple regression model using particulate nitrogen, particulate organic carbon, and phosphate content as independent variables. The shaded area represents 95 % of the confidence interval of the model output.

The $\delta^{13}C_{POC}$ of the sinking particles in the OMZ and beneath it, is the result of the likely reduction in the remineralization rate (i.e. less attenuation flux), probability in response to changes in the zooplankton behaviour due to poor oxygen content, as previous recent studies have pointed. In the current study the C:N ratio increase with deep, suggesting that nitrogen organic compounds are preferably consumed over the rest of the organic matter. This is supported by the multiple regression model, where the main independent variable affecting the $\delta^{13}C_{POC}$ values is the TPN, following by the POC and the phosphate content.

Further works are encouraged on this subject with a better spatial and temporal resolution to elucidate the main variables affecting the $\delta^{15}N_{TPN}$ and the dynamic of the ITCZ position on the POM. It worth noting that the low concentration of dissolved oxygen found during the cruise of this work follows the main conclusion of previous work on the expansion of the OMZ in the tropical regions. Thus, progress in this direction will help to better understand the role of the OMZs in the POM consumption, and, therefore, in the efficiency of the biological carbon pump.

Supplementary Material II

Table S1. Dissolved Oxygen (DO), phosphate (PO_4^{3-}), silicate ($SiOH_4^{4-}$), nitrate (NO_3^-), particulate organic carbon (POC), particulate nitrogen (TPN), carbon and nitrogen ratio (C:N), and stable carbon and nitrogen isotopic composition ($\delta^{13}C$ and $\delta^{15}N$) in the tropical Atlantic Ocean in October of 2018.

Latitude (°N)	Depth (m)	DO (µmol/kg)	PO_4^{3-} (µmol/kg)	$SiOH_4^{4-}$ (µmol/kg)	NO_3^- (µmol/kg)	POC (µmol/L)	TPN (µmol/L)	C:N	$\delta^{13}C$ (‰)	$\delta^{15}N$ (‰)
15.00	5	206.36	0.06	0.58	na	4.06	0.47	8.59	-22.73	3.47
	53	224.00	0.06	0.38	na	3.43	0.36	9.40	-23.46	1.24
	84	227.84	0.04	0.49	na	2.89	0.33	8.69	-26.61	2.96
	120	186.05	0.24	0.87	2.76	3.11	0.27	11.38	-25.31	6.76
	350	102.48	1.60	11.03	23.63	2.23	0.18	12.09	-25.25	4.70
	746	120.73	1.99	20.98	33.41	2.29	0.16	14.23	-25.51	3.35
	1350	192.69	1.67	17.96	27.22	na	na	na	na	na
	3000	247.54	1.44	31.33	14.89	2.50	0.13	19.13	-27.32	2.56
	4200	245.50	1.49	43.53	24.39	na	na	na	na	na
	5922	247.26	1.41	48.81	24.39	1.35	0.09	15.37	-26.00	3.73
11.98	12	209.32	0.10	0.73	na	5.19	0.62	8.42	-22.92	4.03
	60	188.75	0.19	0.85	1.16	3.59	0.39	9.13	-25.30	1.81
	70	143.06	0.54	1.76	9.38	1.87	0.11	16.82	-25.94	2.64
	445	64.77	1.96	14.77	32.39	2.03	0.15	13.86	-24.98	0.68
	815	121.57	1.70	21.29	33.61	1.76	0.11	16.13	-27.59	1.62
	1400	222.11	1.43	12.66	24.86	5.08	0.46	11.15	-24.55	3.08
	2300	250.55	1.34	23.52	16.54	na	na	na	na	na
	3000	252.68	1.30	31.50	21.21	2.87	0.15	18.62	-25.45	3.90
	3900	248.86	1.36	44.08	22.86	na	na	na	na	na
	4560	247.25	1.17	41.58	27.17	2.02	0.11	18.13	-25.69	6.55
8.01	5	208.87	0.04	23.82	na	3.97	0.50	7.91	-23.29	2.93
	41	218.37	0.79	2.26	11.48	3.12	0.19	16.42	-26.89	1.98
	73	122.12	1.41	30.78	22.30	2.73	0.29	9.33	-26.25	3.20
	209	122.42	0.13	17.89	na	2.33	0.19	12.12	-25.18	4.88
	673	108.23	2.24	20.27	31.79	5.08	na	na	-25.62	na
	1100	167.30	1.63	26.25	32.94	1.61	0.09	17.08	-26.40	3.02
	1800	255.29	1.31	16.60	20.93	na	na	na	na	na
	2700	255.57	1.33	29.15	22.25	1.60	0.09	16.92	-26.08	3.36
	3600	256.37	1.24	40.98	17.44	na	na	na	na	na
	4233	250.81	1.46	49.68	23.06	1.93	0.11	18.08	-26.55	1.36
6.00	5	207.16	0.10	0.15	na	4.14	0.47	8.81	-23.01	1.05
	53	195.39	0.14	1.82	na	3.17	0.39	8.07	-24.47	3.89
	178	128.20	1.01	12.54	30.34	1.97	0.16	12.27	-26.56	4.03
	393	106.33	1.91	19.84	41.75	2.52	0.21	12.25	-26.66	2.58
	764	138.90	2.16	30.29	36.39	2.24	0.15	15.17	-26.02	3.19
	1300	196.18	1.63	22.79	27.84	na	na	na	na	na
	2140	259.72	0.93	15.82	20.22	1.54	na	na	-26.36	na
	3400	260.15	1.33	33.50	21.46	na	na	na	na	na
	4250	244.68	1.56	65.09	21.29	1.56	0.09	17.11	-27.42	2.44

	4538	240.59	1.14	77.26	25.93	2.81	0.13	21.05	-25.26	5.31
4.00	16	206.41	0.19	21.00	na	4.52	0.43	10.54	-23.75	1.03
	90	202.68	0.14	0.78	na	5.13	0.39	13.00	-24.94	3.90
	360	138.94	1.56	11.94	23.83	2.57	0.16	16.04	-26.45	2.21
	554	110.73	1.99	19.60	22.92	1.77	0.11	16.27	-27.46	2.70
	809	141.40	2.23	30.08	31.26	1.57	0.12	13.57	-27.62	1.85
	1250	191.00	1.69	25.34	25.83	na	na	na	na	na
	2040	260.84	1.26	18.88	16.80	1.51	0.09	16.87	-26.93	3.10
	2940	253.18	1.36	37.02	24.32	na	na	na	na	na
	4000	255.81	1.36	44.54	17.16	2.12	0.14	14.86	-26.77	3.89
	4256	243.79	1.63	59.34	28.72	2.51	0.12	21.49	-27.08	4.10
2.01	14	206.25	0.07	0.72	na	4.91	0.71	6.95	-21.69	3.51
	84	189.69	0.17	1.45	na	3.01	0.38	7.93	-24.45	2.25
	249	140.11	1.34	9.99	17.47	2.15	0.15	13.96	-23.68	2.95
	458	103.80	1.74	19.81	34.08	3.85	0.24	15.99	-27.35	2.13
	760	153.58	2.17	32.01	33.16	1.52	0.12	12.48	-27.53	2.03
	1350	202.14	1.54	26.21	28.03	na	na	na	na	na
	2105	260.36	1.13	21.29	24.64	1.65	0.10	16.50	-27.36	1.47
	2940	255.31	1.24	31.24	16.59	na	na	na	na	na
	3714	262.68	1.33	33.82	11.70	0.98	0.06	15.10	-27.57	2.73
	4440	230.19	1.83	72.86	25.16	1.52	0.08	18.67	-27.11	2.67
-0.01	5	206.55	0.20	0.76	na	2.91	0.14	21.47	-26.35	4.36
	69	205.66	0.23	0.81	na	5.04	0.51	9.80	-24.69	4.84
	103	206.47	0.24	0.67	na	4.39	0.41	10.76	-24.83	4.28
	289	143.49	1.24	8.46	30.38	3.67	0.20	18.83	-26.21	4.99
	393	151.18	1.76	14.48	20.38	1.73	0.13	13.79	-25.86	3.59
	756	154.85	2.17	30.39	33.91	1.63	0.12	14.08	-26.91	3.80
	1250	196.24	1.61	25.37	23.76	na	na	na	na	na
	2193	261.05	1.14	21.08	20.53	na	na	na	na	na
	3815	262.07	1.24	34.79	15.31	3.25	0.25	12.85	-25.00	2.34
	4430	227.83	1.87	97.95	29.44	2.10	0.11	19.06	-25.33	4.24

CAPÍTULO V:

Síntese da discussão e conclusões

Os principais resultados desta dissertação foram divididos em dois manuscritos, o primeiro com foco na quantificação da contribuição das águas subtropicais modais nas camadas centrais do oceano Atlântico Tropical e o segundo, abordando a dinâmica da MOP em função dos processos oceanográficos através de um transecto meridional (38°W), desde o equador até 15°N. O primeiro manuscrito permitiu descrever, quantificar, e atualizar a dinâmica das massas de água dentro da picnoclina através da análise otimizada com parâmetros múltiplos utilizando o banco de dados do *World Ocean Database 2018*.

No Hemisfério Norte, a contribuição da EDW, esta confinada nas camadas mais rasas da Água Central do Atlântico Norte (ACAN). Sua distribuição espacial segue a Corrente Equatorial do Norte, e sua contribuição está restrita principalmente nos níveis isopicnais superiores a 26,6 kg m^{-3}. Já a *Madeira Mode Water* (MMW) (~ 27,0 kg m^{-3}), contribui principalmente nos níveis mais

profundos, sendo o limite leste entre a ACAN e a Água Central do Atlântico Sul (ACAS) marcado em torno a 10°N. Estimativas da contribuição das águas modais à ACAN permitiram reforçar o conhecimento da mistura das massas de água nesta região, onde estudos prévios não foram capazes de ter uma boa resolução em níveis superiores devido aos resíduos de conservação de massa elevados.

No Hemisfério Sul, as principais contribuintes para a camada da ACAS são a *Subtropical Mode Water of 18°C* ($STMW_{18}$), que é superficialmente distribuída pela Corrente de Benguela e a Corrente Sul Equatorial, e a *Subtropical Mode Water of 12°C* ($STMW_{12}$) restrita à parte sul do giro subtropical. Além disso, a $STMW_{12}$ é a principal contribuinte nas isopicnais maiores que 26,4 kg m^{-3}, e é misturada com a *Subtropical Mode Water of 14°C* ($STMW_{14}$) e a *Subtropical Indian Mode Water* (STIMW) na região zonal que vai de 20ºS a 30ºS. Dentro desta zona, a influência da STIMW é importante atingindo contribuições à mistura de até 80%, e exibindo uma distribuição oblíqua (em profundidade) associada com o deslocamento isopicnal em direção ao noroeste dos vórtices. Com base nesses resultados, é revelado o esquema de mistura das principais variedades das águas modais na ACAS, ampliando e apoiando estudos anteriores neste tema.

Segundo as análises feitas pode-se inferir que a fonte da STIMW como contribuição à ACAS está associada aos vórtices das Agulhas formados na zona de retroflexão da Corrente das Agulhas. Os resultados são consistentes e suportados pelos dois conjuntos de dados diferentes avaliados, permitindo a detecção de 58 vórtices usando o banco de dados AVISOme (de 1993 a 2019) e 55 vórtices utilizando o banco do TOeddies (de 1993 a 2017), que foram amostrados por transectos oceanográficos. Com base nisso, as principais massas de água que contribuem para a camada central mais quente que 9ºC são a $STMW_{12}$ (~ 45%), a STIMW (~ 34%) e a $STMW_{14}$ (~ 18%). Além disso, não há diferença significativa entre os vórtices ciclônicos e anticiclônicos em relação à contribuição da STIMW. Por esse motivo, acredita-se que na evolução dos vórtices das Agulhas iniciais, estes podem gerar outras estruturas de mesoescala com uma contribuição dessa variedade de massa de água à ACAS.

Além disso, foi possível obter uma estimativa média aproximada de 5,5 ± 3,2 Sv entrando no Atlântico Sul, levando em consideração apenas os vórtices das Agulhas e assumindo que eles são transportados principalmente pela Corrente de Benguela.

Já no segundo manuscrito, os resultados pertencem ao transecto meridional realizado em outubro do 2018. Neste, as propriedades hidrográficas (temperatura, salinidade, oxigênio, e nutrientes) junto com a MOP e os seus isótopos estáveis analisados mostraram uma integração de processos envolvendo as interações atmosfera-oceano (através da zona de convergência intertropical, ZCIT), o sistema de correntes que mantem a ZMO, e o consumo da MOP que está se afundando. Dois efeitos principais da ZCIT foram evidenciados, (i) a divergência de Ekman no Equador, que eleva as isopicnais em cerca de 200 m na faixa de latitude 5°-10°N, tornando mais rasos (e mais altos) os valores de clorofila; e (ii) a possível entrada de partículas terrígenas da poeira do Sahara, que provavelmente aumentam o efeito de lastro no MOP, incrementando a velocidade de afundamento e reduzindo o consumo da MOP (valores maiores de $\delta^{13}C_{COP}$).

Os valores de $\delta^{13}C_{COP}$ das partículas que estão assentando na ZMO e abaixo dela, são o resultado da provável redução na taxa de remineralização (menor fluxo de atenuação), surgindo que provavelmente seja resposta das mudanças no comportamento do zooplâncton devido ao baixo teor de oxigênio dissolvido, conforme indicado por estudos recentes. Por outro lado, a razão C:N aumenta com a profundidade, sugerindo que os compostos orgânicos de nitrogênio são consumidos preferencialmente sobre o resto da matéria orgânica. Isso é suportado pelo modelo de regressão múltipla, onde a principal variável independente que afeta os valores de $\delta^{13}C_{COP}$ é o nitrogênio total particulado (NTP), seguida pelo carbono orgânico particulado (COP) e pelo conteúdo de fosfato.

Novos trabalhos são encorajados sobre este assunto com uma melhor resolução espacial e temporal, a fim de elucidar as principais variáveis que afetam o $\delta^{15}N_{NTP}$ e a dinâmica da posição ZCIT na MOP. Assim, o avanço nesta

direção ajudará a entender melhor o papel das ZMO no consumo da MOP e, portanto, na eficiência da bomba de biológica.

Referências bibliográficas

Anderson, L. a, Sarmiento, J.L., 1994. Redfield ratios of the remineralization determined by nutrient data analysis. Global Biogeochem. Cycles 8, 65–80. https://doi.org/10.1029/93GB03318.

Azevedo, J.L.L., Mata, M.M., 2010. O mecanismo de autopropulsão de vórtices oceânicos: uma revisão. Revista Brasileira de Geofísica 28 (3), 153–172.

Baker, A.R., Jickells, T.D., 2017. Atmospheric deposition of soluble trace elements along the Atlantic Meridional Transect (AMT). Prog. oceanogr. 158, 41–51. https://doi.org/10.1016/j.pocean.2016.10.002

Ballalai, J.M., Santos, T.P., Lessa, D.O., Venancio, I.M., Chiessi, C.M., Johnstone, H.J.H., Kuhnert, H., Claudio, M.R., Toledo, F., Costa, K.B., Albuquerque, A.L.S., 2019. Tracking Spread of the Agulhas Leakage Into the Western South Atlantic and Its Northward Transmission During the Last Interglacial. Paleoceanogr. Paleoclimatology 34, 1744–1760. https://doi.org/10.1029/2019PA003653

Barrera, F., Lara, R.J., Krock, B., Garzón-Cardona, J.E., Fabro, E., Koch, B.P., 2017. Factors influencing the characteristics and distribution or surface organic matter in the Pacific-Atlantic connection. J. Mar. Syst. 175, 36–45. https://doi.org/10.1016/j.jmarsys.2017.07.004

Barrett, P.M., Resing, J.A., Buck, N.J., Buck, C.S., Landing, W.M., Measures, C.I., 2012. The trace element composition of suspended particulate matter in the upper 1000m of the eastern North Atlantic Ocean: A16N. Mar. Chem. 142–144, 41–53. https://doi.org/10.1016/j.marchem.2012.07.006

Biastoch, A., Böning, C.W., Schwarzkopf, F.U., Lutjeharms, J.R.E., 2009. Increase in Agulhas leakage due to poleward shift of Southern Hemisphere westerlies. Nature 462, 495–498. https://doi.org/10.1038/nature08519.

Boyer, T.P., O.K. Baranova, C. Coleman, H.E. Garcia, A. Grodsky, R.A. Locarnini, A.V. Mishonov, C.R. Paver, J.R. Reagan, D. Seidov, I.V. Smolyar, K.W. Weathers, M.M. Zweng (2018). World Ocean Database 2018. A. V. Mishonov, Technical Editor, NOAA Atlas NESDIS 87. www.nodc.noaa.gov

Brandt, P., Bange, H.W., Banyte, D., Dengler, M., Didwischus, S.H., Fischer, T., Greatbatch, R.J., Hahn, J., Kanzow, T., Karstensen, J., Körtzinger, A., Krahmann, G., Schmidtko, S., Stramma, L., Tanhua, T., Visbeck, M., 2015. On the role of circulation and mixing in the ventilation of oxygen minimum zones with a focus on the eastern tropical North Atlantic. Biogeosciences 12, 489–512. https://doi.org/10.5194/bg-12-489-2015

Casanova-Masjoan, M., Pelegrí, J.L., Sangrà, P., Martínez, A., Grisolía-Santos, D., Pérez-Hernández, M.D., Hernández-Guerra, A., 2017. Characteristics and evolution of an Agulhas ring. J. Geophys. Res. Ocean. 122, 7049–7065. https://doi.org/10.1002/2017JC012969.

Castellanos, P., Campos, E.J.D., Piera, J., Sato, O.T., Silva Dias, M.A.F., 2017. Impacts of Agulhas leakage on the tropical Atlantic western boundary systems. J. Clim. 30, 6645–6659. https://doi.org/10.1175/JCLI-D-15-0878.1.

Carvalho, A. da C. de O., Mendes, C.R.B., Kerr, R., Azevedo, J.L.L. de, Galdino, F., Tavano, V.M., 2019. The impact of mesoscale eddies on the phytoplankton community in the South Atlantic Ocean: HPLC-CHEMTAX approach. Mar. Environ. Res. 144, 154–165. https://doi.org/10.1016/j.marenvres.2018.12.003

Cavan, E.L., Trimmer, M., Shelley, F., Sanders, R., 2017. Remineralization of particulate organic carbon in an ocean oxygen minimum zone. Nat. Commun. 8. https://doi.org/10.1038/ncomms14847

Cutter, G., Casciotti, K., Croot, P., Geibert, W., Heimbürger, L., Lohan, M., Planquette, H., Flierdt, T., 2017. Sampling and Sample-handling Protocols for GEOTRACES Cruises. Page, https://www.geotraces.org/methods-cookbook/

Da Silveira, I.C.A., De Miranda, L.B., Brown, W.S., 1994. On the origins of the North Brazil Current. J. Geophys. Res. 99, 501–512. https://doi.org/10.1029/94jc01776

Degens, E.T., 1969. Biogeochemistry of Stable Carbon Istopes, in: Eglinton, G., and Murphy, M.T.J. (Eds.), Organic Geochemistry Methods and Results. Springer-Verlag Berlin Heidelberg 1969, Germany, pp. 304-328.

De La Rocha, C.L., Passow, U., 2007. Factors influencing the sinking of POC and the efficiency of the biological carbon pump. Deep. Res. Part II Top. Stud. oceanogr. 54, 639–658. https://doi.org/10.1016/j.dsr2.2007.01.004

De La Rocha, C.L., Passow, U., 2014. 8.4 The Biological Pump, in: Turekian, K., Holland, H., (Eds.), Teatrise On Geochemistry, Second ed., Elsevier, Amsterdan, pp. 94-115.

Dencausse, G., Arhan, M., Speich, S., 2010. Routes of Agulhas rings in the southeastern Cape Basin. Deep. Res. Part I oceanogr. Res. Pap. 57, 1406–1421. https://doi.org/10.1016/j.dsr.2010.07.008.

Devol, A.H., Hartnett, H.E., 2001. Role of the oxygen-deficient zone in transfer of organic carbon to the deep ocean. Limnol. oceanogr. 46, 1684–1690. https://doi.org/10.4319/lo.2001.46.7.1684

Dotto, T., Kerr, R., Mata, M., Garcia, C., 2016. Multidecadal freshening and lightening in the deep waters of the Bransfield Strait, Antarctica. J. Geophys. Res. Ocean. 121, 3741–3756. https://doi.org/10.1002/2015JC011228.Received

Duncombe Rae, C.M., 1991. Agulhas retroflection rings in the South Atlantic Ocean: An overview. South African J. Mar. Sci. 11, 327–344. https://doi.org/10.2989/025776191784287574.

Eadie, B.J., Jeffrey, L.M., 1973. δ13C analyses of oceanic particulate organic matter. Mar. Chem. 1, 199–209. https://doi.org/10.1016/0304-4203(73)90004-2

Eadie, B.J., Jeffrey, L.M., Sackett, W.M., 1978. Some observations on the stable carbon isotope composition of dissolved and particulate organic carbon in the marine environment. Geochim. Cosmochim. Acta 42, 1265–1269. https://doi.org/10.1016/0016-7037(78)90120-5

Engel, A., Wagner, H., Le Moigne, F.A.C., Wilson, S.T., 2017. Particle export fluxes to the oxygen minimum zone of the eastern tropical North Atlantic. Biogeosciences 14, 1825–1838. https://doi.org/10.5194/bg-14-1825-2017

Falkowski, P.G., Barber, R.T., Smetacek, V., 1998. Biogeochemical controls and

feedbacks on ocean primary production. Science (80-.). 281, 200–206. https://doi.org/10.1126/science.281.5374.200

Fernandez, D., Sutton, P., Bowen, M., 2017. Variability of the subtropical mode water in the Southwest Pacific. J. Geophys. Res. Ocean. 122, 7163–7180. https://doi.org/doi:10.1002/2017JC013011.

Ferreira, M.L. de C., Kerr, R., 2017. Source water distribution and quantification of North Atlantic Deep Water and Antarctic Bottom Water in the Atlantic Ocean. Prog. oceanogr. 153, 66–83. https://doi.org/10.1016/j.pocean.2017.04.003.

Fischer, G., 1991. Stable carbon isotope ratios of plankton carbon and sinking organic matter from the Atlantic sector of the Southern Ocean. Mar. Chem. 35, 581–596. https://doi.org/10.1016/S0304-4203(09)90044-5

Fischer, G., Müller, P.J., Wefer, G., 1998. Latitudinal δ13C(org) variations in sinking matter and sediments from the South Atlantic: Effects of anthropogenic CO2 and implications for paleo-PCO2 reconstructions. J. Mar. Syst. 17, 471–495. https://doi.org/10.1016/S0924-7963(98)00059-1

Fratantoni, D.M., Kwon, Y.O., Hodges, B.A., 2013. Direct observation of subtropical mode water circulation in the western North Atlantic Ocean. Deep. Res. Part II Top. Stud. oceanogr. 91, 35–56. https://doi.org/10.1016/j.dsr2.2013.02.027.

Garzón, J.E.C., Martínez, A.M., Barrera, F., Pfaff, F., Koch, B.P., Freije, R.H., Gómez, E.A., Lara, R.J., 2016. The Pacific-Atlantic connection: Biogeochemical signals in the southern end of the Argentine shelf. J. Mar. Syst. 163, 95–101. https://doi.org/10.1016/j.jmarsys.2016.07.008

Giering, S.L.C., Sanders, R., Lampitt, R.S., Anderson, T.R., Tamburini, C., Boutrif, M., Zubkov, M. V., Marsay, C.M., Henson, S.A., Saw, K., Cook, K., Mayor, D.J., 2014. Reconciliation of the carbon budget in the ocean's twilight zone. Nature 507, 480–483. https://doi.org/10.1038/nature13123

Gordon, A.L., 1996. Comment on the South Atlantic's Role in the Global Circulation, in: Wefer, G., Berger, W.H., Siedler, G., Webb, D.J. (Eds.), The South Atlantic: Present and Past Circulation. Springer, Berlin, Heidelberg,

pp. 121–124. https://doi.org/10.1007/978-3-642-80353-6_7

Gordon, A.L., Lutjeharmst, J.R.E., Gründlingh, M., 1987. Stratification and circulation at the Agulhas Retroflection. Deep. Res. 34, 565–599. https://doi.org/https://doi.org/10.1016/0198-0149(87)90006-9.

Gordon, A.L., Weiss, R.F., Smethie, W.M., Warner, M.J., 1992. Thermocline and Intermediate Water Communication Between the South Atlantic and Indian Oceans. J. Geophys. Res. 97, 7223–7240. https://doi.org/https://doi.org/10.1029/92JC00485.

Guerra, L.A.A., Paiva, A.M., Chassignet, E.P., 2018. On the translation of Agulhas rings to the western South Atlantic Ocean. Deep Sea Research Part I: oceanographic Research Papers 139, 104–113. https://doi.org/10.1016/j.dsr.2018.08.005

Hahn, J., Brandt, P., Schmidtko, S., Krahmann, G., 2017. Decadal oxygen change in the eastern tropical North Atlantic. Ocean Sci. 13, 551–576. https://doi.org/10.5194/os-13-551-2017

Hall, C., Lutjeharms, J.R.E., 2011. Cyclonic eddies identified in the Cape Basin of the South Atlantic Ocean. J. Mar. Syst. 85, 1–10. https://doi.org/10.1016/j.jmarsys.2010.10.003

Ham, Y.G., Kug, J.S., Park, J.Y., 2013. Two distinct roles of Atlantic SSTs in ENSO variability: North Tropical Atlantic SST and Atlantic Niño. Geophys. Res. Lett. 40, 4012–4017. https://doi.org/10.1002/grl.50729

Hanawa, K., Talley, L.D., 2001. Mode waters. Ocean circulation and climate. In: Siedler, G., Church, J., Gould, J. (Eds.), International Geophysical Series. vol. 77. Academic Press, San Diego, CA, pp. 373–386.

Hansen, H.P., and Koroleff, E., 1999. Determination of nutrients, in: Grasshoff, K., Kremling, K., Ehrhardt, M., (Eds.), Methods of Seawater Analysis. Wiley-VCH, Toronto, pp. 159-228.

Hazeleger, W., Drijfhout, S., 2006. Subtropical cells and meridional overturning circulation pathways in the tropical Atlantic. J. Geophys. Res. 111, 1–13. https://doi.org/10.1029/2005JC002942.

Helly, J.J., Levin, L.A., 2004. Global distribution of naturally occurring marine hypoxia on continental margins. Deep. Res. Part I oceanogr. Res. Pap. 51, 1159–1168. https://doi.org/10.1016/j.dsr.2004.03.009

Holmes, M.E, Lavik, G., Fischer, G., Wefer, G., 2003. Nitrogen Isotopes in Sinking Particles and Surface Sediments in the Central and Southern Atlantic, in: Wefer, G., Mulitza, S., Ratmeyer, V., (eds), 2003, The South Atlantic in the Late Quaternary: Reconstruction of Material Budgets and Current Systems. Springer-Verlag Berlin Heidelberg New York Tokyo, pp 143-165

Holte, J.W., Talley, L.D., Chereskin, T.K., Sloyan, B.M., 2012. The role of air-sea fluxes in Subantarctic Mode Water formation. J. Geophys. Res. 117, 1–17. https://doi.org/10.1029/2011JC007798.

Honjo, S., Manganini, S.J., Krishfield, R.A., Francois, R., 2008. Particulate organic carbon fluxes to the ocean interior and factors controlling the biological pump: A synthesis of global sediment trap programs since 1983. Prog. oceanogr. 76, 217–285. https://doi.org/10.1016/j.pocean.2007.11.003

Huang, C., Jiang, Q., Yao, L., Yang, H., Lin, C., Huang, T., Zhang, Y., 2018. Variation pattern of particulate organic carbon and nitrogen in oceans and inland waters. Biogeosciences 15, 1827–1841. https://doi.org/10.5194/bg-15-1827-2018

Jeffrey, A.W.A., Pflaum, R.C., Brooks, J.M., Sackett, W., 1983. Vertical trends in particulate organic carbon 13C:12C ratio in the upper water column. Deep Sea Res. 30, 971–983. https://doi.org/10.1016/0198-0149(83)90052-3

Karstensen, J., Fiedler, B., Schütte, F., Brandt, P., Körtzinger, A., Fischer, G., Zantopp, R., Hahn, J., Visbeck, M., Wallace, D., 2015. Open ocean dead zones in the tropical North Atlantic Ocean. Biogeosciences 12, 2597–2605. https://doi.org/10.5194/bg-12-2597-2015.

Karstensen, J., Stramma, L., Visbeck, M., 2008. Oxygen minimum zones in the eastern tropical Atlantic and Pacific oceans. Prog. oceanogr. 77, 331–350. https://doi.org/10.1016/j.pocean.2007.05.009.

Karstensen, J., Quadfasel, D., 2002. Formation of Southern Hemisphere

thermocline waters: Water mass conversion and subduction. J. Phys. oceanogr. 32, 3020–3038. https://doi.org/10.1175/1520-0485(2002)032<3020:FOSHTW>2.0.CO;2

Keil, R.G., Neibauer, J.A., Biladeau, C., Van Der Elst, K., Devol, A.H., 2016. A multiproxy approach to understanding the “enhanced” flux of organic matter through the oxygen-deficient waters of the Arabian Sea. Biogeosciences 13, 2077–2092. https://doi.org/10.5194/bg-13-2077-2016

Kelly, K.A., Dong, S., 2013. The contributions of atmosphere and ocean to North Atlantic Subtropical Mode Water volume anomalies. Deep. Res. Part II Top. Stud. oceanogr. 91, 111–127. https://doi.org/10.1016/j.dsr2.2013.02.020.

Kelley, D., Richards, C. (2019). oce: Analysis of oceanographic Data. R package version 1.1-1. https://CRAN.R-project.org/package=oce.

Kerr, R., Mata, M.M., Garcia, C.A.E., 2009a. On the temporal variability of the weddell sea deep water masses. Antarct. Sci. 21, 383–400. https://doi.org/10.1017/S0954102009001990.

Kerr, R., Wainer, I., Mata, M.M., 2009b. Representation of the weddell sea deep water masses in the ocean component of the NCAR-CCSM model. Antarct. Sci. 21, 301–312. https://doi.org/10.1017/S0954102009001825.

Kitidis, V., Brown, I., Hardman-Mountford, N., Lefèvre, N., 2017. Surface ocean carbon dioxide during the Atlantic Meridional Transect (1995–2013); evidence of ocean acidification. Prog. oceanogr. 158, 65–75. https://doi.org/10.1016/j.pocean.2016.08.005.

Klein, B., Tomczak, M., 1994. Identification of diapycnal mixing through optimum multiparameter analysis 2. Evidence for unidirectional diapycnal mixing in the front between North and South Atlantic Central Water. J. Geophys. Res. 99, 275–280. https://doi.org/10.1029/94jc01948.

Landrum, J.P., Altabet, M.A., Montoya, J.P., 2011. Basin-scale distributions of stable nitrogen isotopes in the subtropical North Atlantic Ocean: Contribution of diazotroph nitrogen to particulate organic matter and mesozooplankton. Deep. Res. Part I oceanogr. Res. Pap. 58, 615–625.

https://doi.org/10.1016/j.dsr.2011.01.012

Lara, R.J., Alder, V., Franzosi, C.A., Kattner, G., 2010. Characteristics of suspended particulate organic matter in the southwestern Atlantic: Influence of temperature, nutrient and phytoplankton features on the stable isotope signature. J. Mar. Syst. 79, 199–209. https://doi.org/10.1016/j.jmarsys.2009.09.002

Larqué, L., Maamaatuaiahutapu, K., Garçon, V., 1997. On the intermediate and deep water flows in the South Atlantic Ocean. J. Geophys. Res. Ocean. 102, 12425–12440. https://doi.org/10.1029/97JC00629.

Lauvset, S.K., Tanhua, T., 2015. A toolbox for secondary quality control on ocean chemistry and hydrographic data. Limnol. oceanogr. Methods 13, 601–608. https://doi.org/10.1002/lom3.10050

Laxenaire, R., Speich, S., Blanke, B., Chaigneau, A., Pegliasco, C., Stegner, A., 2018. Anticyclonic Eddies Connecting the Western Boundaries of Indian and Atlantic Oceans. J. Geophys. Res. Ocean. 123, 7651–7677. https://doi.org/10.1029/2018JC014270.

Laxenaire, R., Speich, S., Stegner, A., 2019. Evolution of the Thermohaline Structure of One Agulhas Ring Reconstructed from Satellite Altimetry and Argo Floats. J. Geophys. Res. Ocean. https://doi.org/10.1029/2018JC014426.

Lehahn, Y., d'Ovidio, F., Lévy, M., Amitai, Y., Heifetz, E., 2011. Long range transport of a quasi isolated chlorophyll patch by an Agulhas ring. Geophysical Research Letters 38. https://doi.org/10.1029/2011GL048588

Li, Z., 2012. Interannual and decadal variability of the subtropical mode water formation in the South Pacific Ocean. Ocean Model. 47, 96–112. https://doi.org/10.1016/j.ocemod.2012.02.001

Lourey, M.J., Trull, T.W., Sigman, D.M., 2003. Sensitivity of δ 15 N of nitrate, surface suspended and deep sinking particulate nitrogen to seasonal nitrate depletion in the Southern Ocean. Global Biogeochem. Cycles 17, n/a-n/a. https://doi.org/10.1029/2002gb001973

Lozier, M.S., Owens, W.B., Curry, R.G., 1995. The climatology of the North Atlantic. Prog. oceanogr. 36, 1–44. https://doi.org/10.1016/0079-6611(95)00013-5.

Luyten, J.R., Pedlosky, J., Stommel, H., 1983. The Ventilated Thermocline. J. Phys. oceanogr. 13, 292–309. https://doi.org/10.1175/1520-0485

MacKas, A.L., Denman, K.L., Bennett, A.F., 1987. Least squares multiple tracer analysis of water mass composition. J. Geophys. Res. 92, 2907–2918. https://doi.org/10.1029/JC092iC03p02907.

MacKenzie, K.M., Robertson, D.R., Adams, J.N., Altieri, A.H., Turner, B.L., 2019. Structure and nutrient transfer in a tropical pelagic upwelling food web: From isoscapes to the whole ecosystem. Prog. oceanogr. 178. https://doi.org/10.1016/j.pocean.2019.102145

Mason, E., Pascual, A., McWilliams, J.C., 2014. A new sea surface height-based code for oceanic mesoscale eddy tracking. J. Atmos. Ocean. Technol. 31, 1181–1188. https://doi.org/10.1175/JTECH-D-14-00019.1

Marcello, F., Wainer, I., Rodrigues, R.R., 2018. South Atlantic Subtropical Gyre Late Twentieth Century Changes. J. Geophys. Res. Ocean. 123, 5194–5209. https://doi.org/10.1029/2018JC013815

McCartney, M.S., 1977. Subantarctic mode water. In: Angel, M. (Ed.), A Voyage of Discovery: George Deacon 70th Anniversary Volume. Pergamon and Publishing House, New York, pp. 103–119.

McCartney, M.S, Talley, L., 1982. The Subpolar Mode Water of the North Atlantic Ocean. J. Phys. oceanogr. 12, 1169–1188. https://doi.org/10.1175/1520-0485(1982)012<1169:tsmwot>2.0.co;2.

Middelburg, J., 2019. Marine Carbon Biogeochemistry A Primer for Earth System Scientist, Springer Open, Switzerland.

Olsen, A., Key, R.M., Van Heuven, S., Lauvset, S.K., Velo, A., Lin, X., Schirnick, C., Kozyr, A., Tanhua, T., Hoppema, M., Jutterström, S., Steinfeldt, R., Jeansson, E., Ishii, M., Pérez, F.F., Suzuki, T., 2016. The global ocean data analysis project version 2 (GLODAPv2) - An internally consistent data

product for the world ocean. Earth Syst. Sci. Data 8, 297–323. https://doi.org/10.5194/essd-8-297-2016

Orselli, I. B. M.; Goyet, C.; Kerr, R.; Azevedo, J. L. L. de; Araujo, M.; Galdino, F.; Touratier, F.; Garcia, C. A. E. The Effect of Agulhas Eddies on Absorption and Transport of Anthropogenic Carbon in the South Atlantic Ocean. Climate 2019, 7 (6), 84.a

Orselli, I.B.M., Kerr, R., Azevedo, J.L.L. d., Galdino, F., Araujo, M., Garcia, C.A.E., 2019. The sea-air CO2 net fluxes in the South Atlantic Ocean and the role played by Agulhas eddies. Prog. oceanogr. 170, 40–52. https://doi.org/10.1016/j.pocean.2018.10.006.b

Orselli, I.B.M., Kerr, R., Ito, R.G., Tavano, V.M., Mendes, C.R.B., Garcia, C.A.E., 2018. How fast is the Patagonian shelf-break acidifying? J. Mar. Syst. 178, 1–14. https://doi.org/10.1016/j.jmarsys.2017.10.007.

Passow, U., Carlson, C.A., 2012. The biological pump in a high CO2 world. Mar. Ecol. Prog. Ser. 470, 249–271. https://doi.org/10.3354/meps09985

Peterson, R.G., Stramma, L., 1991. Upper-level circulation in the South Atlantic Ocean. Prog. oceanogr. 26, 1–73. https://doi.org/10.1016/0079-6611(91)90006-8

Poole, R., Tomczak, M., 1999. Optimum multiparameter analysis of the water mass structure in the Atlantic Ocean thermocline. Deep. Res. Part I oceanogr. Res. Pap. 46, 1895–1921. https://doi.org/10.1016/S0967-0637(99)00025-4.

Price, James. F., 2001. Subduction. Ocean circulation and climate. In: Siedler, G., Church, J., Gould, J. (Eds.), International Geophysical Series. vol. 77. Academic Press, San Diego, CA, pp. 357–371.

Provost, C., Escoffier, C., Maamaatuaiahutapu, K., Kartavtseff, A., Garçon, V., 1999. Subtropical mode waters in the South Atlantic Ocean. J. Geophys. Res. Ocean. 104, 21033–21049. https://doi.org/10.1029/1999jc900049.

Qiu, B., Chen, S., 2006. Decadal variability in the formation of the North Pacific subtropical mode water: Oceanic versus atmospheric control. J. Phys.

oceanogr. 36, 1365–1380. https://doi.org/10.1175/JPO2918.1

R Core Team (2019). R: A language and environment for statistical computing.R Foundation for Statistical Computing, Vienna, Austria. URL https://www.R-project.org/.

Rasse, R., Dall'Olmo, G., 2019. Do Oceanic Hypoxic Regions Act as Barriers for Sinking Particles? A Case Study in the Eastern Tropical North Atlantic. Global Biogeochem. Cycles 33, 1611–1630. https://doi.org/10.1029/2019GB006305

Rau, G.H., Takahashi, T., Des Marais, D.J., Repeta, D.J., Martin, J.H., 1992. The relationship between δ13C of organic matter and [CO2(aq)] in ocean surface water: Data from a JGOFS site in the northeast Atlantic Ocean and a model. Geochim. Cosmochim. Acta 56, 1413–1419. https://doi.org/10.1016/0016-7037(92)90073-R

Rau, G.H., Takahashi, T., Des Marais, D.J., Sullivan, C.W., 1991. Particulate organic matter δ13C variations across the Drake Passage. J. Geophys. Res. 96, 131–135. https://doi.org/10.1029/91jc01253

Redfield, A.C., Ketchum, B.H., Richards, F.A., 1963. The influence of organisms on the composition of sea-water. In: Hill, M.N. (Ed.) The Sea: Ideas and Observations on Progress in the Study of the Seas, Vol, 2. Wiley, London, pp. 26-77.

Reid, J.R., 1996. On the Circulation of the South Atlantic Ocean, in: Wefer, G., Berger, W.H., Siedler, G., Webb, D.J. (Eds.), The South Atlantic: Present and Past Circulation. Springer, Berlin, Heidelberg, pp. 13–44. https://doi.org/10.1007/978-3-642-80353-6_2

Rey, M., Rodríguez-Fonseca, B., Polo, I., 2015. Atlantic opportunities for ENSO prediction. Geophys. Res. Lett. 42, 6802–6810. https://doi.org/10.1002/2015GL065062

Rhein, M., S.R. Rintoul, S. Aoki, E. Campos, D. Chambers, R.A. Feely, S. Gulev, G.C. Johnson, S.A. Josey, A. Kostianoy, C. Mauritzen, D. Roemmich, L.D. Talley and F. Wang, 2013: Observations: Ocean. In: Climate Change 2013:

The Physical Science Basis. Contribution of Working Group I to the Fifth Assessment Report of the Intergovernmental Panel on Climate Change [Stocker, T.F., D. Qin, G.-K. Plattner, M. Tignor, S.K. Allen, J. Boschung, A. Nauels, Y. Xia, V. Bex and P.M. Midgley (eds.)]. Cambridge University Press, Cambridge, United Kingdom and New York, NY, USA.

Richardson, P.L., 2007. Agulhas leakage into the Atlantic estimated with subsurface floats and surface drifters. Deep. Res. Part I oceanogr. Res. Pap. 54, 1361–1389. https://doi.org/10.1016/j.dsr.2007.04.010.

Rodrigues, R.R., Rothstein, L.M., Wimbush, M., 2007. Seasonal variability of the South Equatorial Current bifurcation in the Atlantic Ocean: A numerical study. J. Phys. oceanogr. 37, 16–30. https://doi.org/10.1175/JPO2983.1

Roullier, F., Berline, L., Guidi, L., Durrieu De Madron, X., Picheral, M., Sciandra, A., Pesant, S., Stemmann, L., 2014. Particle size distribution and estimated carbon flux across the Arabian Sea oxygen minimum zone. Biogeosciences 11, 4541–4557. https://doi.org/10.5194/bg-11-4541-2014

Rühs, S., Schwarzkopf, F.U., Speich, S., Biastoch, A., 2019. Cold vs. warm water route-sources for the upper limb of the Atlantic Meridional Overturning Circulation revisited in a high-resolution ocean model. Ocean Sci. 15, 489–512. https://doi.org/10.5194/os-15-489-2019.

Salt, L.A., van Heuven, S.M.A.C., Claus, M.E., Jones, E.M., de Baar, H.J.W., 2015. Rapid acidification of mode and intermediate waters in the southwestern Atlantic Ocean. Biogeosciences 12, 1387–1401. https://doi.org/10.5194/bg-12-1387-2015.

Santos, G.C., Kerr, R., Azevedo, J.L.L., Mendes, C.R.B., da Cunha, L.C., 2016. Influence of Antarctic Intermediate Water on the deoxygenation of the Atlantic Ocean. Dyn. Atmos. Ocean. 76, 72–82. https://doi.org/10.1016/j.dynatmoce.2016.09.002.

Sato, O.T., Polito, P.S., 2014. Observation of South Atlantic subtropical mode waters with Argo profiling float data. J. Geophys. Res. Ocean. 119, 2860–2881. https://doi.org/10.1002/ 2013JC009438.

Sarmiento, J., and Gruber, N., 2006. Ocean Biogeochemical Dynamics,

Princeton University Press, United Kingdom.

Schlax, M.G., Chelton, D.B., 2016. The “Growing Method” of Eddy Identification and Tracking in Two and Three Dimensions. College of Earth, Ocean and Atmospheric Sciences. Oregon State University, Corvallis, Oregon July 8, 2016.

Schlitzer, R., 2019. Ocean Data View, <http://odv.awi.de>.

Schlosser, C., Klar, J.K., Wake, B.D., Snow, J.T., Honey, D.J., Woodward, E.M.S., Lohan, M.C., Achterberg, E.P., Moore, C.M., 2014. Seasonal ITCZ migration dynamically controls the location of the (sub)tropical Atlantic biogeochemical divide. Proc. Natl. Acad. Sci. 111, 1438–1442. https://doi.org/10.1073/pnas.1318670111

Schmidtko, S., Stramma, L., Visbeck, M., 2017. Decline in global oceanic oxygen content during the past five decades. Nature 542, 335–339. https://doi.org/10.1038/nature21399

Schouten, M.W., de Ruijter, W.P.M., van Leeuwen, P.J., Lutjeharms, J.R.E., 2000. Translation, decay and splitting of Agulhas rings in the southeastern Atlantic Ocean. J. Geophys. Res. Ocean. 105, 21913–21925. https://doi.org/10.1029/1999jc000046

Siedler, G., Kuhl, A., Zenk, W., 1987. The Madeira Mode Water. J. Phys. oceanogr. 17, 1561–1570. https://doi.org/https://doi.org/10.1175/1520-0485(1987)017<1561:TMMW>2.0.CO;2.

Souza, A.G.Q. de, Kerr, R., Azevedo, J.L.L. de, 2018. On the influence of Subtropical Mode Water on the South Atlantic Ocean. J. Mar. Syst. 185, 13–24. https://doi.org/10.1016/j.jmarsys.2018.04.006.

Souza, J.M.A.C., Montégut, C.D.B., Cabanes, C., Klein, P., 2011. Estimation of the Agulhas ring impacts on meridional heat fluxes and transport using ARGO floats and satellite data. Geophys. Res. Lett. 38, 1–5. https://doi.org/10.1029/2011GL049359.

Stramma, L., England, M., 1999. On the water masses and mean circulation of the South Atlantic Ocean. J. Geophys. Res. Ocean. 104, 20,863-20,883.

https://doi.org/10.1029/1999JC900139.

Stramma, L., Hüttl, S., Schafstall, J., 2005. Water masses and currents in the upper tropical northeast Atlantic off northwest Africa. J. Geophys. Res. Ocean. 110, 1–18. https://doi.org/10.1029/2005JC002939

Stramma, L., Johnson, G.C., Sprintall, J., Mohrholz, V., 2008. Expanding oxygen-minimum zones in the tropical oceans. Science (80-.). 320, 655–658. https://doi.org/10.1126/science.1153847.

Stramma, L., Schott, F., 1999. The mean flow field of the tropical Atlantic Ocean. Atlantic 46, 279–303. https://doi.org/https://doi.org/10.1016/S0967-0645(98)00109-X.

Takahashi, T., Broecker, W.S., Langer, S., 1985. Redfield ratio based on chemical data from isopycnal surfaces. J. Geophys. Res. 90, 6907–6924. https://doi.org/10.1029/JC090iC04p06907.

Tanhua, T., Van Heuven, S., Key, R.M., Velo, A., Olsen, A., Schirnick, C., 2010. Quality control procedures and methods of the CARINA database. Earth Syst. Sci. Data 2, 35–49. https://doi.org/10.5194/essd-2-35-2010

Tomczak, M., 1981. A multi-parameter extension of temperature/salinity diagram techniques for the analysis of non-isopycnal mixing. Prog. oceanogr. 10, 147–171. https://doi.org/https://doi.org/10.1016/0079-6611(81)90010-0.

Tomczak, M., Godfrey, J.S., 1994. CHAPTER 7 - Arctic oceanography; the path of North Atlantic Deep Water, in: Tomczak, M., Godfrey, J.S. (Eds.), Regional oceanography. Pergamon, Amsterdam, pp. 89–111d. https://doi.org/10.1016/B978-0-08-041021-0.50011-4

Tomczak, M., Large, D.G., 1989. Optimum Multiparameter Analysis of Mixing in the Thermocline of the Eastern Indian Ocean. J. Geophys. Res. 94, 16,141-16,149. https://doi.org/https://doi.org/10.1029/JC094iC11p16141.

Tsubouchi, T., Suga, T., Hanawa, K., 2007. Three types of South Pacific subtropical mode waters: Their relation to the large-scale circulation of the South Pacific subtropical gyre and their temporal variability. J. Phys. oceanogr. 37, 2478–2490. https://doi.org/10.1175/JPO3132.1

Vanegas, S.A., Mysak, L.A., Straub, D.N., 1998. An interdecadal climate cycle in the South Atlantic and its links to other ocean basins. J. Geophys. Res. Ocean. 103, 24723–24736. https://doi.org/10.1029/98JC02443

Van Mooy, B.A.S., Keil, R.G., Devol, A.H., 2002. Impact of suboxia on sinking particulate organic carbon: Enhanced carbon flux and preferential degradation of amino acids via denitrification. Geochim. Cosmochim. Acta 66, 457–465. https://doi.org/10.1016/S0016-7037(01)00787-6

Volk, T., Hoffert, M.I., 1985. Ocean carbon pumps: analysis of relative strengths and efficiencies in ocean-driven atmospheric CO2 changes. carbon cycle Atmos. CO2 Nat. Var. Archean to Present 32, 99–110.

Wada, E., Terazaki, M., Kabaya, Y., Nemoto, T., 1987. 15N and 13C abundances in the antarctic ocean with emphasis on biogeochemical structure of food web. Deep Sea Res. 34, 829–841. https://doi.org/10.1016/0198-0149(87)90039-2

Weijer, W., De Ruijter, W., Dijkstra, H., 2001. Stability of the Atlantic overturning circulation: competition between Bering Strait freshwater flux and Agulhas heat and salt sources. J. Phys. oceanogr. 31, 2385–2402.

Worthington, V., L., 1958. The 18° water in the Sargasso Sea. Deep Sea Res. 5, 297–305. https://doi.org/10.1016/0146-6313(58)90026-1.

Yasuda, T., Kitamura, Y., 2003. Long-term variability of North Pacific Subtropical Mode Water in response to spin-up of the subtropical gyre. J. oceanogr. 59, 279–290. https://doi.org/10.1023/A:1025507725222